

GEOPHYSICAL EVIDENCE FOR QUATERNARY DEFORMATION WITHIN THE  
OFFSHORE SAN ANDREAS FAULT SYSTEM, NORTHERN CALIFORNIA

AS  
36  
2012  
GEOL  
.576

A thesis submitted to the faculty of  
San Francisco State University  
In partial fulfillment of  
The Requirements for  
The Degree

Master of Science  
In  
Geosciences

by

Brian Andrew Stozek

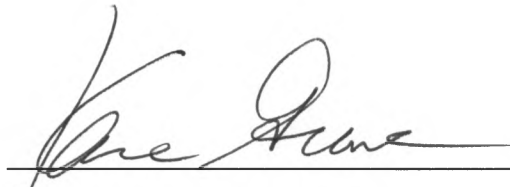
San Francisco, California

May 2012

Copyright by  
Brian Andrew Stozek  
2012

CERTIFICATION OF APPROVAL

I certify that I have read *Geophysical evidence for Quaternary deformation within the offshore San Andreas Fault System, Northern California* by Brian Andrew Stozek, and that in my opinion this work meets the criteria for approving a thesis submitted in partial fulfillment of the requirements for the degree: Master of Science in Geosciences at San Francisco State University



---

Dr. Karen Grove

Professor, Geosciences Department, SFSU



---

Dr. John Caskey

Associate Professor, Geosciences Department, SFSU



---

Holly Ryan

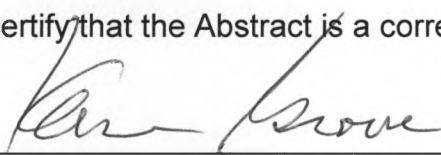
Research Geologist, U.S. Geological Survey

GEOPHYSICAL EVIDENCE FOR QUATERNARY DEFORMATION WITHIN THE  
OFFSHORE SAN ANDREAS FAULT SYSTEM, NORTHERN CALIFORNIA

Brian Andrew Stozek  
San Francisco, California  
2012

Offshore multichannel and mini-sparker seismic reflection profiles collected north of San Francisco indicate varying tectono-stratigraphic conditions since the Late Miocene. Near the Point Reyes Peninsula headland, Miocene units have been vertically offset at least 2 km on the Point Reyes fault (PRF); deformation began during the Late Miocene, probably in response to a change in relative plate motions. North of the peninsula, multiple Quaternary sequences formed above a subsiding Plio-Pleistocene unconformity (PPU) during eustatic sea-level fluctuations. The mechanism for subsidence may be related, in part, to isostatic loading from thick Pleistocene deposits derived from the Russian River. West of the Gualala Block, preserved sequences have been folded, probably starting ~500 ka, by transpressional structures associated with the Gualala fault. South and adjacent to the headland, few Pleistocene sediments are preserved. The PPU and overlying Holocene deposits are undeformed, suggesting that the PRF has become increasingly inactive since the Middle Pleistocene and that its hazard potential in current fault and tsunami hazard models should be reduced.

I certify that the Abstract is a correct representation of the content of this thesis.



Chair, Thesis Committee

5/9/2012  
Date

## ACKNOWLEDGEMENTS

This thesis would not have been possible without the guidance and support of my thesis committee: Karen Grove, John Caskey and Holly Ryan. I would also like to thank Ray Sliter, Dennis Mann, Tom Parsons, Bob McLaughlin and Stephanie Ross with the USGS for their assistance and feedback. Finally, I would like to thank the SFSU Department of Geosciences and my friends and family for their support. Funding for the project was provided by the USGS STEP program and the SFSU ORSP.

## TABLE OF CONTENTS

List of Tables.....	viii
List of Figures.....	ix
List of Appendices.....	xii
1.0 Introduction.....	1
2.0 Geologic Background.....	4
2.1 Stratigraphic Units.....	4
2.2 Faults of the San Andreas Fault System (SAFS).....	7
2.2.1 Peninsula and North Coast SAF.....	8
2.2.2 San Gregorio fault (SGF).....	10
2.2.3 Point Reyes fault (PRF).....	11
3.0 Methods.....	12
3.1 Exploratory Well Logs.....	13
3.2 Seismic Reflection Profiles.....	14
3.3 Multibeam Bathymetric Data.....	16
3.4 Seismic Reflection Correlation and Velocity Models.....	16
3.5 Isopach Maps.....	18
4.0 Results.....	19
4.1 Middle Miocene Section.....	21
4.2 Upper Miocene Section.....	24
4.3 Pliocene Section.....	27
4.4 Timing and amount of deformation.....	28
4.5 Pleistocene Section.....	31
4.6 Holocene Section.....	33
4.7 Quaternary sequences north of Point Reyes.....	34

5.0 Discussion.....	40
5.1 Implications for movement on the Point Reyes fault.....	41
5.2 Controls on the formation of Quaternary sequences.....	47
5.3 Late Quaternary deformation model.....	50
5.4 Suggestions for future work.....	52
6.0 Conclusions.....	53
7.0 References.....	55
8.0 Appendices.....	118

## LIST OF TABLES

Table	Page
1. Well 27-1.....	60
2. Well 39-1.....	61
3. Well 41-1.....	62
4. Well 51-2.....	63
5. Well 53-1.....	64
6. Well 55-1.....	65
7. Well 55-2.....	66
8. Well 58-1.....	67

## LIST OF FIGURES

Figure	Page
1: Study area map.....	68
2: Revised offshore SAFS fault and fold map for the Point Reyes Peninsula region.....	69
3: Geologic map of Point Reyes Peninsula (adapted from Clark and Brabb, 1997).....	70
4: Seismic reflection profile datasets.....	71
5: Multibeam dataset (acquired by California State Monterey Bay).....	72
6: Offshore/onshore stratigraphic correlation diagram (amended from Heck et al., 1990).....	73
7: Offshore/onshore stratigraphic correlation diagram (amended from Heck et al., 1990).....	74
8: Velocity model for geologic units above the Monterey Formation.....	75
9: Velocity model for geologic units below the top of the Monterey Formation....	76
10: MCS profile WSF-076 (in TWTT).....	77
11: Depth converted MCS profile WSF-080.....	78
12: Depth converted MCS profile WSF-086.....	79
13: Depth converted MCS profile WSF-088.....	80
14: Depth converted MCS profile WSF-090.....	81
15: MCS profile WSF-001 (in TWTT).....	82

16: MCS profile WSF-094 (in TWTT).....	83
17: MCS profile WSF-098 (in TWTT).....	84
18: MCS profile WSF-102 (in TWTT).....	85
19: Depth converted MCS profile WNC82-106.....	86
20: Depth converted MCS profile WNC82-112.....	87
21: MCS profile WSF-203 (in time).....	88
22: MCS profile W482-112 (in TWTT).....	89
23: MCS profile W482-106 (in TWTT).....	90
24: MCS profile W482-102 (in TWTT).....	91
25: Depth converted mini-sparker seismic reflection profile PR-14.....	92
26: Depth converted mini-sparker seismic reflection profile PR-27.....	93
27: Depth converted mini-sparker seismic reflection profile PR-34.....	94
28: Depth converted mini-sparker seismic reflection profile PR-02.....	95
29: Depth converted mini-sparker seismic reflection profile PR-19.....	96
30: Depth converted mini-sparker seismic reflection profile PR-43.....	97
31: Depth converted mini-sparker seismic reflection profile PR-45.....	98
32: Depth converted mini-sparker seismic reflection profile PR-55.....	99
33: Depth converted mini-sparker seismic reflection profile PR-69.....	100
34: Depth converted mini-sparker seismic reflection profile PR-66.....	101
35: Depth converted mini-sparker seismic reflection profile PR-65.....	102
36: Depth converted mini-sparker seismic reflection profile PR-63A/63.....	103

37: Depth converted mini-sparker seismic reflection profile PR-95.....	104
38: Depth converted mini-sparker seismic reflection profile PR-109/109A.....	105
39: Depth converted mini-sparker seismic reflection profile PR-122.....	106
40: Depth converted mini-sparker seismic reflection profile PR-133.....	107
41: Depth converted mini-sparker seismic reflection profile PR-143.....	108
42: Isopach map of Upper Miocene units.....	109
43: Isopach Map of Pliocene units.....	110
44: Isopach Map of Quaternary units.....	111
45: Isopach Map of Pleistocene units.....	112
46: Isopach Map of Holocene units.....	113
47: Stratigraphic column depicting two Quaternary sequences.....	114
48: Marine Isotope Stage curve (Bassinot, 2007).....	115
49: GPS velocity field vectors (compiled by the WGCEP).....	116
50: Late Quaternary deformation summary.....	117

## LIST OF APPENDICES

Appendix	Page
A. Velocity Models for Offshore Wells.....	118
B. Uncertainty in the Velocity Regression Equations.....	120
C: Individual Well Velocity Models.....	122

## 1.0 Introduction

At the latitude of the San Francisco Bay Area, the San Andreas Fault System (SAFS) consists of an approximately 75-km-wide network of generally subparallel right-lateral faults (Fig. 1). Although the amount and timing of slip on many of the onland SAFS faults have been well characterized through field study (e.g., McLaughlin et al., 1996; Hall et al., 1999; Wakabayashi, 1999) and the development of three-dimensional models (e.g., Chéry et al., 2001; d'Alessio et al., 2005), offshore components of the SAFS are still not well understood. Recent studies that have interpreted offshore seismic reflection profiles collected across the offshore SAFS (Bruns et al., 2002; Ryan et al., 2008) have advanced our understanding of offshore structures, including dip-slip faults adjacent to the San Andreas fault (SAF) and San Gregorio fault (SGF). Although the SAFS is predominantly a right-lateral fault system, blind thrust events such as the 1983 Coalinga ( $M_w$  6.4) and 2003 San Simeon ( $M_w$  6.5) earthquakes in central California attest to the seismic hazard associated with dip-slip structures as well (Hardebeck et al., 2004). In the Bay Area, the 1989  $M_w$  6.9 Loma Prieta earthquake involved a large component of reverse motion on a fault adjacent to the SAF (Beroza, 1996) and young (<0.4 Ma) contractional structures have been mapped throughout the region (Page et al., 1998).

North of San Francisco, the SAF separates the Point Reyes Peninsula from mainland California (Fig. 2) and is the location where the largest amount of dextral offset was measured on the SAF after the great 1906 San Francisco earthquake (Lawson, 1908). A recent investigation of emergent marine terraces on the Point Reyes Peninsula showed significant uplift west of the SAF during the past 80 k.y., indicating that contractional processes have affected the region as well (Grove et al., 2010). Grove et al. (2010) suggested that this uplift was in part related to active reverse faults in the offshore region. The youngest marine terrace (~80 ka) on the western slope of Inverness Ridge is at progressively higher elevations to the south, indicating uplift rates that increase from ~0.2 mm/yr on the coast east of Drakes Bay to ~1.0 mm/yr near Bolinas (Fig. 3; Grove et al., 2010). Correlations of older terrace surfaces implied that uplift of the southern end of the peninsula has accelerated during the past 300 k.y., only achieving the ~1.0 mm/yr rate by ~125 ka (Fig. 3; Grove et al., 2010). Grove et al. (2010) proposed that deformation could be the result of late Pleistocene movement on offshore reverse faults, such as the Point Reyes fault (PRF; Fig. 1). Because the SAF is parallel to the plate-motion direction at the latitude of Point Reyes (Argus and Gordon, 2001), Quaternary uplift of the peninsula is likely produced by intersecting faults that create restraining geometries (Grove et al., 2010).

Other evidence is consistent with reverse-fault motion in the Point Reyes region. A kinematic fault model incorporating slip only on the dextral San Andreas and San Gregorio faults was unable to explain observed uplift of the Point Reyes Peninsula (Ryan et al., 2008), suggesting that additional (vertical-slip) fault movements are needed. In 1999, a  $M_w$  4.6 reverse-sense earthquake with a 8-km-deep hypocenter occurred near Bolinas, California (Fig. 2) (Baise et al., 2003). The fault plane solution for the earthquake indicates almost entirely reverse motion on a northwest-striking,  $47^\circ$ -dipping fault (Baise et al., 2003). The east-dipping nodal plane would correspond to a fault that projects to the ocean floor 7–8 km offshore in the same area where the PRF has been mapped on the seafloor (Fig. 1; Ryan et al., 2008). Potential seismic hazard was assigned to the PRF by the 2008 Working Group on California Earthquake Probabilities (WGCEP, 2008); they indicated a late Quaternary slip rate of 0.3 mm/yr and a maximum earthquake size of  $M_w$  6.7–6.9 for the fault.

Industry multichannel seismic (MCS) reflection profiles and offshore exploratory well data collected in the 1960s through the 1980s are now in the public domain, and provide the opportunity to more thoroughly study the geologic history of the offshore region west of the Point Reyes Peninsula. I used these data, together with recently collected high-resolution seismic reflection data, to study the timing and movement history of the PRF and other offshore faults and to create a revised offshore SAFS fault and fold map (Fig. 2). The PRF zone

was mapped to the north and south of the peninsula to determine whether the PRF connects with the SAF to the north, and/or the SGF to the south (Figs. 1, 2). The resultant offshore map of faults and folds and the interpretations presented herein indicate that, to the south, the PRF may have connected with the western SGF (SGF-W) as recently as the Late Pleistocene, but to the north the PRF is buried by probable Quaternary sedimentary sequences and does not appear to have been active since at least the Middle Pleistocene. The new interpretations suggest that the hazard potential of the Point Reyes fault in current fault and tsunami hazard models should be re-evaluated. A late Quaternary deformation model was created to explain the mechanisms for observed onshore/offshore Quaternary deformation; it is proposed that rapid uplift on the southern Point Reyes Peninsula is currently due to complex fault interactions at the active SGF-E/SAF junction near Bolinas.

## **2.0 Geologic Background**

### **2.1 *Stratigraphic Units***

The onshore stratigraphy of the Point Reyes Peninsula consists of Upper Cretaceous granitoid and older metamorphic basement rocks overlain by Tertiary marine sedimentary rocks comprising three unconformity-bounded sequences and overlain by discontinuous Quaternary surficial deposits (Fig. 3; Clark et al., 1984; Clark and Brabb, 1997). The basement rocks are exposed on the limbs of

the Point Reyes syncline, at the Point Reyes headland to the west and along Inverness Ridge and Tomales Point to the east (Fig. 3). The Tertiary sedimentary sequences are part of the 3700 km<sup>2</sup> Bodega Basin (Fig. 1). The sequences are separated by basin-wide unconformities attributed to successive marine transgressions alternating with episodes of uplift and erosion (McCulloch, 1989). The oldest sequence consists of 210 m of interbedded conglomerate and sandstone of the Paleocene Point Reyes Conglomerate (Galloway, 1977) that nonconformably overlies granitic rocks and was probably deposited in an upper to mid submarine-fan-channel complex (Clark et al., 1984). Overlying the Point Reyes Conglomerate, the Middle to Upper Miocene sequence is as much as 1,600 m thick and consists of a basal transgressive shallow-marine unit, the Laird Sandstone, and overlying siliceous mudstone and chert beds of the Monterey Formation that reflect progressive deepening of the sedimentary basin to mid-bathyal depths (Clark et al., 1984; McCulloch, 1989). An angular unconformity separates the Monterey Formation from the overlying Upper Miocene to Pliocene sequence that is as much as 2,500 m thick and consists of the basal transgressive glauconitic Santa Margarita Sandstone that grades upward into the Santa Cruz (siliceous) Mudstone (Clark et al., 1984). Basin filling is recorded by a coarsening-upward sequence from the Santa Cruz Mudstone (bathyal depths) to mudstone to fine sandstone of the Purisima Formation (shelf depths) (McCulloch, 1989). Discontinuous Quaternary surficial deposits throughout the

peninsula consist of uplifted marine-terrace, sand-dune and beach deposits (Fig. 3).

Most of the Bodega Basin is located offshore (Fig. 1). It was first described in detail by Hoskins and Griffiths (1971), who used industry seismic and exploratory well data collected in the 1960s to describe the basin's offshore stratigraphy and major structures. In the offshore, the Bodega Basin consists predominately of Upper Miocene and younger marine strata unconformably overlying Middle Miocene siliceous mudstone, Eocene deep-marine strata and Cretaceous granitoid basement rock. The basin is bounded on the west by the Pigeon Point and Farallon Highs and on the east by the San Gregorio and San Andreas faults (Hoskins and Griffiths, 1971; McCulloch, 1989). Hoskins and Griffiths (1971) noted that the pre-Miocene section is much more complexly faulted than the Miocene and Pliocene strata, and probably had a different structural grain that included development of the central cross-basin high that is manifested today as the Point Reyes Peninsula. Following Eocene–Oligocene deformation and uplift, Middle Miocene seas transgressed across the entire basin, forming a sequence similar to what is visible on the Point Reyes Peninsula. The basal shallow-marine Laird Sandstone is overlain by deeper-water chert beds of the Monterey Formation (Hoskins and Griffiths, 1971). In the southern part of the basin, an angular unconformity like that observed on land separates the Monterey Formation from the overlying Upper Miocene–Pliocene

sequence that consists of the basal shallow-marine Santa Margarita Sandstone overlain by the deep-water Santa Cruz Mudstone and the shallower-marine Purisima Formation (Hoskins and Griffiths, 1971; McCulloch, 1989). The offshore basin contains a relatively thin cover of Quaternary sediments, consisting of sand, silty sand, sandy silt, and silt that have filled in topographic lows above the most recent basin-wide unconformity (Chin et al., 1997).

## **2.2 *Faults of the San Andreas Fault System (SAFS)***

The SAFS forms the boundary between the Pacific plate and Sierra Nevada–Great Valley microplate; the boundary between the Sierran microplate and the North American plate is located on the eastern side of the Sierra Nevada in eastern California (Argus and Gordon, 2001). At the latitude of the San Francisco Bay region the ~75 km wide SAFS accommodates ~4 cm/yr of the total ~5 cm/yr relative motion between the Pacific and North American plates (DeMets et al., 2010), and the remaining ~1 cm/yr of relative motion is accommodated by faults along the eastern edge of the Sierran microplate (Argus and Gordon, 2001). In central California, south of the Bay Area, the ~4 cm/yr of right-lateral strike-slip motion between the Pacific and Sierran plates is accommodated almost entirely on the SAF. In the San Francisco Bay region, strike-slip motion is distributed on multiple subparallel faults of the SAFS including the San Gregorio, San Andreas, Rodgers Creek-Hayward, Green

Valley-Concord-Calaveras, and Antioch fault systems (d'Alessio et al., 2005). This study is focused primarily on Quaternary deformation related to the San Andreas, San Gregorio and Point Reyes faults located in the near-offshore region of the Point Reyes Peninsula.

### *2.2.1 Peninsula and North Coast SAF Segments*

The offshore section of the San Francisco Peninsula segment of the SAF (PSAF) lies between Mussel Rock and Bolinas (Fig. 1). At Bolinas, the eastern strand of the SGF merges with the PSAF to become the North Coast San Andreas fault (NCSAF) (Fig. 2). From Bolinas to Bodega Head, the NCSAF separates accretionary rocks of the Mesozoic Franciscan Complex to the east and continental granitic basement rocks of the Salinian terrane to the west (Figs. 2, 3). Along the eastern edge of the Point Reyes Peninsula, the NCSAF is a 1–3 km wide zone that forms a prominent linear valley; the 1906 earthquake ruptured a strand in the center of the valley (Fig. 3). At the edges of the valley, Galloway (1977) mapped the eastern and western boundary faults near Bolinas; farther north, Grove and Niemi (2005) mapped bounding faults in the valley south of Tomales Bay where they truncate late Pleistocene deposits (Fig. 3). The estimated slip rate of  $24 \pm 3$  mm/yr on the NCSAF at Point Reyes (Niemi and Hall, 1992) is higher than the estimated slip rate of  $17 \pm 4$  mm/yr on the PSAF (Hall et

al., 1999) because the NCSAF combines slip on the SGF and PSAF north of where the two faults merge near Bolinas (Fig. 2).

The NCSAF at the Point Reyes Peninsula is the boundary between fundamentally different basement rock types because it has been active since the inception of the SAF (Atwater, 1989). South of the Point Reyes Peninsula, however, the northernmost part of the PSAF is located entirely within Franciscan Complex rocks and the Pilarcitos fault is the boundary between Salinian and Franciscan basement rocks (Brabb et al., 1998). It is likely that the Pilarcitos fault accommodated plate motion before ~3 Ma (Parsons and Zoback, 1997). McLaughlin et al. (2007) suggested that slip was incrementally transferred from the Pilarcitos fault to the PSAF between 5.4 Ma and 1.0–1.6 Ma.

North of the Point Reyes Peninsula, the NCSAF between Fort Ross and Point Arena (Fig. 1) separates Franciscan rocks from those of the Gualala block, which is either a part of the Salinian terrane or a fragment of Franciscan-type rocks analogous to the Franciscan slice currently located between the PSAF and the inactive Pilarcitos fault (Dickenson et al., 2005). The Gualala fault (Fig. 2) is the western boundary of the Gualala block; it extends subparallel to the coastline ~4–5 km offshore and may be an extension of the Pilarcitos fault that has been offset by SAF motions (Dickenson et al., 2005).

### 2.2.2 *San Gregorio Fault (SGF)*

The SGF zone is part of the San Gregorio–Hosgri fault system that extends north from southern California and merges with the SAF on the Golden Gate Platform south of Bolinas (Fig. 2) (Bruns et al., 2002; Dickinson et al., 2005). Dickinson et al. (2005) estimated a net dextral offset along the San Gregorio–Hosgri fault zone of  $156 \pm 4$  km based on stratigraphic correlations. Geologic similarities between the Miocene Santa Margarita and Santa Cruz formations located in the central Santa Cruz Mountains and on the Point Reyes Peninsula indicate 70–90 km of offset during the past 6–8 Ma (Clark et al., 1984). The total ~150 km of offset is further demonstrated by correlations between Cretaceous granitoid basement rock and overlying Paleogene deep-marine deposits with distinctive conglomerate beds located at Point Reyes (west side of fault) and near Monterey (east side of fault; Clark et al., 1984). The difference between estimated long-term and current slip rates on the SGF suggests that the slip rate has slowed over time, from a maximum of ~25 mm/yr at the time of fault initiation to ~8 mm/yr during the late Quaternary (Dickinson et al., 2005). Based on the difference in slip between the NCSAF and the PSAF, the Working Group on California Earthquake Probabilities (WGCEP, 2003) estimated a late Quaternary slip rate of 7 mm/yr for the San Gregorio fault.

The main eastern strand of the SGF (SGF-E) north of Half Moon Bay (Fig. 1) bends from a strike of N35°W to a more northerly orientation of N20°W and the structural zone between the eastern and western strands widens to at least 8 km south of Bolinas (Figs. 1, 2) (Bruns et al., 2002; Ryan et al., 2008). The San Gregorio structural zone (SGSZ) was identified by Bruns et al. (2002) on the basis of multiple folds and reverse faults observed in high-resolution multichannel seismic reflection lines. Bruns et al., (2002) suggested that these reverse faults might merge at depth into a single fault. The SGF-E appears to connect with the western boundary fault at Bolinas; to the west the SGF-W bends to a more northwesterly strike and appears to merge with the Point Reyes fault (Fig. 1; Ryan et al., 2008).

### *2.2.3 Point Reyes Fault (PRF)*

The PRF is an offshore component of the SAFS that is probably responsible for the majority of the uplift of the western Point Reyes Peninsula (McCulloch, 1989; Ryan et al., 2008). The presence of a reverse fault offshore of Point Reyes was first suggested by gravity anomalies just south of the Point Reyes headland (Chapman and Bishop, 1968). Galloway (1977) suggested that the nearly east-west orientation of the south-facing cliff of the Point Reyes headland is an eroded fault-line scarp, with the down-thrown block to the south. The age of offset on the offshore PRF was first estimated by Hoskins and

Griffiths (1971), who used geophysical data to suggest that the fault and an associated anticline are of Early Pleistocene age. McCulloch (1989) reported uncertainty over the age of the PRF but suggested that it might be a low-angle thrust at depth, similar to late Neogene thrust faults located along the San Joaquin basin margin adjacent to the SAF in central California. McCulloch (1989) also suggested that the PRF could be a reactivated normal or oblique-slip fault that formed during Miocene transtension and later developed a sinuosity similar to adjacent faults and folds in the Bodega Basin during late Neogene transpression and fault inversion.

### **3.0 Methods**

To better understand offshore fault motions and interactions, I used mini-sparker seismic reflection data acquired by the USGS in 2009 (Fig. 4) and multibeam bathymetric data, acquired by the California State University at Monterey Bay within the 3-mile (5-km) limit offshore of the Point Reyes Peninsula (Fig. 5), to reinterpret the tectono-stratigraphic framework of the SAFS and to interpret probable Quaternary sequences newly identified in the offshore region north of the Point Reyes Peninsula. Eight offshore Shell exploratory well logs (Fig. 1, Tables 1–8) that provide velocity and lithologic data were used in conjunction with industry multichannel (deep-penetration) seismic (MCS) reflection profiles (Fig. 4) to provide age control, extend analyses beyond the 3-

mile limit of the high-resolution data and to connect offshore observations with onshore observations and well data (Figs. 1, 6, 7). Velocity models were created from well log velocity regressions and were used to correlate exploratory well logs with seismic reflection profiles in two-way travel time (TWTT). Basin-wide velocity models (Figs. 8, 9) were then used to convert stratigraphic horizons interpreted in TWTT to depth and to create isopach maps of five stratigraphic intervals.

### **3.1 *Exploratory Well Logs***

The U.S. Minerals Management Service released Shell Oil Company offshore Bodega Basin exploratory well data (Fig. 1) into the public domain in the 1990s. The well data include core descriptions, paleontology logs, resistivity logs, and velocity logs for eight wells that were drilled within the Bodega Basin between 1963 and 1967 (Tables 1–8). Boundaries between the stratigraphic units were previously identified in the well logs based on lithologic and paleontologic data (Webster and Yenne, 1987; Heck et al., 1990). I used the depth and velocity data to tie stratigraphic units identified in the wells to formation boundary horizons on seismic reflection profiles throughout the offshore region.

Six onshore wells were drilled for the Chevron/Standard Oil Company (Clark and Brabb, 1997) between the Point Reyes headland and Bolinas Bay in the late 1940s and early 1950s (Figs. 1, 6 and 7). I used the onshore well logs to

compare stratigraphic units between their onshore and offshore locations. I modified two stratigraphic cross sections based on correlations among offshore and onshore wells (Figs. 6, 7) to better depict lateral variations in stratigraphic units across the PRF and within the Bodega Basin. The first correlation diagram (Fig. 6) combines all eight offshore wells with onshore wells Tevis-1 and Lockhart R.C.A. 3-1 located north of Bolinas. The second correlation diagram (Fig. 7) combines offshore wells 39-1 and 41-1 with onshore wells Mendoza No. 2 and Molseed No. 1 located northeast of the Point Reyes headland—it depicts stratigraphic variations across the PRF and onto the Point Reyes headland.

### **3.2 Seismic Reflection Profiles**

Multichannel seismic (MCS) data were collected by WesternGeco between 1976 and 1982, and extend from the near offshore to the edge of the continental shelf (Figs. 4, 10–24). These data have been released into the public domain, and are available with metadata on the USGS National Archive of Marine Seismic Surveys website (<http://walrus.wr.usgs.gov/NAMSS/>). The MCS data have a penetration of up to 4 km and a vertical resolution of 20–30 m. Older seismic reflection profile data from the 1960s were previously used in conjunction with Shell exploratory well data to describe geologic units in the offshore portion of the Bodega Basin in the context of petroleum exploration (Hoskins and Griffiths, 1971). McCulloch (1989) used WesternGeco data combined with

USGS seismic surveys to provide a generalized tectonic interpretation for the central California offshore region. The recently released MCS data provide a denser and more extensive network of well-tied seismic reflection profiles than those used in previous studies.

The USGS collected high-resolution mini-sparker seismic data offshore of the Point Reyes Peninsula in the summer of 2009 (Figs. 4, 25–41). The mini-sparker data were collected within the three-mile (5-km) limit of California state waters, with the addition of two lines that extend farther offshore and tie to Shell exploratory wells (Fig. 4). The mini-sparker seismic technique has a penetration of approximately 500 m and a vertical resolution of two–five m. The data were collected using a SIG ELC50 mini-sparker system that produces 500 J of high voltage electrical discharge that was received by a towed SIG ELC820 12 m single-channel hydrophone streamer containing 12 elements. The mini-sparker system was fired every 0.5 seconds at 4 to 4.5 knots (2.1 to 2.3 m/s), which gave a data trace spacing of 1 to 3 m.

During my investigation, I integrated high-resolution mini-sparker seismic data with the older, deep-penetration MCS seismic data. By integrating the data sets, interpretations made on one type of seismic reflection profile could be tied and extended to another data type through the use of 2D seismic interpretation software. The high-resolution seismic data were used to interpret recent

deformation and Quaternary-aged sedimentary sequences preserved north of the Point Reyes headland. The deeper-penetration, lower-resolution MCS seismic reflection profiles were used to interpret deeper structures and the tops of the Neogene units.

### **3.3 *Multibeam Bathymetric Data***

Multibeam bathymetric data were collected between Point Arena and Año Nuevo between 2006 and 2007 by the Seafloor Mapping Lab of California State University in Monterey as part of the North Central California Coast State Waters Mapping Project (<http://seafloor.csumb.edu/projects.html>). The multibeam data extend 3 miles (5 km) from shore and show surficial sediments and bedrock outcrops (Fig. 5). This dataset was used to aid interpretations of lithologic units on seismic-reflection profiles by providing further constraints on the characteristics of the units where they are exposed at the seafloor.

### **3.4 *Seismic Reflection Correlation and Velocity Models***

Depths to the tops of geologic units (Tables 1–8) are based on Shell exploratory well logs and offshore petroleum resource reports that integrate original core descriptions and velocity data (Webster and Yenne, 1987; Heck et al., 1990). Where there are discrepancies in the depth interpretations, preference was given to the Heck et al. (1990) interpretation, because the report

took into account original well data, previous interpretations, and the regional seismic reflection interpretations of McCulloch (1989). The Heck et al. (1990) report did not take into account paleontologic data that mostly agreed with Webster and Yenne's (1987) depth-to-formation estimates for the Monterey Formation, with the exception of offshore well 51-2, where the Shell Oil paleontologic data estimated the depth of the Monterey Formation to be approximately 120 m above previous interpretations. In terms of larger-scale stratigraphic interpretations, this discrepancy appears to be minor because resolution of the MCS data is only on the order of 20–30 m, so the difference between interpretations only corresponds to a three–four seismic reflector error and is for only one of the eight wells within the basin.

To correlate well depths to stratigraphic horizons on seismic reflection profiles, a method was required to estimate the TWTT to the top of geologic units within the Bodega Basin. TWTT is the time it takes for an acoustic signal to travel from a signal source near the surface to a layer with an acoustic impedance contrast at depth and then back to a surface receiver. Acoustic-wave velocity regressions were created for each offshore well (Appendix C) to estimate TWTTs to the top of the Purisima Formation, Santa Cruz Formation and Monterey Formation (Tables 1–8). The methods used for creating the TWTT equations and individual well regressions are described in Appendix A.

Once the stratigraphic horizons were interpreted in TWTT and extended across the network of Bodega Basin profiles (Fig. 4), the interpretations were converted to depth. This conversion was done by using velocity (as a function of TWTT) models that were developed for above (Fig. 8) and below (Fig. 9) the Monterey Formation for the entire basin (Appendix A) and enabled me to create isopach maps of five key stratigraphic intervals. Velocity log data were available for a few MCS profiles and were used to convert the profiles to depth, allowing a more accurate measurement of dips and structural relief on horizon surfaces. Uncertainty involved in the creation of the regression models is described in Appendix B.

### **3.5 *Isopach Maps***

To analyze thickness variations across the offshore Bodega Basin, I produced isopach maps of five stratigraphic intervals (Figs. 42–46). The isopachs were created by exporting UTM coordinates and thickness values (depth converted to meters) into ArcView GIS software. The data were then gridded, using inverse distance weighting of thickness values, so that data could be interpolated between seismic reflection track lines (Fig. 4). The isopach maps depict varying thicknesses of specific stratigraphic intervals and are discussed in the Results section.

## 4.0 Results

Lateral stratigraphic variations were analyzed within five Neogene sedimentary packages that were identified in offshore exploratory wells and on multichannel seismic reflection profiles (Mio–Pliocene) and on high-resolution seismic reflection profiles above the regional Plio–Pleistocene Unconformity (PPU) surface (Pleistocene–Holocene). The Holocene package was identified by the acoustically transparent layer (ATL) that is visible at the top of most high-resolution seismic reflection profiles (Figs. 25–41). The resulting correlations were used to create isopach maps for Upper Miocene, Pliocene, Pleistocene and Holocene sedimentary sequences. A Quaternary isopach map was also created to incorporate Pleistocene and Holocene sections overlying the PPU. A Middle-Miocene isopach map was not created because the Monterey Formation was deposited in a transtensional setting (Atwater, 1989) of discontinuous offshore basins prior to the establishment of the more-continuous offshore Bodega Basin (McCulloch, 1989) and it is beyond the scope of this study, which is focused on the younger Plio–Pleistocene deformation. The five post-Monterey sedimentary packages are described in time-specific sections below.

The revised offshore SAFS fault and fold map (Fig. 2) depicts structures that deform Miocene and younger units on MCS and mini-sparker seismic reflection profiles (Figs. 4, 10–41). South of the Point Reyes Peninsula, I have

reinterpreted the SAFS structures, including the SGF-W, PRF, PRF-W anticline, and PRF-E monocline that are located west of the junction of the SGF-E and SAF near Bolinas (Fig. 2). The southern end of the study area also includes the San Gregorio structural zone described by Bruns et al. (2002). The zone is a structurally complex region located between the western and eastern strands of the SGF that comprises folds and thrust faults (Bruns et al., 2002). South of the Golden Gate, the San Gregorio structural zone is buried beneath relatively undeformed strata, but near Bolinas, recent uplift has exhumed the buried structure at the sea floor and is an active, ongoing process (Bruns et al., 2002). This deformation is evident in the south end of the study area, where folds are visible on the eastern ends of seismic reflection lines located southwest of Bolinas (MCS profiles WSF-076 and WSF-080—Figs. 4, 10, 11; high-resolution profiles PR-14 and PR-27—Figs. 4, 25, 26).

Adjacent to the Point Reyes headland (Fig. 2), the PRF is mapped where Salinian granitoid rocks have been uplifted on the hanging-wall of the fault and Tertiary marine sedimentary units have been vertically offset at least 2 km. North of the Point Reyes Peninsula, the PRF is buried beneath probable Pleistocene deposits and it is mapped where the fault is observed to offset seismic reflectors at depth. The map also depicts the PRF-W anticline, PRF-E monocline and post-Purisima folds. These structures may be the result of faulting at depth that is not observed within the penetration or resolution of the seismic reflection profiles. At

the northern end of the study area, shortened and vertically offset reflectors are observed within Pleistocene units and are mapped as Pleistocene fault and fold structures (Fig. 2). All other contraction structures are mapped as post-Purisima anticlines and synclines, based on the youngest unit they are observed to deform (Fig. 2).

#### **4.1 Middle Miocene Section**

The Monterey Formation records widespread Middle Miocene deposition across and beyond the Bodega Basin (Clark et al., 1984; McCulloch, 1989). Its thickness varies considerably, probably a result of both varying depositional depths and post-depositional deformation. The formation was encountered in only one of the three northern onshore wells (Molseed No. 1, Fig. 1), which was drilled approximately 7 km northeast of the Point Reyes headland, on the western limb of the Point Reyes syncline. The Molseed No. 1 well log (Fig. 7) shows approximately 30 m of Monterey Formation at 466 m below ground surface overlying granite, whereas Mendoza wells No. 1 and No. 2, drilled ~3 km northeast of the Point Reyes headland, do not show any Monterey Formation sediments. The onshore wells drilled on the eastern limb of the Point Reyes syncline northwest of Bolinas encountered much thicker Middle Miocene sections (Fig. 6). The Tevis-1 well (Figs. 1, 6), drilled ~10 km northwest of Bolinas on Double Point, encountered 1,000 m of Monterey Formation starting at 450 m

below ground surface. The Lockhart R.C.A. 3-1 well, drilled ~2.5 km northwest of Bolinas, encountered 1500 m of Monterey Formation at 1050 m below ground surface.

The Shell Oil Company offshore wells show less variation in the thickness of the Middle Miocene section while also providing evidence of significant post-Middle Miocene vertical displacement across the PRF. West of the Point Reyes Peninsula, offshore wells encountered 200–300 m of Monterey Formation in wells 39-1, 41-1 and 51-2, and 30–100 m in the more northerly wells 53-1, 55-1, 55-2 and 58-1 (Tables 2–8; Fig. 6). Offshore wells and MCS tie-lines near the 58-1 well provided sufficient detail to identify the upper contact of the Monterey Formation on the PR-95 high-resolution profile (Fig. 37). This contact interpretation is supported by the irregular, jagged topography along the PPU surface that results from resistant beds within the Monterey Formation. Offshore well 27-1 encountered 173 m of Monterey Formation at a depth of 226 m (hanging wall of the PRF), where it is truncated by the PPU surface and underlying 119 m of probable Quaternary-aged deposits (Table 1; Fig. 6). The change in depth of the Monterey Formation indicates at least 2 km of vertical displacement across the PRF.

The Middle Miocene section exhibits both Miocene– and Plio–Pleistocene-aged deformation. West of the PRF, the Monterey Formation appears to be

disconformable with post-Middle Miocene units in the northwest portion of the Bodega Basin (e.g., Figs. 18, 21). In the southern part of the basin, however, the Monterey Formation is separated from overlying units by a pronounced angular unconformity; seismic reflection profile WSF-001, that extends southeast from the Point Reyes headland (Figs. 4, 15), shows the angular unconformity and a probable detachment surface between the tilted Monterey Formation and underlying granitoid basement rock (below shot point 450). This structure may be a remnant of a Miocene-aged east-west structural grain, which may have created a cross-basin high (Hoskins and Griffiths, 1971). The irregular upper contact and distribution of the Monterey Formation (Figs. 11–14) suggests that Middle Miocene deposition may have been controlled, in part, by east–west-oriented normal faults. Miocene extension occurred after the passing of the unstable Mendocino Triple Junction (Atwater, 1989) and may have created normal-fault-bounded sub-basins. Normal faults are visible on the southwestern end of MCS profiles (Figs. 13, 14), just east of the Farallon High, and show a growth fault geometry where Middle Miocene units appear to thicken into the structure. Miocene normal faults, particularly well expressed on profiles shown in Figs. 11–14, appear to have been subsequently reactivated and inverted during Plio–Pleistocene transpression. Normal fault inversion has been described in many locations, including the coastal region throughout California (e.g.; Gutierrez-Alonso and Gross, 1997).

## **4.2 Upper Miocene Section**

The Upper Miocene stratigraphic sequence in the Bodega Basin comprises the Santa Margarita Sandstone and the Santa Cruz Mudstone; it overlies the Monterey Formation and is overlain by the Pliocene Purisima Formation. As described in the previous section, in the southern part of the basin the lower boundary is an angular unconformity, but in the northern part of the basin no angular discordances were observed. The upper boundary of the Santa Cruz Mudstone appears to be conformable throughout the study area, although unconformities have been observed in other localities (Powell et al., 2007). Based on interpretations of surface exposures along the western coast of the Point Reyes Peninsula, the basal Santa Margarita Sandstone was deposited in shallow water at shelf depths and the Santa Cruz Mudstone was deposited in deeper water at slope depths. These exposures show a gradational boundary between the Santa Margarita Sandstone and the Santa Cruz Mudstone, indicating a gradually-subsiding basin.

Onshore Chevron Oil Company exploratory wells encountered thick Upper Miocene sections near Bolinas, but only the thin basal Santa Margarita Sandstone in wells near the Point Reyes headland. Wells drilled near the headland (Mendoza No. 2 and Molseed No.1, Fig. 7) encountered 10–50 m of Santa Margarita Sandstone overlying either granite (Mendoza No. 2) or a thin

section of Monterey Formation (Molseed No. 1). On the southern Point Reyes Peninsula near Bolinas, wells (Robson No. 1 and Lockhart R.C.A. 3-1, Figs. 1, 6) encountered approximately 16 m of Santa Margarita Sandstone beneath thick sections of Santa Cruz Mudstone. The Santa Cruz Mudstone was encountered at ground surface within the wells drilled near Bolinas and the unit decreases in thickness to the north due to erosion. On the southernmost Point Reyes Peninsula near Bolinas, the Lockhart R.C.A. 3-1 well encountered 1030 m of Santa Cruz Mudstone (Fig. 6). Northwest of Bolinas on Double Point, Tevis-1 (Figs. 1, 6) encountered only approximately 450 m of Santa Cruz Mudstone (Fig. 6), and farther north, outcrop exposures pinch out on the eastern limb of the Point Reyes syncline at about the latitude of the Point Reyes headland (western limb) where no Santa Cruz Mudstone is found (Fig. 3). North-southeast-oriented MCS reflection profiles show that Santa Cruz Mudstone is preserved to the north and south of the headland. Parallel reflectors extend upward toward the headland, rather than onlapping what would have been a pre-existing high, showing that the unit was deposited and then eroded following uplift of the headland.

All eight offshore exploratory wells encountered the Upper Miocene section. The southern offshore wells (39-1, 41-1) encountered a thinner section at shallower depths due to uplift and erosion, while the northern wells (51-2, 53-1, 55-1, 55-2 and 58-1) encountered thicker sections preserved at greater

depths. The basal Santa Margarita Sandstone was encountered in only one offshore well (53-1; Fig. 1; Table 5), but the unit may have been overlooked in other wells because it is so thin. Adjacent to the Point Reyes headland, wells 39-1 and 41-1 encountered 530 m and 310 m of Santa Cruz Mudstone at depths of 302 m and 84 m below sea level (Figs. 1, 6; Tables 2, 3), respectively. The more northerly offshore wells drilled to the west of the PRF, encountered the top of the Santa Cruz Mudstone at greater depths, between 576 m (well 51-2, Table 4) and 1,012 m (well 58-1, Table 8) below sea level. Thicknesses encountered in the northern offshore wells were relatively consistent, with approximately 1,000 m reported in wells 51-2, 53-1, 55-1, 55-2 and 58-1 (Tables 4–8). No Santa Cruz Mudstone was encountered in well 27-1 (Table 1), which was drilled into the anticline above the PRF.

The Upper Miocene isopach map (Fig. 42) of stratigraphic thicknesses between the Pliocene Purisima Formation and the top of the Monterey Formation covers part of the offshore Bodega Basin west of the PRF between the latitudes of Bolinas and Bodega Head, where offshore well control was sufficient to interpret boundaries on the seismic reflection profiles. The Upper Miocene isopachs vary from 1,700 m at the northern end of the map (west of well 27-1), to 230 m at the southern end of the map and on the PRF-W anticline southwest of the Point Reyes headland (Fig. 42). The thickest isopachs northwest of the Point Reyes Peninsula represent a region where Upper Miocene units were unaffected

by uplift associated with the PRF. The thinnest isopachs are present in the areas of Plio–Pleistocene uplift southwest of the headland and at the southern end of the study area, where the Upper Miocene and younger units onlap the eastern side of the Farallon High (Figs. 11–14).

### **4.3 Pliocene Section**

The Mio–Pliocene Purisima Formation is bounded by the Pliocene–Pleistocene unconformity (PPU; above) and the Upper Miocene Santa Cruz Mudstone (below). Onshore wells Mendoza No. 2 and Molseed No. 1 encountered 370 m and 410 m of Purisima Formation on the west limb of the Point Reyes syncline (Fig. 7). The onshore wells near Bolinas, however, did not encounter Purisima Formation (Fig. 6) due to erosion on the eastern limb of the syncline (Fig. 3). Thicknesses of the Pliocene section in the offshore wells are uncertain because the top was not always designated and therefore could not be used to correlate with reflection horizons (for example, undesignated Purisima top in well 55-2; Table 7). Seismic reflection tie-line analysis also suggests an erroneous estimate of Purisima Formation thickness in well 39-1, where the logging may have been initiated below the top of the formation. Purisima well control is probably lacking because offshore well-logging activities, in their assessment of hydrocarbon-bearing units, were more focused on the deeper Santa Cruz, Santa Margarita, and Monterey Formations.

The Pliocene isopach map (Fig. 43) includes strata between the PPU and the top of Santa Cruz Mudstone. The isopachs vary from 0 m to approximately 700 m in thickness. The thinnest parts of the isopach map are on the uplifted (hanging wall) side of the PRF, adjacent to the Point Reyes headland in the region of well 41-1, and on the western boundary of the Bodega Basin, where the Purisima Formation onlaps the eastern side of the Farallon High (Figs. 12–14). The thickest isopachs are located approximately 30 km west of Bodega Head (~700-m thick) and 30 km west of Bolinas (~500-m thick), two regions relatively unaffected by uplift on the PRF and PRF-W anticline.

#### **4.4 *Timing and amount of deformation***

Seismic reflection profiles collected across the PRF and PRF-W structures show Plio–Pleistocene uplift and contractional deformation overprinting older Upper Miocene deformation. Given the nature of the plate boundary, which had transitioned to transform type (Atwater, 1989), we can infer that the deformation was occurring within a transpressional regime, but in the seismic reflection profiles only the contractional component is clearly visible. Evidence for older Miocene contractional deformation is visible on profiles WSF-086 and WSF-098 (Figs. 12, 17), where multiple low-amplitude folds deform Upper Miocene units (Santa Margarita Sandstone and Santa Cruz Mudstone) but do not appear to deform the overlying Pliocene Purisima Formation. Evidence of ongoing

contraction is visible on the southwestern side of the basin, where Upper Miocene Santa Cruz Mudstone is onlapping basement rocks on the Farallon High, and the overlying Purisima Formation is, in turn, onlapping the Santa Cruz Mudstone (Figs. 1, 11–14, 16). In contrast, on the eastern side of the basin, MCS profiles collected between 37.8°N and 38.4°N (Figs. 4, 11–14; 16–17; 19–20) primarily show mostly concordant deformation within the Upper Miocene and overlying Mio-Pliocene units across the PRF and PRF-W structures where younger Plio-Pleistocene deformation appears to have reactivated and inverted Miocene normal faults.

MCS profile WSF-094 (Figs. 4, 16), collected north of the Point Reyes headland, shows thickening of the Pliocene section west of where it onlaps the PRF-W anticline. The thickening and onlap suggest that late Pliocene deposition may have been synchronous with uplift on the PRF-W anticline. A strong seafloor multiple within the MCS data, however, obscures any evidence of onlap on profiles collected to the south and north of WSF-094. The Purisima Formation is absent in wells 27-1 and 41-1 (Figs. 6, 7), where it has been entirely removed on the crests of the anticlines related to uplift on the PRF and PRF-W structures (Fig. 2). This geometry is also visible in high-resolution mini-sparker profiles PR-19 and PR-55 (Figs. 29, 32).

Structural observations of the Plio–Pleistocene deformation, such as structural relief due to folding, dip angles of deformed units and vertical offset across faults, were estimated from depth-converted seismic reflection profiles. Because the Pliocene section has been eroded across the PRF and PRF-W, structural relief measurements on folds at the contact between the Santa Cruz Mudstone and Purisima Formation (considered the Mio–Pliocene boundary) were used to measure the amount of younger Plio–Pleistocene deformation. West of Bolinas, the Mio–Pliocene boundary exhibits approximately 400–500 m of structural relief on the 5–10° inclined forelimb shown on MCS profiles WSF-080 and WSF-086 (Figs. 11, 12). Mini-sparker profiles that extend farther landward show steeper dips (15–20°) on folds adjacent to the coastline (Figs. 25, 26). Structural relief increases northward and just south of the Point Reyes headland MCS reflection profiles WSF-088 and WSF-090 (Figs. 13, 14) show a minimum of 500–600 m of structural relief on the Mio–Pliocene boundary, where horizons dip up to 35° and the Upper Miocene section has been folded and uplifted to the seafloor above the PRF. North of the Point Reyes Peninsula, MCS profiles collected between Bodega Head and the outlet of the Russian River (Figs. 4, 19–20) show a minimum of 700–800 m of structural relief on the Mio–Pliocene boundary, with Pliocene horizons dipping up to 45° on the forelimb of the PRF fold. The highest measureable vertical offset due to faulting across the PRF occurs in the region of offshore well 27-1, where the Monterey Formation was

logged at the PPU surface on the hanging wall of the PRF, indicating a minimum of ~2 km of post Middle Miocene uplift across the PRF (Fig. 6). Adjacent to the Point Reyes headland (Fig. 18), vertical offset of the granitoid basement across the PRF appears to be comparable to the ~2 km minimum estimated on the Monterey Formation to the north. A more accurate estimate of vertical offset across the PRF at the headland is not possible because units are also uplifted on the west side (foot wall) of the PRF due to folding associated with the PRF-W anticline (Fig. 18). The largest structural relief measurement on the PRF-W anticline (~750 m) was estimated on the top of the Monterey Formation directly west of the Point Reyes headland (Fig. 18).

#### **4.5 *Pleistocene Section***

The Pleistocene section consists of deposits preserved between the base of the acoustically transparent layer (ATL) and the PPU. The majority of these deposits are sequences that are found north of Point Reyes and are interpreted to be the result of sea-level fluctuations in a subsiding part of the offshore region (see Section 4.7). An approximate Pleistocene thickness, plus a thin probable Holocene-aged veneer, is reported in the Shell offshore logs (Tables 1–8) as pre-log sediment that ranges in thickness from eight m in well 41-1 to 162 m in well 58-1 (Tables 1–8; Figs. 6 and 7).

The Pleistocene isopach map (Fig. 45) is based on correlations using the mini-sparker data set and depicts Pleistocene thicknesses from 0–200 m. The thinnest areas of the isopach map are along the coastline (present-day wave-cut platform). One exception to this pattern is located south of the Point Reyes headland, where layered reflectors on profile PR-34 (Fig. 27) appear to be preserved above the PPU and below the ATL. It is possible that the preserved deposit is associated with the Younger Dryas cold period (12.5–11.5 ka) when global eustatic sea level was between about -60 and -70 m (Lambeck et al., 2002). The thickest area on the Pleistocene isopach map is located ~7 km offshore of the region between Gualala and Fort Ross, where the PPU appears to have been subsiding during the Quaternary, allowing for the deposition of multiple sea level-controlled sequences (see Section 4.7).

Observations of deformation within the Pleistocene section are limited to the region north of the Point Reyes headland, where eustatic sea level-controlled deposits have been preserved above the subsiding PPU. Any evidence of deformation within Pleistocene deposits south of the headland has been removed above the PPU surface. Non-preservation of Pleistocene deposits to the south suggests a lack of accommodation space due to either uplift or quiescent tectonics during the Quaternary. Deformation within the Pleistocene deposits observed north of the Point Reyes Peninsula is described in Section 4.7.

Just north of the headland, PR-69 (Fig. 33) shows a paleo-channel incised into granite north of the headland. The preserved channels appear to be similar to the buried channels described by McCulloch (1982) south of the Point Reyes Peninsula within Drakes Bay, and by Anima et al. (2002) near Santa Cruz. The paleo-channel was probably filled by sediment following the Holocene marine transgression.

#### **4.6 *Holocene Section***

The Holocene isopach map depicts the thickness of sediment deposited above the base of the interpreted ATL (Fig. 46). The region with the thickest Holocene-aged deposits (~30 m) is located at the drainage outlet of the Russian River into the Pacific Ocean, approximately 15 km north of Bodega Head (Figs. 1, 46). The thinnest accumulations of Holocene deposits are in the regions southwest of Bolinas, just north of the Point Reyes headland and adjacent to Bodega Head where granite is exposed at the sea floor (Figs. 1, 5, 46). The Holocene deposits in these regions are thin due to either active uplift or lack of accommodation space adjacent to relict topography. Thickness variations in the Holocene map appear to reflect a depositional pattern defined by regions of source material from rivers and topographically high regions of the Holocene coastline. Mini-sparker lines, collected directly southwest of the headland (PR-43, Fig. 30; PR-45, Fig. 31) image two folds truncated by the PPU and overlain

by an acoustically-transparent Holocene sediment mound. The more northerly line, PR-45 (Fig. 31), images mounded Holocene-aged deposits above the truncated fold interpreted to be a fold between the PRF and the PRF-W anticline. The mounding appears in the multi-beam data set as well (Fig. 5), and is most likely a depositional (not structural) feature formed by currents interacting with the uplifted and exposed headland.

#### **4.7 *Quaternary sequences north of Point Reyes***

High-resolution mini-sparker seismic reflection profiles collected within the 3-mile offshore limit west of the Point Reyes Peninsula (Fig. 4) show a distinct angular unconformity (the PPU) separating underlying tilted Tertiary-aged units from overlying probable Quaternary-aged sequences and Holocene-aged acoustically-transparent sediments. The PPU surface has been described in previous marine geology studies (e.g., Chin et al., 1988; Chin et al., 1997, Grossman et al., 2006) along the central California Coast. Chin et al. (1997) named the regional unconformity surface in the Gulf of the Farallones the “basal unconformity surface”. In the Gulf of the Farallones region, the unconformity is probably a composite erosional surface that is overlain by a thin veneer of acoustically-transparent sediment (Chin et al., 1997) analogous to the acoustically-transparent layer (ATL) that overlies the PPU surface within the near-offshore region between Bolinas and Tomales Point (Figs. 25–34).

Grossman et al. (2006) described a similar surface that they termed the R1 unconformity, which truncates tilted Purisima and Santa Cruz Mudstone units offshore of Santa Cruz, California. The R1 unconformity was described as a Pleistocene–Holocene erosional surface that correlates to other similar-aged erosional surfaces described on the central California shelf (Grossman et al., 2006).

Mini-sparker (Figs. 35–41) and MCS (Fig. 21) profiles collected north of the peninsula, from Tomales Point to Gualala, show a northward-deepening angular unconformity (PPU) and an accompanying thickening of overlying sediments arranged in distinct sequences that have not been previously described in this part of the offshore zone. These sequences, deposited above the PPU, are most likely eustatic sea-level-controlled Quaternary deposits similar to the Pleistocene Merced Formation on the San Francisco Peninsula (Hunter et al., 1984; Clifton et al., 1988) and deposits observed within the offshore Eel River Basin (Burger et al., 2002). Sea-level high stands are represented by acoustically-transparent sections that are similar to the acoustically-transparent section interpreted to represent Holocene high stand deposits throughout my study area and along the central California coast (Chin et al., 1997; Grossman et al., 2006). As sea level begins to fall, coastal environments prograde seaward to create a coarsening-upward sequence (Fig. 47). As observed in the Merced and other Pleistocene units, successive shallowing-upward sequences (regression)

are separated by erosional unconformities formed during the transgressive part of the cycle (Fig. 47). Strong reflectors are created at these transgressive ravinements because of the acoustic contrast between the underlying coarse-grained sediments and the overlying fine-grained shelf sediments (Fig. 47). Because of the numerous sea-level fluctuations during the Pleistocene Epoch (Fig. 48), a large number of sequences can be preserved if a basin is subsiding to create sufficient vertical space.

A few lines of evidence corroborate the Quaternary age for these deposits. The sequences are overlying the Purisima Formation, which is truncated by the PPU surface in well 53-1 (Table 5). Additionally, the offshore well logs show these deposits as pre-log Quaternary sediment overlying Pliocene and older units (Section 4.5). To the west of the PRF, multiple MCS profiles (Figs. 19–21) show that the angular unconformity changes to a disconformity, and continues west to the Farallon Ridge and Cordell Bank, and to the northwest across the Bodega Basin. From south to north, the sequences overlying the PPU are first imaged on seismic reflection profile PR-65 (Figs. 4 and 35) and to the north they are imaged on all of the mini-sparker profiles collected beyond the 3-mile limit (Figs. 36–41), where the PPU surface has apparently subsided during the Quaternary.

My description and interpretation of the probable Quaternary-aged sequences does not benefit from age control data, meaning that individual sequences cannot be accurately tied to a specific cycle on the Marine Isotope Stage (MIS) curve that is a proxy for global sea level (Fig. 48). A lack of tie lines prevented the correlation of individual sequences in the mini-sparker dataset, as only one tie line that images the Quaternary sequences was collected. The tie line, PR-147/147B/147C, was collected east of the region with the thickest sequences. Because ages are not available to tie sequences to specific MISs, it was necessary to correlate sequences by appearance and stratigraphic position. Using this method, only the youngest six sequences were correlated with any degree of confidence.

An isopach map of all strata preserved above the PPU was created by subtracting the depth of the PPU from the depth of the seafloor in both the MCS and mini-sparker datasets (Fig. 44). Isopachs above the PPU vary from ~250 m to less than the limit of mini-sparker seismic profile resolution (~4 m). In general, the map shows less than 20 m thickness in the region south of the Point Reyes headland, along much of the coastline, and in areas where granite is interpreted to be near the seafloor, as far north as Bodega Head. These areas with the thinnest strata mostly represent areas with only Holocene-aged deposition. To the north, the sediments thicken, indicating depositional space that has been created by Quaternary subsidence. The main depocenter, with a thickness in

excess of 250 m, is at the northern end of the study area, ~7 km offshore of the area between Fort Ross and Gualala (Fig. 44). The region of subsidence is bounded on the east by the uplifting coastline and on the western edge of the continental shelf (Fig. 44).

The number and cumulative thickness of preserved Quaternary sequences overlying the PPU and above the PRF increases to the north, with one sequence preserved on mini-sparker profile PR-65 (Fig. 35), two on PR-63A/63 (Fig. 36), three on PR-95 (Fig. 37), and five on PR-109/109A (Fig. 38). The top three sequences (1–3) appear to be continuous and of consistent thickness north of mini-sparker profile PR-95 (Figs. 4, 37), where the base of sequence 3 (Figs. 37–41) is preserved at a consistent depth of approximately 150 m below sea level at the west end of the profiles. North of profile PR-109/109A, as many as six sequences are shown (Figs. 39–41), with an unclear number of additional sequences obscured below a strong multiple in the mini-sparker data set. This section of additional sequences (labeled 4 and greater) is responsible for the pattern of thick isopachs on the Pleistocene and Quaternary isopach maps north of Bodega Head (Figs. 45, 44). Offshore of Stewart's Point and north of PR-143 (Figs. 4, 41, 44), the sequences appear to decrease in number and total thickness.

North of Bodega Head, mini-sparker seismic reflection profiles image shortening within the sequences beginning in the region west of where the offshore NCSAF continues onshore to the east (PR-122, Fig. 39). The amount of shortening appears to increase to the north (PR-133 and PR-143, Figs. 40 and 41) where the Gualala fault (bounding the Gualala Block to the west) diverges from the NCSAF. The folding also appears to become more asymmetrical to the north (Fig. 41). The deformed Pleistocene deposits exhibit forelimb dips of between  $10^{\circ}$  (PR-122, PR-133; Figs. 39, 40) and  $20^{\circ}$  (PR-143; Fig. 41). The shortening within the sequences appears to represent transpression west of the Gualala Block and may be controlled by structures that interact with the Gualala fault at depth (Fig. 2).

Onlap and truncation relationships visible within the shortened Quaternary sequences give a specific time-horizon marker for the initiation of deformation north of Bodega Head. Sequence 5 appears to be truncated and sequence 4 appears to be onlapping the forelimb of a fold deforming the Pleistocene sediments on mini-sparker profile PR-143 (below shot point 2500, Fig. 41), suggesting that shortening probably initiated prior to the deposition of sequence 4. Sequence 4 also appears to be onlapping the forelimb of the eastern fold on PR-133 (below shot point 3000, Fig. 40). The lack of age control for individual Quaternary sequences prohibits precise MIS correlation, but assuming the

preservation of ~100 k.y.-long glacial cycles, truncation and onlapping relationships suggest that the deformation initiated 400–500 ka.

## **5.0 Discussion**

As the first study to focus on Quaternary deformation within the offshore SAFS north of the Golden Gate Platform, this thesis provides a foundation for future tectono-stratigraphic investigations of the region west of the Point Reyes Peninsula. By integrating well log data with seismic reflection profile data, I was able to describe the complex late Neogene tectono-stratigraphic relations, create a revised offshore SAFS fault-and-fold map (Fig. 2) and interpret the nature and timing of deformation associated with the offshore SAFS. In the following sections, I discuss my results in terms of their implications for movement on the Point Reyes fault since the Late Miocene at three locations: north of the Point Reyes headland, at the headland, and south of the headland. I discuss the possible controls that have caused Quaternary sequences to form and be preserved north of the Point Reyes Peninsula. Finally, I present a diagram that summarizes the evidence for late Quaternary deformation and ideas about future work that could help clarify the observations and interpretations presented herein.

### **5.1 *Implications for movement on the Point Reyes fault***

Inherited structures have influenced the pattern of uplift on the PRF, as normal faults that formed during Miocene extension were reactivated and inverted during post-Middle Miocene uplift. The basement structures and associated fault-bounded basins formed during Miocene extension at least partially controlled the location and pattern of Pliocene and Quaternary deformation, as observed in other parts of coastal California (Lettis et al., 2004). For example, deposition in normal-fault-controlled grabens could explain some thickness variations in the Monterey Formation across the PRF (Fig. 6). The younger Santa Cruz Mudstone and Purisima Formation appear to have filled in pre-existing undulating bathymetry and thickness variations are mostly due to onlapping relations at the edges of the Bodega Basin and subsequent erosion during the major Plio–Pleistocene deformation event. Some of the thickness variations could also be due to right-lateral offset on the Point Reyes fault during the Mio–Pliocene, when the fault may have accommodated slip from the SGF-W. South of the headland, Salinian granite on the hanging-wall of the PRF is overlain by less than 500 m of Mio–Pliocene units and a reverse fault of opposite vergence to the PRF may be part of a positive flower-structure (Figs. 14, 15) and a remnant from a time when more strike-slip motion was accommodated by offshore faults.

Movement on the PRF is most evident along the west coast of the Point Reyes Peninsula, where the elevation of the headland appears to be due to movement on the PRF during a major Plio–Pleistocene deformational event. The uplifted granite on the hanging-wall of the PRF is above sea level, forming the headland, and all younger units have been removed. Mio–Pliocene deep to shallow marine stratigraphic units that are truncated at the seafloor adjacent to the headland show larger amounts of shortening and higher dips, compared to the folding observed south of the headland (Figs. 14, 16). Similarly, uplift of Pliocene-aged strata above the PRF-W anticline is greatest in the region just southwest of the headland (Figs. 2, 43). Pliocene strata are thinnest adjacent to the headland, where the strata were folded and then truncated by erosion (PPU surface; Fig. 43). Well 41-1, drilled into the crest of the PRF-W anticline, did not encounter the Purisima Formation, indicating it had been entirely eroded at the drill site (Fig. 7; Table 3). In the vicinity of the headland, the shallow granite basement may have acted as a resilient block, or buttress, during Plio–Pleistocene uplift. The similar sinuosity of the PRF and PRF-W anticline in the region of the headland also supports syn-deformation of the structures due to post-fault buttressing (McCulloch, 1982).

Deformation of Mio–Pliocene units was clearly observed in seismic profiles, but the paucity of Quaternary deposits does not provide strong constraints on the duration of the Plio–Pleistocene deformational event. Uplifted

coastal terraces indicate Late Pleistocene uplift on the southeastern part of the Point Reyes Peninsula (Grove et al., 2010), but the timing of uplift at the Point Reyes headland and within the Point Reyes syncline is still poorly constrained. A marine terrace deposit overlying granite on the Point Reyes headland did not provide consistent age estimates and the deposit could be much older than the 20–100 ka ages obtained through luminescence dating (Grove et al., 2010). Other deposits that unconformably overlie the onland Purisima Formation just west of Drakes Estero are part of a broad terraced surface in the center of the Point Reyes syncline that has been incised by stream valleys (Galloway, 1977), but has not yet been dated. Axelrod (1983) reinterpreted Galloway's (1977) description of pine cones (*Pinus radiata*) and Gowan Cypress (*Cupressus goveniana*) found within a siltstone deposit unconformably overlying the Purisima Formation near Drakes Bay. A tentative age of 500 ka was given to the deposit based on a presumed rate in the evolution of cone size.

Adjacent to the headland in the offshore region, the composite PPU surface truncates folded Mio–Pliocene units and the surface appears to be undeformed in the high-resolution mini-sparker profiles across the PRF and the PRF-W anticline (Figs. 28–32). Wave erosion on the composite ravinement surface (PPU) has removed all evidence of Quaternary uplift, except on the Point Reyes headland, where more resistant granite uplifted on the hanging-wall of the PRF protected the headland deposits from wave attack. Seismic reflection

profile observations adjacent to the headland show no evidence of uplift away from the exposed granite and suggest that the uplifted marine terrace deposits on the headland are probably older than the 5e MIS high-stand (125 ka). The elevation of the preserved deposits (~100 m above sea level) on the headland would require an uplift rate of ~1 mm/yr that is not observed above the PRF on high-resolution seismic reflection profiles adjacent to the headland since the last marine transgression. The deposits could be as old as 400–500 ka (MIS 11 or 13; Fig. 48), or even older.

A 400 ka age for the headland deposits would coincide with the incipient rise of the present-day Coastal Ranges, following Plio–Pleistocene folding, uplift and erosion (Page et al., 1998). The post-400 ka tectonic pulse may have occurred as a response to horizontal contraction and thickening in the middle crust (Page et al., 1998). Hearty et al. (1999) suggest that the MIS 11 (~400 ka) eustatic sea-level high stand may have been at high as 20+ meters above present-day sea level. If the marine deposit overlying granite on the headland was deposited at 20+ meters above sea-level approximately 400 ka, then an uplift rate of approximately 0.2 mm/yr would be sufficient to uplift the deposit to its present elevation of 106 m above sea-level. We can only speculate that this uplift rate may be the result of a coherent uplift of the Salinian terrane, similar to uplift observed throughout the Coast Ranges since 400 ka (Page et al., 1998). In any case, it appears that the majority of uplift in the headlands region occurred

prior to the Middle Pleistocene and that any uplift since then has been occurring at a slower rate than that observed in the southeast part of the peninsula, near Bolinas.

South of the headland, deformed late Neogene units have been truncated by the PPU at the seafloor, and are overlain by a thin (<10 m) Holocene veneer of sediment. The Holocene veneer represents the only preserved Quaternary sediments above the PPU surface, suggesting that the region has uplifted or remained stable during the late Quaternary. High-resolution reflection profiles collected south of the headland show undeformed Holocene deposits and no evidence of uplift associated with the PRF since the Holocene marine transgression. West of the southern Point Reyes Peninsula near Double Point, multibeam data (Fig. 5) show deformed Neogene units exposed at the seafloor. The multibeam data and mini-sparker profiles collected in this region (Figs. 5, 25, 26), show post-Purisima folds to be truncated by deformation probably related to the active uplift of marine terraces along structures associated with the SGF-E/SAF junction. This pattern of deformation may be because of restraining geometries that have been created as offshore faults have become less active and more of the dextral slip has been transferred eastward to the SGF-E and SAF. Uplift rates as high as 1 mm/yr, measured from uplifted coastal terraces near Bolinas, appear to have accelerated at the south end of the Point Reyes Peninsula during the late Quaternary, as reverse faults south of Bolinas, and

associated with the SGF-E/SAF junction, have become more active and migrated northward (Bruns et al, 2002).

North of the Point Reyes headland, the PRF-W anticline diminishes in amplitude and Mio–Pliocene uplift and shortening east of the PRF appears to be distributed across multiple NW–SE-trending folds (Fig. 2). Plio–Pleistocene deformation to the north must have occurred prior to at least Middle Pleistocene time because the PPU is overlain by multiple relatively undeformed eustatic-sea-level-controlled Quaternary sequences. Sequences observed to be onlapping the western edge of the folded PPU surface above the PRF on mini-sparker profiles PR-65, PR-63A/63 and PR-95 (Figs. 35–37) were probably deposited sometime after the initial erosion of the PPU surface and may be synchronous with the most recent uplift on the PRF north of the headland. Age control on these deposits could help improve timing constraints on uplift associated with the PRF north of the peninsula.

The majority of the deformation visible on offshore seismic reflection profiles is clearly post-Purisima in age and is probably related to a change in relative plate motion between the Pacific and North American plates at 8–6.6 Ma (Atwater and Stock, 1998; Argus and Gordon, 2001). Thickening and onlapping of the Purisima Formation just west of the PRF-W anticline (WSF-094, Fig. 16) may record incipient deformation related to this change in relative plate motion.

How long deformation has continued is unclear because younger sediments have been removed due to truncation on the composite PPU surface south of the headland and there is a lack of age control for probable eustatic sea-level controlled sequences north of the peninsula.

The new time constraint interpretations for movement on the PRF suggest that the hazard potential of the Point Reyes fault in current fault and tsunami hazard models should be re-evaluated, as the majority of the motion occurred prior to the Middle Pleistocene and any motion since then has been at a very slow rate. The current seismic hazard potential assigned to the PRF by the 2008 Working Group on California Earthquake Probabilities (WGCEP, 2008) includes a late Quaternary slip rate of 0.3 mm/yr and a maximum earthquake size of  $M_w$  6.7–6.9 for the fault. My interpretations suggest that the hazard potential of the PRF may be less, especially because relatively undisturbed Quaternary sequences bury PRF-related deformation north of the Point Reyes Peninsula.

## **5.2 Controls on the formation of Quaternary sequences**

North of the Point Reyes Peninsula, subsidence has provided space for up to 260 m of sea-level-controlled marine sequences to be preserved above the regional PPU surface (Fig. 44). The sequences increase in number and total thickness north of mini-sparker line PR-66 (Fig. 4). The Quaternary isopach map (Fig. 44) shows that the thickest section of Quaternary deposits lies west of the

Pleistocene deformation associated with the Gualala fault (Fig. 2), approximately 25 km northwest of the thickest portion of the Holocene isopach map centered at the outlet of the Russian River (Figs. 44 and 46). Based on the estimated slip rates of  $24 \pm 3$  mm/yr on the NCSAF (Niemi and Hall, 1992), the region with the thickest Quaternary deposits would have been located at the latitude of Russian River at  $\sim 1$  Ma and may represent the region of incipient subsidence that was partly in response to the isostatic loading of the Russian River derived sediments.

The age of the oldest sequence overlying the time transgressive PPU surface is unknown, but was probably deposited  $\sim 1$  Ma. Prior to  $\sim 2$  Ma, the Russian River drained a larger area of the northern California Coast Ranges; after a drainage reversal associated with the passing of the Mendocino Triple Junction, the primary drainage outlet changed from the southern Russian River outlet to the north-flowing Eel River (Lock et al., 2006). The Delgada fan, Russian River gravel, and Wilson Creek Formation were all deposited during the time the Russian River was the primary drainage outlet, from 6–2 Ma (Lock et al., 2006). It appears unlikely, however, that the sea-level-controlled marine sequence deposits are older than 2 Ma if the PPU has been subsiding consistently during the Quaternary and preserving  $\sim 100$  k.y.-long glacial cycles. Assuming each sequence represents  $\sim 100$  k.y. of deposition, the number of glacial cycles suggests an age of  $\sim 1$  Ma for the oldest preserved sequences.

Deformation within the sequences is visible on high-resolution mini-sparker seismic reflection profiles collected offshore of Fort Ross, where Pleistocene deposits are folded west of the offshore Gualala fault, with the amount of shortening increasing to the north (Figs. 2, 39–41). The folding appears to have initiated prior to the deposition of sequence 4 in the region of mini-sparker profile PR-143 (Figs. 4, 41), and has continued during the subsidence and preservation of sequences 1–3. Again assuming that sequences represent ~100 k.y.-long glacial cycles, truncation and onlapping relationships suggest that the deformation in the region of profile PR-143 (Figs. 4, 41) initiated 400–500 ka.

Due to the regional extent of the PPU subsidence and the continuity of the subsiding surface across offshore structures, the most likely mechanism for the observed subsidence is the isostatic loading of Pleistocene deposits and underlying late Neogene units combined with a change of basement (northern terminus of the Salinian terrane). Alternatively, the PPU subsidence and preservation of the Quaternary sequences could be the result of perturbations of heat flow in the lower lithosphere, due to the passing of the Mendocino Triple Junction (Furlong and Schwartz, 2004).

### **5.3 *Late Quaternary deformation model***

The late Quaternary deformation model (Fig. 50) summarizes the mechanisms for observed active uplift of the Point Reyes Peninsula near Bolinas and Quaternary subsidence of the regional PPU surface north of the Point Reyes Peninsula. The lack of evidence for deformation of the PPU surface south of the Point Reyes Peninsula, observations of the present day velocity field (Fig. 49), and the lack of historically observed offshore seismicity suggest that the PRF has probably become less active since the Middle Pleistocene. High-resolution seismic reflection data collected normal to the strike of the PRF (Figs. 25–38) do not show any evidence of deformation of the PPU surface across the PRF or the PRF-W anticline. The PPU, however, is a composite ravinement surface that represents multiple cycles of erosion and only records evidence of deformation since the Holocene transgression. It is possible that uplift rates during the Holocene have not resulted in enough uplift to be visible within the resolution of the seismic reflection data set.

The GPS-derived velocity field (Fig. 49), created from the database assembled by the WGCEP (<http://www.wgcep.org/>), indicates that the GPS velocity vectors south of Tomales Point are all nearly parallel to the strike of the SAF. The orientation of the velocity field vectors suggests that it is unlikely that long-term dextral or oblique slip would continue on a fault striking

counterclockwise to the velocity field south of the headland. Instead, it appears more likely that slip is accommodated on faults with orientations similar to that of the NCSAF (~N35°W). Besides the 1999 Bolinas earthquake, there has been no >3  $M_w$  seismicity in the vicinity of the PRF since 1973 (USGS/NEIC, 1973-Present catalog) besides the 1999 Bolinas earthquake (Fig. 2). The focal mechanism for the Bolinas earthquake indicates reverse motion on a northwest-trending, ~47°-east-dipping fault for one of the fault plane solutions (Baise et al., 2003). This earthquake was most likely associated with the active junction of the SGF-E and the SAF near Bolinas in a region where stress redistribution related to the 1906 earthquake could be expected (WGCEP, 2003). An alternative explanation for the lack of historical seismicity in the region of the SGF-W and PRF structures is that they are dependent structures that have been most recently active due to secondary activity (aftershocks) within the SAFS. Due to the lack of seismicity on the locked section of the NCSAF since 1906, there is no seismic evidence to support this scenario. The lack of PPU deformation, the SAF-parallel strike of the GPS derived velocity field, and lack of historical seismicity do not provide any evidence to support an active PRF.

The late Quaternary deformation summary (Fig. 50) shows Quaternary subsidence in the region north of the Point Reyes Peninsula and Quaternary uplift (or lack of subsidence) south of Bodega Head. The model describes differential uplift (near Bolinas) due to the SGF-E/SAF junction and subsidence

(north of the headland) partly due to the isostatic loading of sea-level controlled Quaternary sequences overlying the PPU. The PRF may now be inactive and differential uplift of the southern part of the peninsula on the SAF and associated structures is interpreted to be the result of SGF-E/SAF fault junction near Bolinas that may represent an effective left-restraining bend in the SAFS. Grove et al.'s (2010) observations of marine terraces on the southern Point Reyes Peninsula show that uplift rates have been accelerating on the southern part of the peninsula near Bolinas during the past ~300 k.y., while rates appear to have been decelerating less than 20 km to the north. The differential uplift could be partly explained by a southward migrating SGF-E/SAF fault junction. North of the Russian River outlet, offshore contractional structures have accommodated shortening west of the offshore Gualala fault. Seismic reflection profiles show the structures have deformed the youngest preserved Quaternary sequences and truncation and onlapping relationships suggest that the deformation initiated 400–500 ka.

#### **5.4 *Suggestions for future work***

Additional evaluation of offshore Quaternary deformation within the SAFS would benefit from age control of the Quaternary sequences. The sequences could be sampled by drilling and possibly dated by strontium isotope stratigraphy (as in Ingram and Ingle, 1998) or by identifying the Rockland ash, a widespread

tephrachronologic unit dated at about 0.5 Ma (Lanphere et al., 2004). Better age control would help to correlate sequences to specific Quaternary MIS high stands, and improve timing constraints on offshore subsidence and uplift. The collection of additional mini-sparker high-resolution seismic reflection data west of the 3-mile limit could help to better define the near-surface zone above the PRF and related structures north of the Point Reyes Peninsula. These data could refine the interpretations presented herein that related to the timing of offshore deformation and the subsidence of the PPU surface north of the Point Reyes Peninsula.

## **6.0 Conclusions**

North of the Point Reyes Peninsula, evidence for Quaternary deformation within the offshore SAFS involves Quaternary subsidence of the shelf that has resulted in the preservation of multiple eustatic sea-level controlled stratigraphic sequences above a regional Plio-Pleistocene unconformity. The sequences show little deformation, except to the west of the Gualala fault, where they are deformed by contractional structures. Multichannel seismic reflection profiles primarily show concordant deformation within the Upper Miocene and overlying Mio-Pliocene units across the PRF and PRF-W structures where Plio-Pleistocene deformation appears to have reactivated and inverted Miocene normal faults. Despite seismic reflection profile and exploratory well evidence for ~2 km of uplift

on the PRF since the Mio-Pliocene, there is no geophysical evidence for uplift on the northern PRF since at least the Middle Pleistocene and on the southern PRF since the Holocene marine transgression. These interpretations suggest that the hazard potential of the Point Reyes fault in current fault and tsunami hazard models should be re-evaluated. Post-80-ka uplift at the southern end of the peninsula is probably related to the SGF-E/SAF junction rather than movement on the offshore PRF.

## 7.0 References

- Amina, R.J., Eittrheim, B.D., Edwards, B.D., and Stevenson, A.J., 2002, Nearshore morphology and late Quaternary geologic framework of the northern Monterey Bay Marine Sanctuary, California: *Marine Geology*, v. 181, p. 35-54.
- Argus, D.F., and Gordon, R.G., 2001, Present tectonic motion across the Coast Ranges and San Andreas fault system in central California: *Geological Society of America Bulletin*, v. 113, p.1580-1592.
- Atwater, T., 1989, Plate tectonic history of the northeast Pacific and western North America, *in* Winterer, E. L., Hussong, D. M., and Decker, R. W., eds., *The eastern Pacific Ocean and Hawaii*: Boulder, Colorado, Geological Society of America, *Geology of North America*, v. N, p. 21-72.
- Atwater, T., and Stock, J., 1998, Pacific North America plate tectonics of the Neogene southwestern United States: an update: *International Geology Review*, v. 40, p. 375-402.
- Axelrod, D.I., 1983, New Pleistocene conifer records, coastal California: *University of California Publications in Geological Science*, v. 127, 108 p.
- Baise, L.G., Dreger, D.S., and Glaser, S.D., 2003, The effect of shallow San Francisco Bay sediments on waveforms recorded during the  $M_w$  4.6 Bolinas, California, Earthquake: *Bulletin of the Seismological Society of America*, v. 93, p. 465-479.
- Bassinot, F.C., 2007, Oxygen isotope stratigraphy of the oceans, *in* Elias, S.A., ed., *Encyclopedia of Quaternary Science*, p. 1740-1748.
- Beroza, G.C., 1996, Rupture history of the earthquake from high-frequency strong-motion data, *in* Spudich, P., ed., *The Loma Prieta, California, earthquake of October 17, 1989—Main-shock characteristics*: U.S. Geological Survey Professional Paper 1550-A, p. 9–32.
- Brabb, E.E., Graymer, R.W., and Jones, D.L., 1998, *Geology of the onshore part of San Mateo County, California*: U.S. Geological Survey Open-File Report 98-137, scale 1:62,500 (2 sheets with 13 p. text).
- Bruns, T.R., Cooper, A.K., Carlson, P.R., and McCulloch, D.S., 2002, Structure of the submerged San Andreas and San Gregorio fault zones in the Gulf of the Farallones off San Francisco, California, from high-resolution seismic-reflection data, *in* Parsons, T., ed., *Crustal structure of the coastal and marine San Francisco Bay Region, California*: U.S. Geological Survey Professional Paper 1658, p. 77–117.
- Burger, R.L., Fulthorpe, C.S., Austin, J.A., Jr., and Guillick, S.P.S., 2002, Lower Pleistocene to present structural deformation and sequence stratigraphy of the continental shelf, offshore Eel River Basin, northern California: *Marine Geology*, v. 185, p. 249–281.
- Chapman, R.H., and Bishop, C.C., 1968, Bouguer gravity map of California, San Francisco sheet: *California Division of Mines and Geology*, scale 1:250,000, 1 sheet.

Chéry, J., Zoback, M.D., Hassani, R., 2001, An integrated mechanical model of the San Andreas fault in central and northern California: *Journal of Geophysical Research*, v. 106, p. 22,051-22,066.

Chin, J.L., Karl, H.A., and Maher, N.M., 1997, Shallow subsurface geology of the continental shelf, Gulf of the Farallones, California, and its relationship to surficial seafloor characteristics: *Marine Geology*, v. 137, p. 251-269.

Chin, J.L., Clifton, H.E., and Mullins, H.T., 1988, Seismic stratigraphy and late Quaternary shelf history, South-Central Monterey Bay, California: *Marine Geology*, v. 81, p. 137-157.

Clark, J., and Brabb, E., 1997, Geology of Point Reyes National Seashore and vicinity, California: A Digital Database: U.S. Geological Survey Open-File Report 97-456, scale 1:48,000, 8 p.

Clark, J.C., Brabb, E.E., Greene, G.H., and Ross, D.C., 1984, Geology of Point Reyes Peninsula and Implications for San Gregorio Fault History, *in* Crouch, J.K., and Bachman, S.B., eds., *Tectonics and Sedimentation Along the California Margin: Pacific Section S.E.P.M.*, v. 38, p. 67-86.

Clifton, H.E., Hunter, R.E., and Gardner, J.V., 1988, Analysis of eustatic tectonic and sedimentologic influences on transgressive and regressive cycles in the late Cenozoic Merced Formation, San Francisco, California, *in* Paola, C., Kleinspehn, K.L., eds., *New Perspectives in Basin Analysis*. New York, Springer-Verlag, p. 109-128.

d'Alessio, M.A., Johanson, and I.A., Burgmann, R., 2005, Slicing up the San Francisco Bay area: block kinematics and fault slip rates from GPS-derived surface velocities: *Journal of Geophysical Research*, v. 110, 19 p.

DeMets, C., Gordon, R.G., and Argus, D.F., 2010, Current plate motions: *Geophysical Journal International*, v. 181, p. 1-80.

Dickinson, W.R., Ducea, M., Rosenberg, L.I., Greene, H.G., Graham, S.A., Clark, J.C., Weber, G.E., Kidder, S., Ernst, and W.G., Brabb, E.E., 2005, Net dextral slip, Neogene San Gregorio-Hosgri fault zone, coastal California: geologic evidence and tectonic implications: *Geological Society America Special Paper*, v. 391, 43 p.

Furlong, K. P., and S. Y. Schwartz, 2004, Influence of the Mendocino Triple Junction on the tectonics of coastal California: *Annual Review of Earth and Planetary Sciences*, v. 32, p. 403-433.

Galloway, A. J., 1977, Geology of the Point Reyes Peninsula, Marin County: *California Division of Mines and Geology Bulletin*, v. 202. 72 p.

Grossman, E.E., Eittrheim, S.L., Field, M.E., and Wong, F.L., 2006, Shallow stratigraphy and sedimentation history during high-frequency sea-level changes on the central California shelf: *Continental Shelf Research* v. 26, p. 1217-1239.

Grove, K., and Niemi, T., 2005, Late Quaternary deformation and slip rates in the northern San Andreas fault zone at Olema Valley, Marin County, California: *Tectonophysics*, v. 401, p. 231-250.

Grove, K., Scherer, A.M., Lee, G., Sklar, L., and Davis, J., 2010, Accelerating and spatially-varying crustal uplift and its geomorphic expression, San Andreas fault zone north of San Francisco, California: *Tectonophysics*, v. 495, p. 256-268.

Gutiérrez-Alonso, G., and Gross, M.R., 1997, Geometry of inverted faults and related folds in the Monterey Formation: implications for the structural evolution of the southern Santa Maria basin, California: *Journal of Structural Geology*, vol. 19, p. 1303-1320.

Hall, N.T., Wright, R.H., and Clahan, K.B., 1999, Paleoseismic studies of the San Francisco Peninsula segment of the San Andreas fault zone near Woodside, California: *Journal of Geophysical Research*, v. 104, p. 23215–23236.

Hardebeck, J. L., Boatwright, J., Dreger, D., Goel, R., Graizer, V., Hudnut, K., Ji, C., Jones, L., Langbein, J., Lin, J., Roeloffs, E., Simpson, R., Stark, K., Stein, R., and Tinsley, J.C., 2004, Preliminary report on the 22 December 2003 M 6.5 San Simeon, California earthquake: *Seismological Research Letters*, v. 75, p. 155–172.

Heck, R.G., Edwards, E.B., Kronen, J.D., Jr., and Willingham, C.R., 1990, Petroleum potential of the offshore Outer Santa Cruz and Bodega basins, California, *in* Garrison, R.E., Greene, H.G., Hicks, K.R., Weber, G.E., and Wright, T.L., eds., *Geology and tectonics of the central California Coast region, San Francisco to Monterey*: Pacific Section, American Association of Petroleum Geologists, Book GB67, p. 143-164.

Hoskins, E.G., and Griffiths, J.R., 1971, Hydrocarbon potential of northern and central California offshore, *in* Cram, I.H. ed., *Future petroleum provinces of the United States- their geology and potential*: American Association of Petroleum Geologists Memoir 15, v. 1, p. 212-228.

Hunter, R.E., Clifton, H.E., Hall, N.T., Csaszar, G., Richmond, B.M., and Chin, J.L., 1984, Pliocene and Pleistocene coastal and shelf deposits of the Merced Formation and associated beds, northwestern San Francisco Peninsula, California: *SEPM Field Guide* 3, p. 1–29.

Ingram, B.L., Ingle, J.C., 1998, Strontium isotope ages of the marine Merced Formation near San Francisco, California: *Quaternary Research*, vol. 50, p. 194–199.

Lanphere, M. A., Champion, D. E., Clyne, M. A., Lowenstern, J. B., Sarna-Wojcicki, A. M., and Wooden, J.L., 2004, Age of the Rockland tephra, western USA: *Quaternary Research*, v. 62, p. 94-104.

Lawson, A.C., 1908, The California Earthquake of April 18, 1906, *in* Lawson, A.C., chairman, *Report of the State Earthquake Investigation Commission*: Washington, D.C., Carnegie Institution [reprinted 1969].

Lettis, W. R., K. L. Hanson, J. R. Unruh, M. K. McLaren, and W. U. Savage, 2004, Quaternary tectonic setting of south central coastal California: *U.S. Geological Survey Bulletin* 1995-AA, 24 p.

Lock, J., Kelsey, H., Furlong, K., and Woolace, A., 2006, Late Neogene and Quaternary landscape evolution of the northern California Coast Ranges: Evidence for Mendocino triple junction tectonics: *Geological Society of America Bulletin*, v. 118, p. 1232-1246.

McCulloch, D.S., 1989, Evolution of the offshore central California Margin, in Winterer, E. L., Hussong, D.M., and Decker, R. W., eds., *The eastern Pacific Ocean and Hawaii*: Boulder, Colorado, Geological Society of America, *Geology of North America*, v. N, p. 439–470.

McCulloch, D.S., 1982, The geology beneath Drakes Bay, *in* Murphy, L, ed., *Submerged Cultural Resources Survey*: National Park Service, p. 123–139.

McLaughlin, R. J., Powell, C. L., McDougal-Reid, K., and Jachens, R. C., 2007, Cessation of slip on the Pilarcitos Fault and initiation of the San Francisco Peninsula segment of the (modern) San Andreas Fault, California: *Transactions AGU Fall Meeting*, San Francisco, abstract #T43A-1089.

McLaughlin, R.J., Sliter, W.V., Sorg, D.H., Russell, P.C., and Sarna-Wojcicki, A.M., 1996, Large-scale right-slip displacement on the East San Francisco Bay Region fault system, California: Implications for location of late Miocene to Pliocene Pacific plate boundary: *Tectonics*, v. 15, p. 1–18.

Niemi, T.M., and Hall, N.T., 1992, Late Holocene slip rate and recurrence of great earthquakes on the San Andreas fault in northern California: *Geology*, v. 20, p. 195–198.

Page, B.M., Thompson, G.A., and Coleman, R.G., 1998, Late Cenozoic tectonics of the central and southern Coast Ranges: *Geological Society of America Bulletin*, v. 110, p. 846–876.

Parsons, T., and Zoback, M.L., 1997, Three-dimensional upper crustal velocity structure beneath San Francisco Peninsula, California: *Journal of Geophysical Research*, v. 102, no. B3, p. 5473–5490.

Powell II, C.L., Baron, J.A., Sarna-Wojcicki, A., Clark, J.C., Perry, F.A., Brabb, E.E., and Fleck, R.J., 2007, Age, stratigraphy, and correlation of the Late Neogene Purisima Formation, central California Coast Ranges: *U. S. Geological Survey Professional Paper 1740*, 32 p.

Ryan, H.F., Parsons, T., and Sliter, R.W., 2008, Vertical tectonic deformation associated with the San Andreas fault zone offshore of San Francisco, California: *Tectonophysics*, v. 457, p. 209–223.

U.S. Geological Survey (USGS), 2006, NAMSS: National Archive of Marine Seismic Surveys: <http://walrus.wr.usgs.gov/NAMSS/>.

U.S. Geological Survey (USGS) and California Geological Survey (CGS), 2006, Quaternary fault and fold database for the United States: <http://earthquakes.usgs.gov/regional/qfaults/> (accessed November 2011).

Wakabayashi, J., 1999, Distribution of displacement on and evolution of a young transform fault system: The northern San Andreas fault system, California: *Tectonics*, v. 18, no. 6, p. 1245–1274.

Webster, F. and K.A. Yenne, 1987, Northern and central California lease sale/May 14, 1963: U.S. Department of the Interior Minerals Management Service, Pacific OCS Region, OCS Report MMS 87-0108, 48 p.

Working Group on California Earthquake Probabilities (WGCEP), 2003, Earthquake probabilities in the San Francisco Bay region: 2002 to 2031: U.S. Geological Survey Open-File Report 03-214.

Working Group on California Earthquake Probabilities (WGCEP), 2008, Documentation for the 2008 Update of the United States National Seismic Hazard Maps: U.S. Geological Survey Open-File Report 2008-1128.

Table 1: Well 27-1

Top of Formation	Depth below Sea Level (Feet)	Depth (m)	Thickness (m)	Midpoint Velocity from Regression Model (m/s)	TWTT from Velocity Regression (s)	TWTT from Velocity Log (s)
Water	0	0	106	1500		
Pre-log Sediment	348	106	119	1708	0.141	
Monterey	740	226	173		0.281	0.288
Laird	1308	399	50			
Mindego	1472	449	122			
Point Reyes	1872	571	415			
TD	3234	986				

m- meters

m/s- meters per second

TWTT- Two-way travel time

s- seconds

Table 2: Well 39-1

Top of Formation	Depth below Sea Level (Feet)	Depth (m)	Thickness (m)	Midpoint Velocity from Regression Model (m/s)	TWTT from Velocity Regression (s)	TWTT from Velocity Log (s)
Water	0	0	61	1500		
Pre-log Sediment	200	61	101	1610	0.081	
Purisima	532	162	140	1726	0.207	
Santa Cruz	990	302	530	2033	0.369	
Monterey	2730	832	226		0.891	0.894
Laird	3470	1058	21			
Point Reyes	3540	1079	608			
Granite	5535	1687	30			
TD	5632	1717				

m- meters

m/s- meters per second

TWTT- Two-way travel time

s- seconds

Table 3: Well 41-1

Top of Formation	Depth below Sea Level (Feet)	Depth (m)	Thickness (m)	Midpoint Velocity from Regression Model (m/s)	TWTT from Velocity Regression (s)	TWTT from Velocity Log (s)
Water	0	0	76	1500		
Pre-log Sediment	250	76	8	1536	0.101	
Santa Cruz	277	84	310	1649	0.112	
Monterey	1295	395	297		0.488	0.483
Laird	2270	692	13			
Mindego	2312	705	75			
Point Reyes	2560	780	584			
Granite	4475	1364	69			
TD	4700	1433				

m- meters

m/s- meters per second

TWTT- Two-way travel time

s- seconds

Table 4: Well 51-2

Top of Formation	Depth below Sea Level (Feet)	Depth (m)	Thickness (m)	Midpoint Velocity from Regression Model (m/s)	TWTT from Velocity Regression (s)	TWTT from Velocity Log (s)
Water	0	0	111	1500		
Pre-log Sediment	364	111	87	1502	0.148	
Purisima	650	198	378	1594	0.264	
Santa Cruz	1890	576	1030	2227	0.738	0.745
Monterey	5270	1606	293		1.664	1.676
Laird	6230	1899	8			
Point Reyes	6255	1907	1283			
TD	10466	3190				

m- meters

m/s- meters per second

TWTT- Two-way travel time

s- seconds

Table 5: Well 53-1

Top of Formation	Depth below Sea Level (Feet)	Depth (m)	Thickness (m)	Midpoint Velocity from Regression Model (m/s)	TWTT from Velocity Regression (s)	TWTT from Velocity Log (s)
Water depth	0	0	105	1500		
Pre-log Sediment	344	105	101	1580	0.141	
Purisima	675	206	611	1800	0.268	
Santa Cruz	2680	817	1024	2496	0.947	0.946
Santa Margarita	6040	1841	108	3135	1.768	1.790
Monterey	6395	1949	43		1.837	1.855
Laird	6537	1992	37			
Mindego	6660	2030	241			
Point Reyes	7450	2271	185			
TD	8057	2456				

m- meters

m/s- meters per second

TWTT- Two-way travel time

s- seconds

Table 6: Well 55-1

Top of Formation	Depth below Sea Level (Feet)	Depth (m)	Thickness (m)	Midpoint Velocity from Regression Model (m/s)	TWTT from Velocity Regression (s)	TWTT from Velocity Log (s)
Water depth	0	0	126	1500		
Pre-Log Sediment	413	126	99	1530	0.168	
Purisima	737	225	647	1677	0.297	
Santa Cruz	2860	872	931	2353	1.069	1.036
Monterey	5915	1803	65		1.861	1.842
Laird	6130	1868	12			
Mindego	6170	1881	40			
Point Reyes	6300	1920	359			
TD	7477	2279				

m- meters

m/s- meters per second

TWTT- Two-way travel time

s- seconds

Table 7: Well 55-2

Top of Formation	Depth below Sea Level (Feet)	Depth (m)	Thickness (m)	Midpoint Velocity from Regression Model (m/s)	TWTT from Velocity Regression (s)	TWTT from Velocity Log (s)
Water Depth	0	0	128	1500		
Pre-log Sediment	420	128	489*	1637	0.171	
Purisima (not top)	2025	617	387	1904	0.768	
Santa Cruz	3295	1004	962	2541	1.175	1.150
Monterey	6450	1966	100		1.932	1.942
Laird	6778	2066	86			
Point Reyes	7060	2152	61			
TD	7297	2213				

m- meters

m/s- meters per second

TWTT- Two-way travel time

s- seconds

\*- includes unknown thickness of Purisima, as the actual top of the Purisima was not logged.

Table 8: Well 58-1

Top of Formation	Depth below Sea Level (Feet)	Depth (m)	Thickness (m)	Midpoint Velocity from Regression Model (m/s)	TWTT from Velocity Regression (s)	TWTT from Velocity Log (s)
Water depth	0	0	134	1500		
Pre-log Sediments	440	134	162	1577	0.179	
Purisima	970	296	716	1820	0.384	
Santa Cruz	3320	1012	1033	2650	1.171	1.174
Monterey	6710	2045	31		1.951	1.975
Laird	6812	2076	55			
Mindego	6992	2131	134			
Point Reyes	7430	2265	137			
TD	7881	2402				

m- meters

m/s- meters per second

TWTT- Two-way travel time

s- seconds

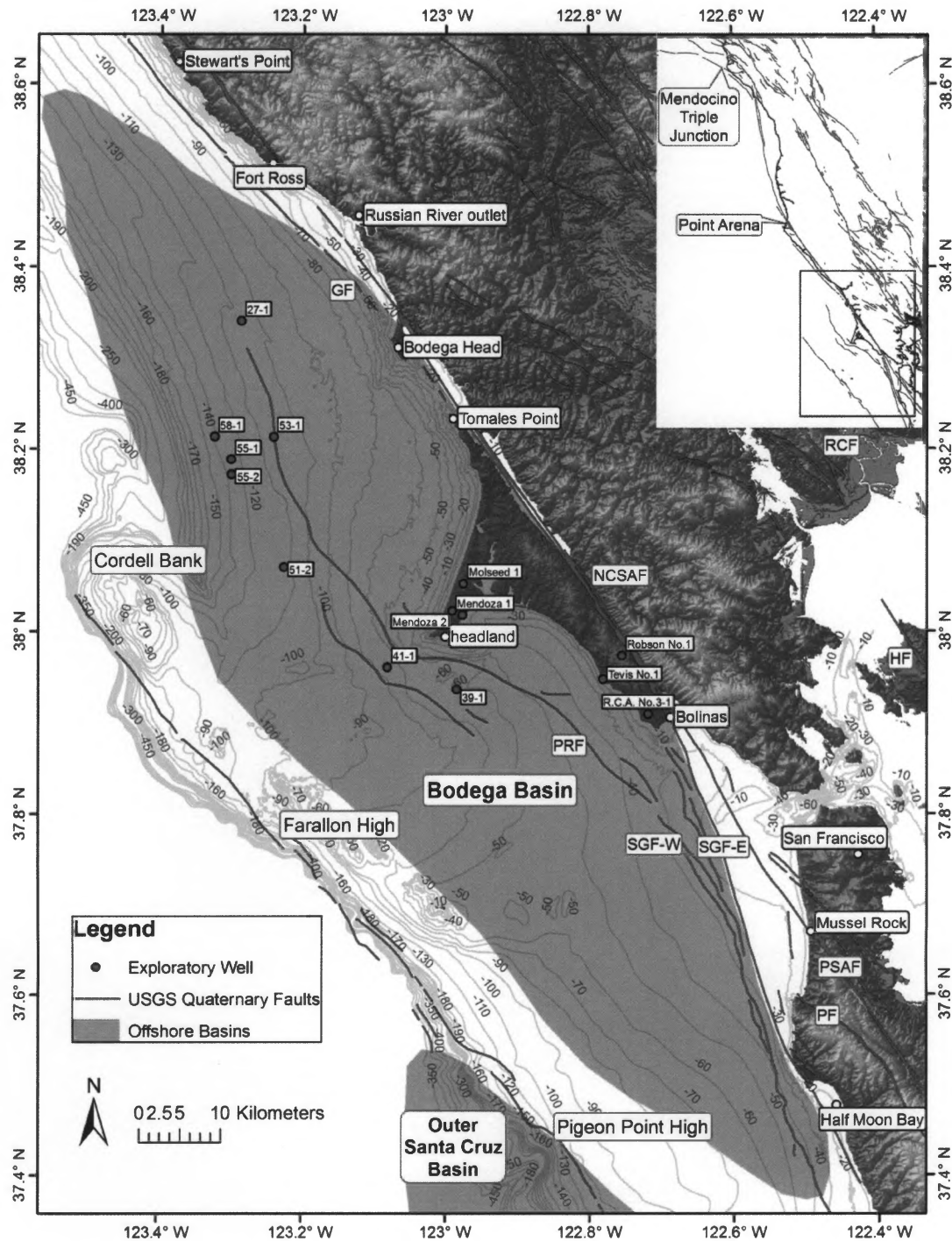


Figure 1: Study area map with USGS Quaternary faults (USGS and CGS, 2006), Bodega Basin (Ryan et al., 2008), locations of onshore (Clark and Brabb, 1997) and offshore (Heck et al., 1990) exploratory wells. Bathymetric contours in meters. Inset shows location within northern California.

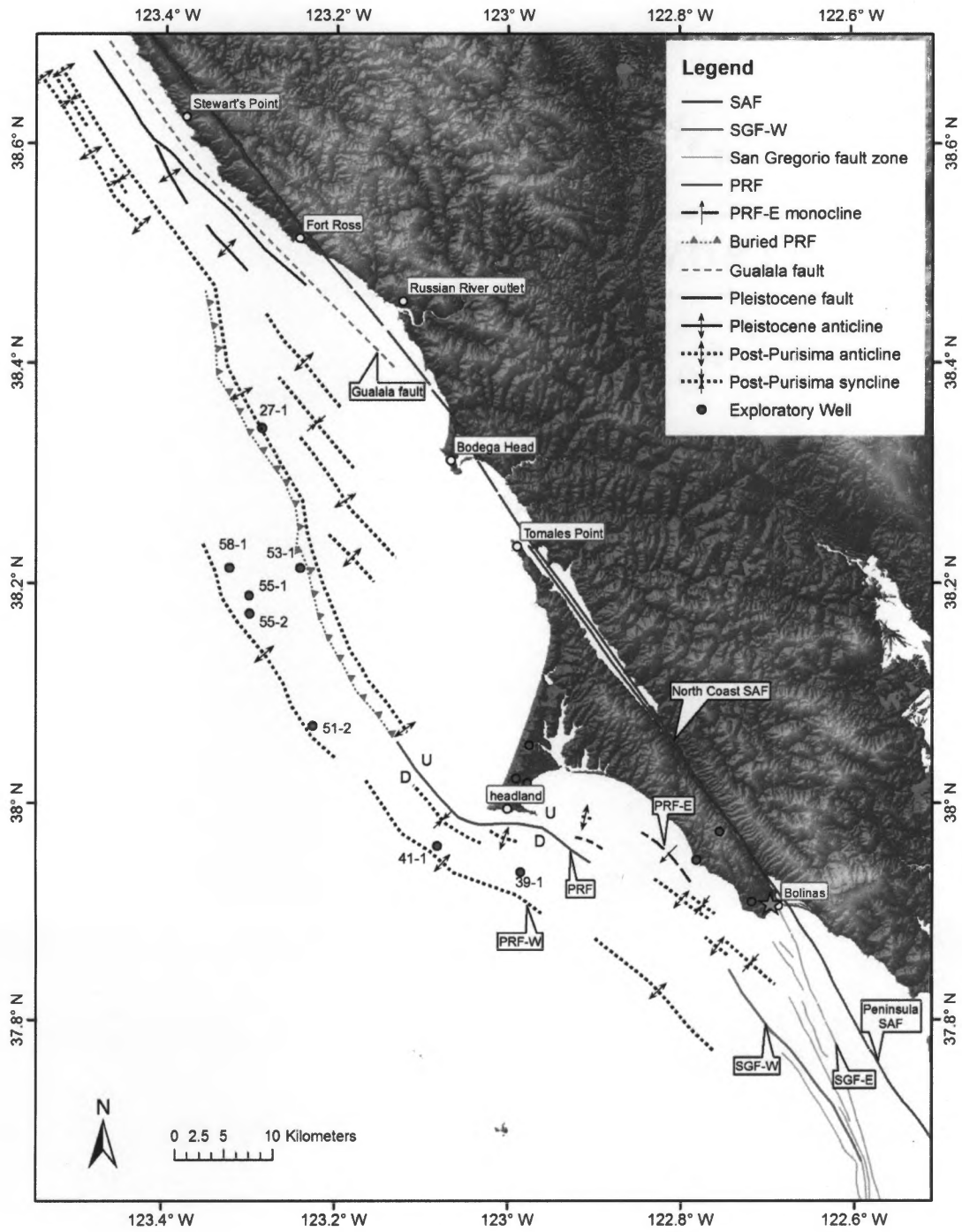


Figure 2: Revised offshore SAFS fault and fold map for Point Reyes Peninsula region. The light blue star represents the epicenter of the 1999 Bolinas earthquake.

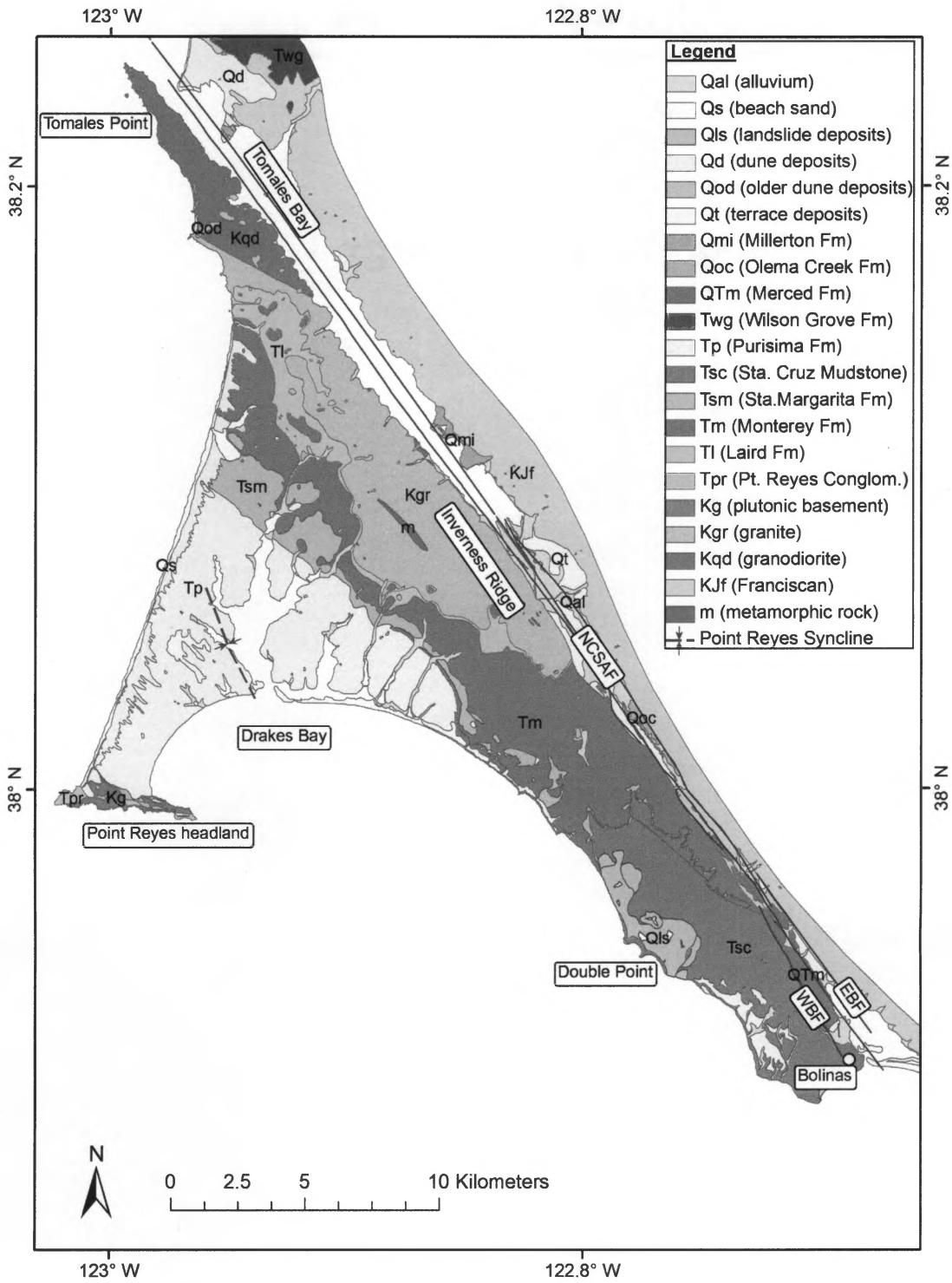


Figure 3: Geologic map of Point Reyes Peninsula adapted from Clark and Brabb (1997).

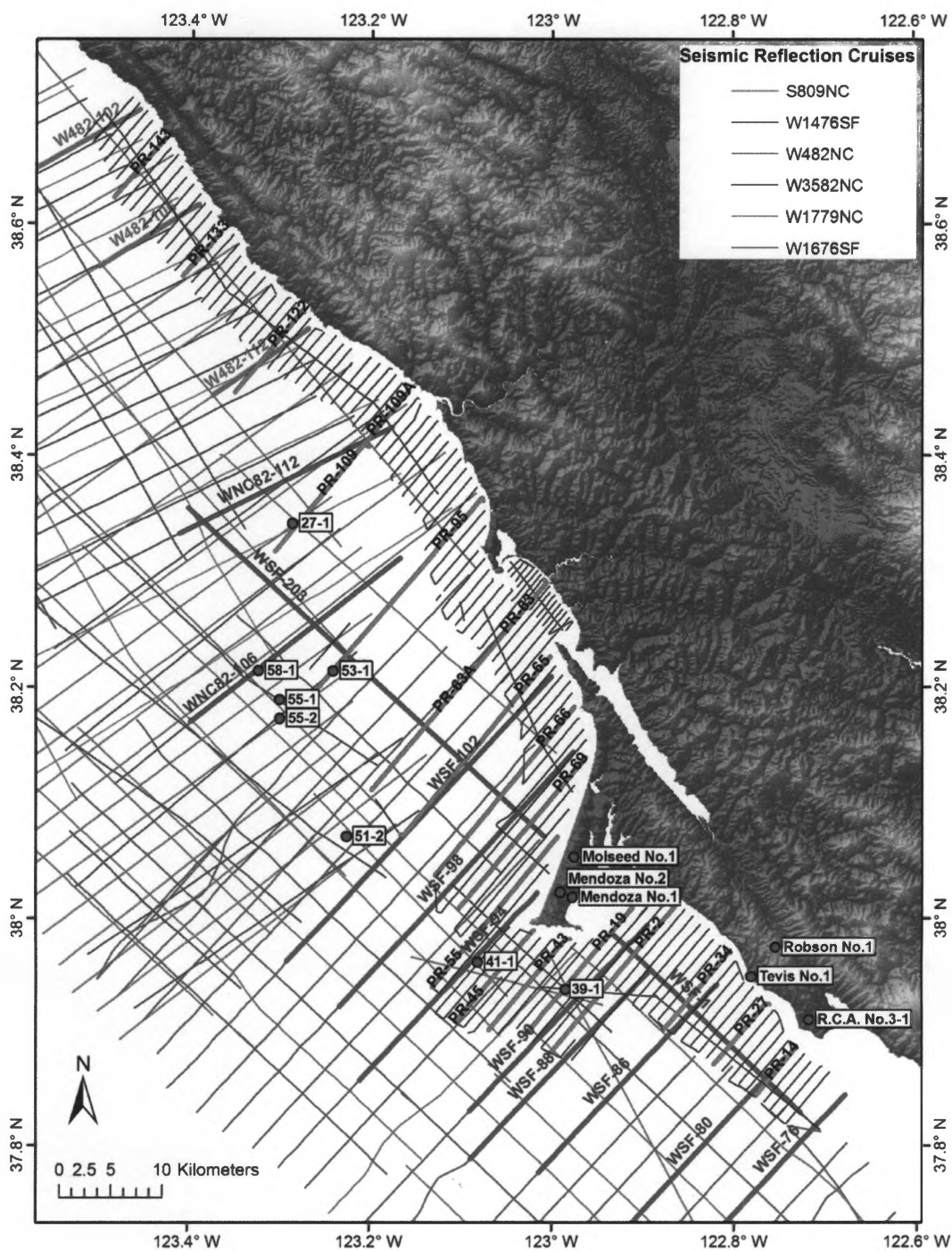


Figure 4: Seismic reflection profile datasets. Key profiles (Figs. 10-41) are labeled and shown in bold. Mini-sparker seismic reflection profiles are shown in pink; all other colors represent MCS reflection profiles (USGS, 2006).

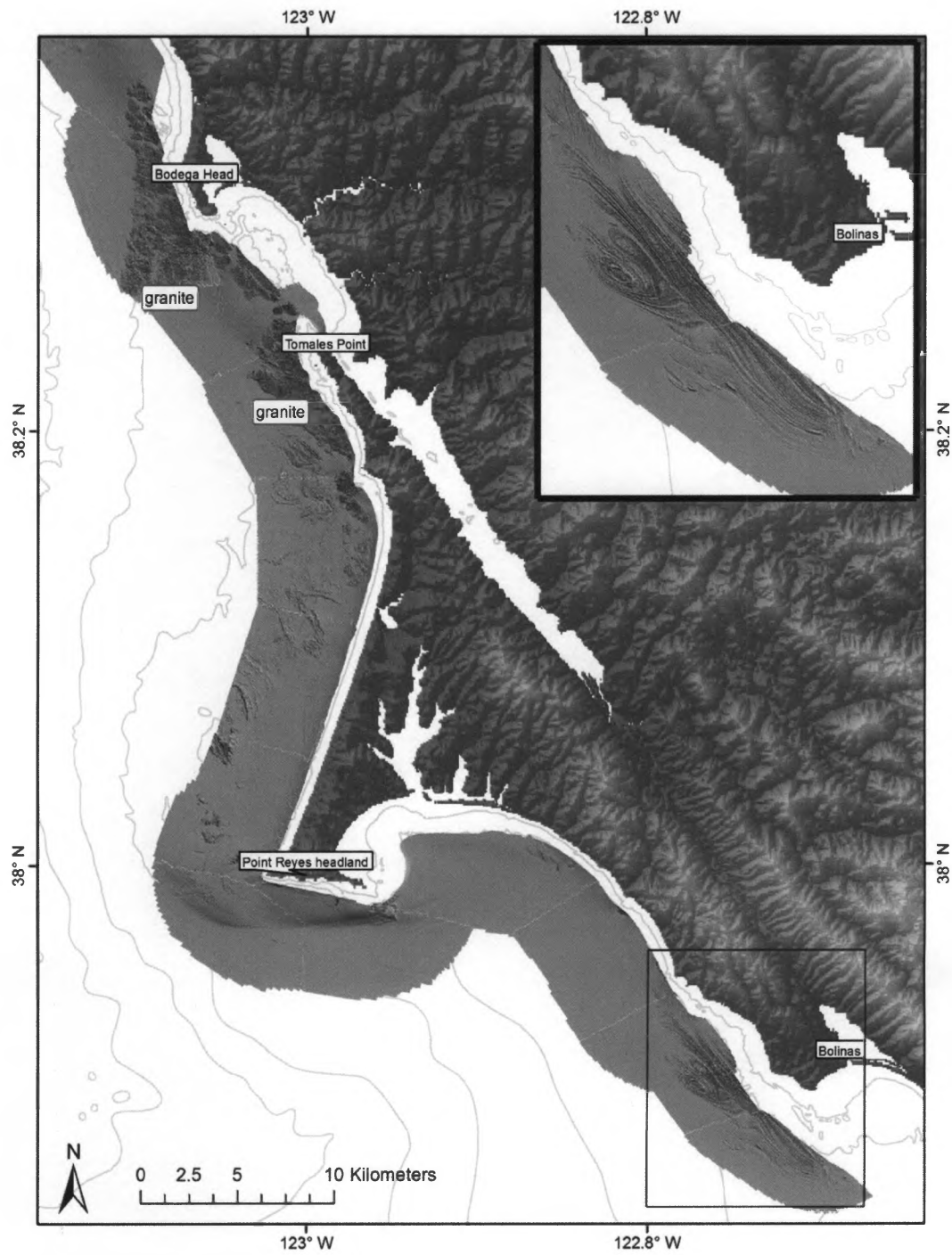


Figure 5: Multibeam dataset acquired by California State University, Monterey Bay as part of the California Coast State Waters Mapping Project (<http://seafloor.csUMB.edu/projects.html>). The inset shows a larger-scale map of the multibeam dataset west of Bolinas.

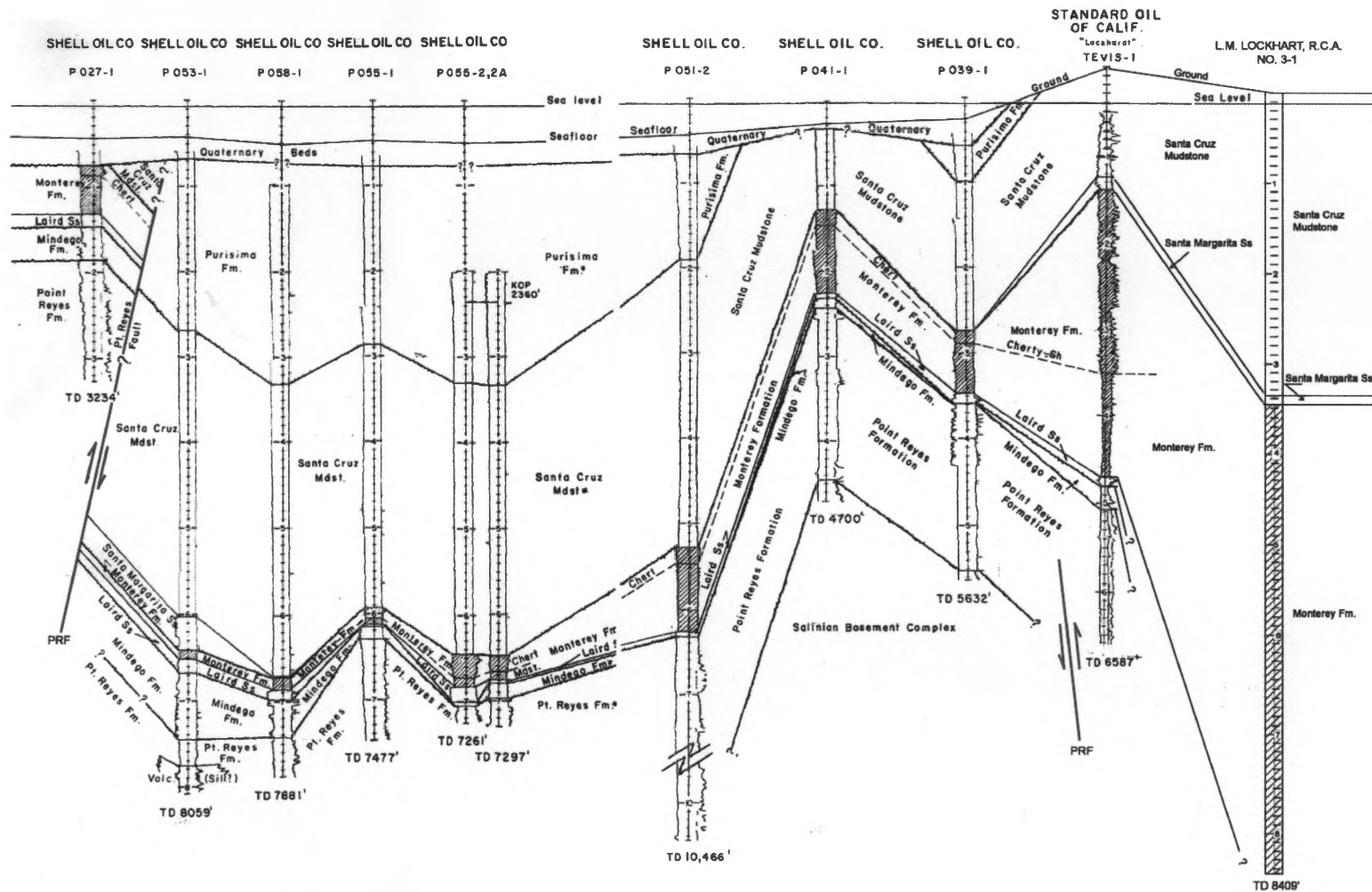


Figure 6: Offshore/onshore stratigraphic correlation diagram, amended from Heck et al., 1990. For well locations see Fig. 1. Note that the distance between well locations does not follow a uniform scale and there is a large amount of vertical exaggeration that is not uniform across the diagram. The PRF is included as a location marker only and fault dip is not meant to be accurate.

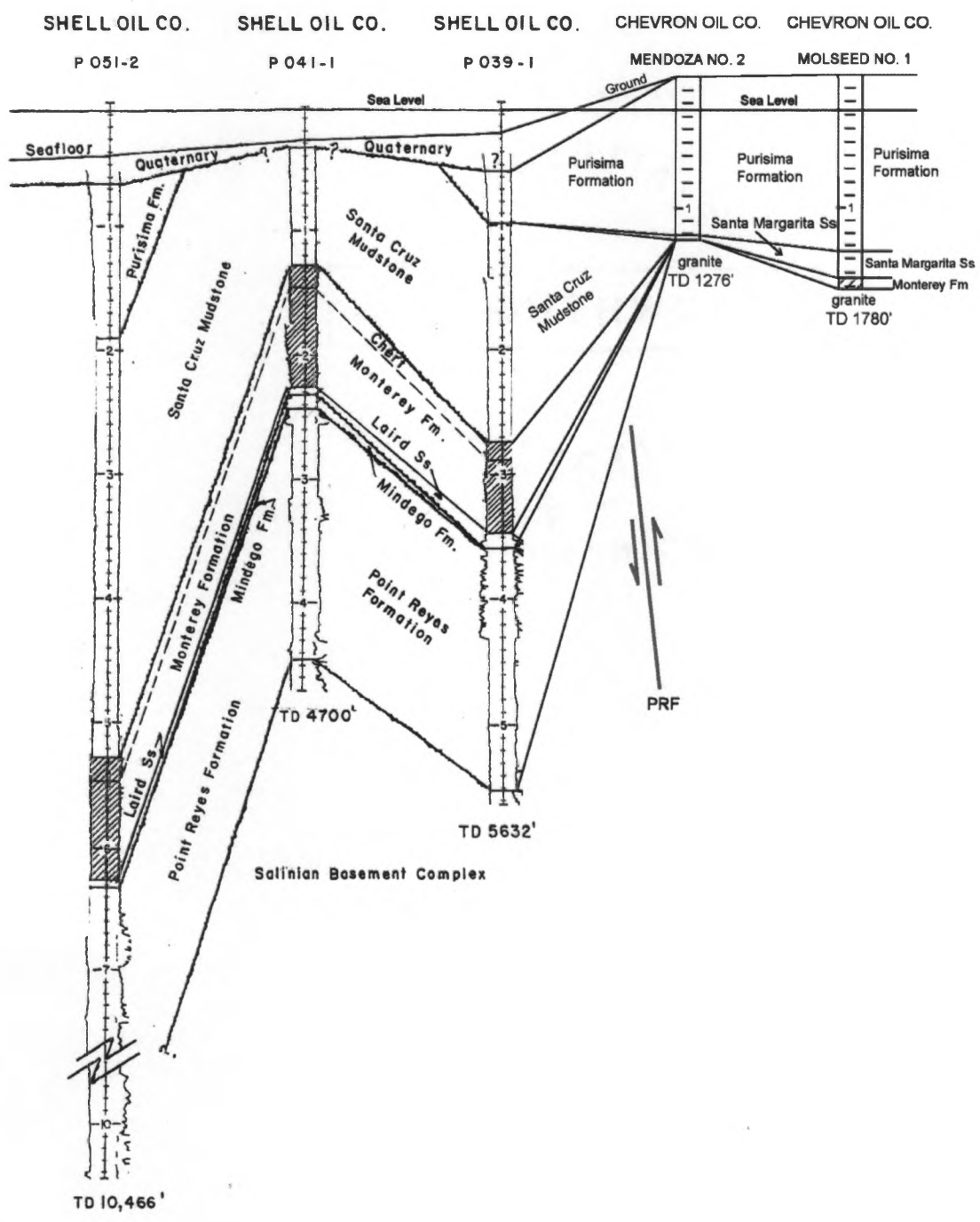


Figure 7: Offshore/onshore stratigraphic correlation diagram, amended from Heck et al., 1990. For well locations see Fig. 1. Note that the distance between well locations does not follow a uniform scale and there is a large amount of vertical exaggeration that is not uniform across the diagram. The PRF is included as a location marker only and fault dip is not meant to be accurate.

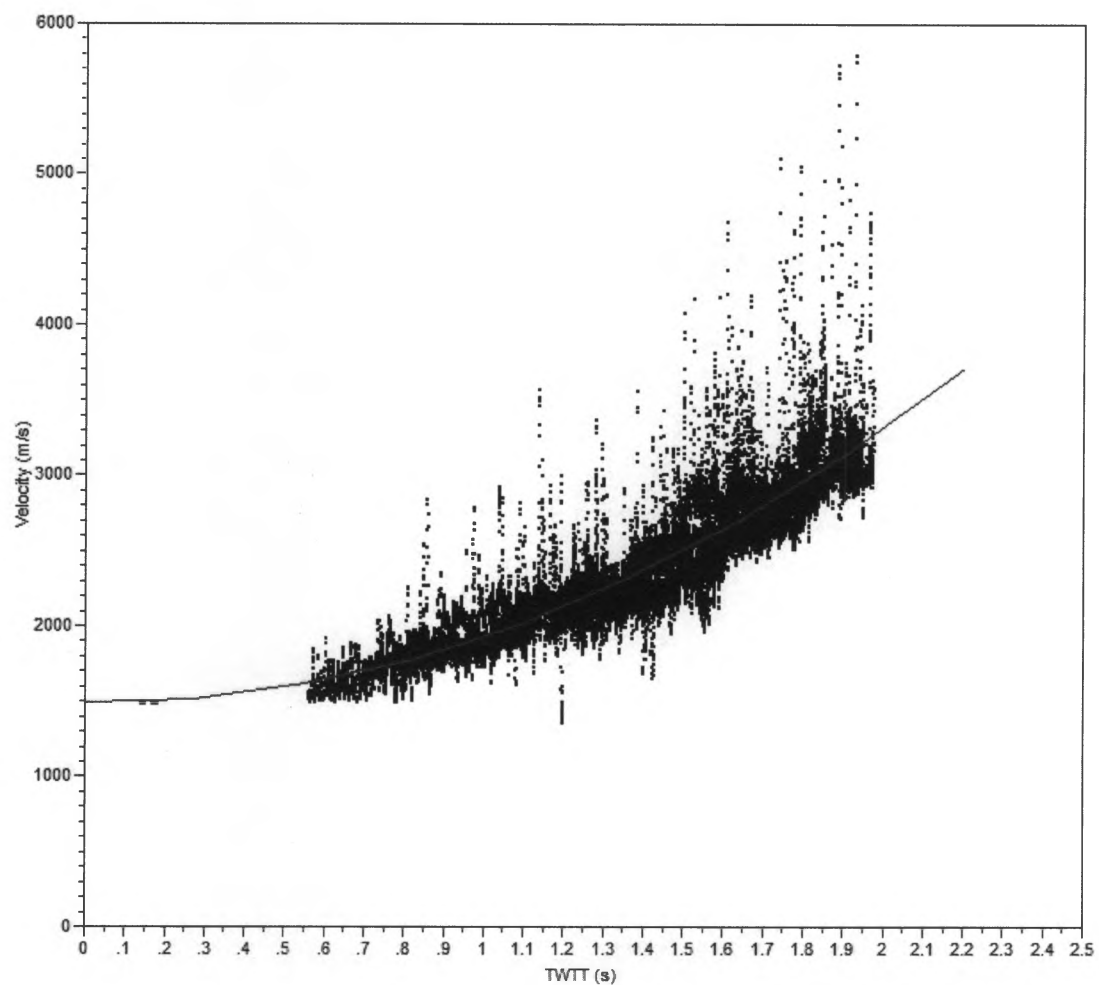


Figure 8: Velocity model for geologic units above Monterey Formation: Velocity as a function of TWTT fit with a second order polynomial curve forced through the y-axis (velocity) at 1500 m/s for geologic units above the top of the Monterey Formation within the Bodega Basin.

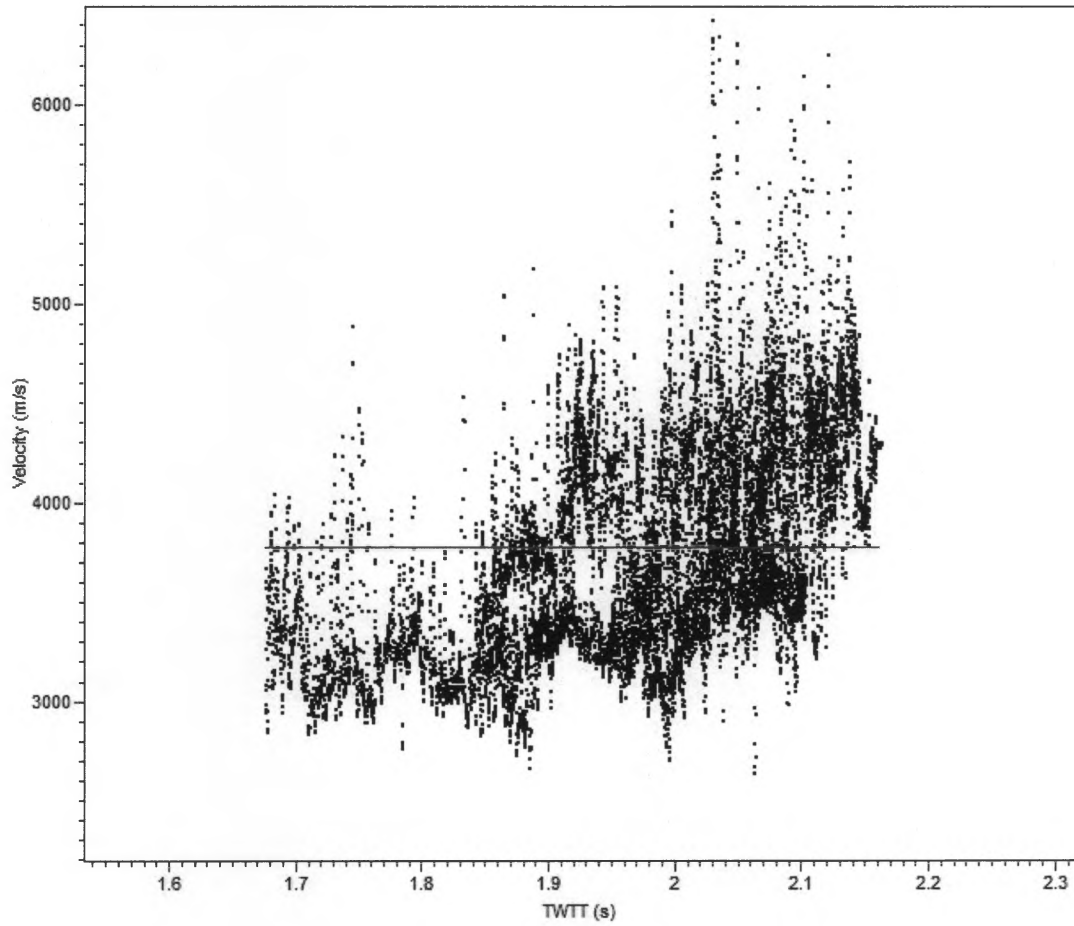


Figure 9: Velocity model for geologic units below the top of the Monterey Formation: Velocity as a function of TWTT fit with a mean velocity line for geologic units below the top of the Monterey Formation within the Bodega Basin.

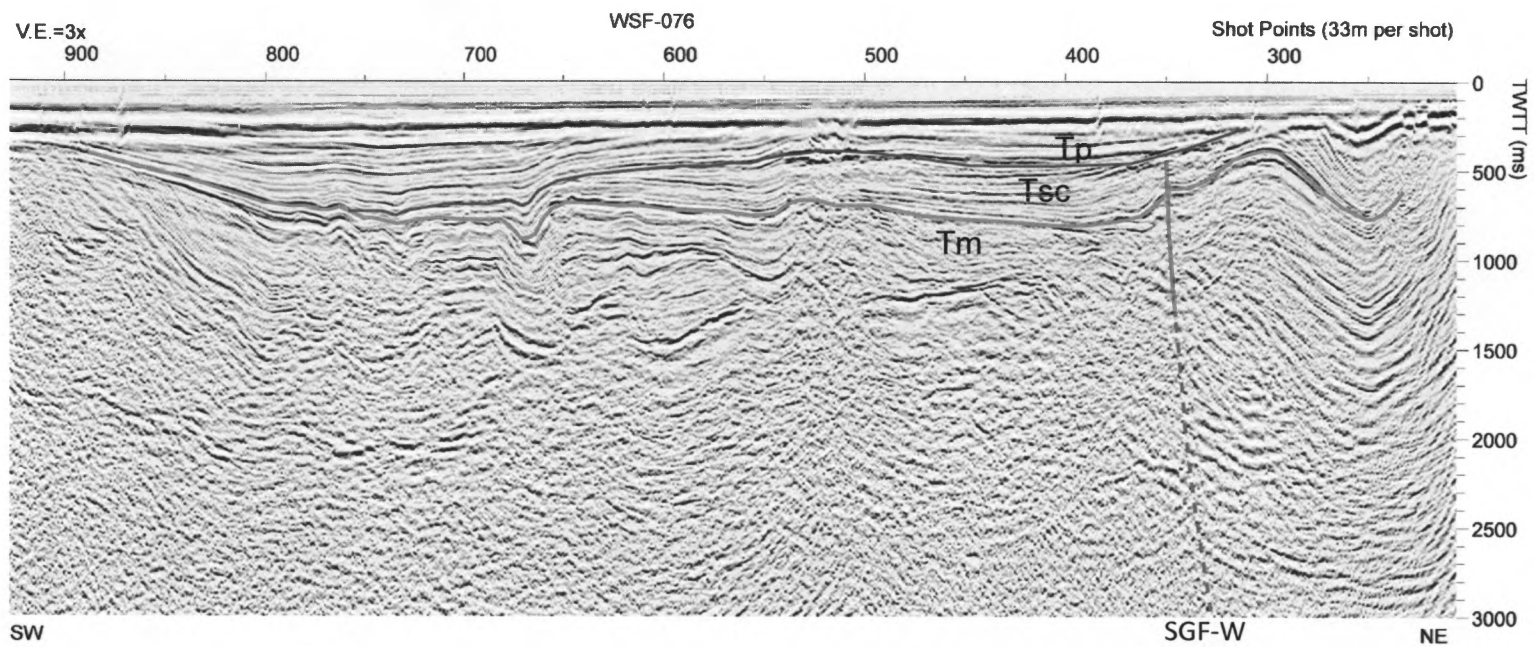


Figure 10: MCS profile WSF-076 (in TWTT). Dark blue is top of the Santa Cruz Mudstone; green is the top of the Monterey Formation; SGF-W is labeled. Location of profile shown in Fig. 4.

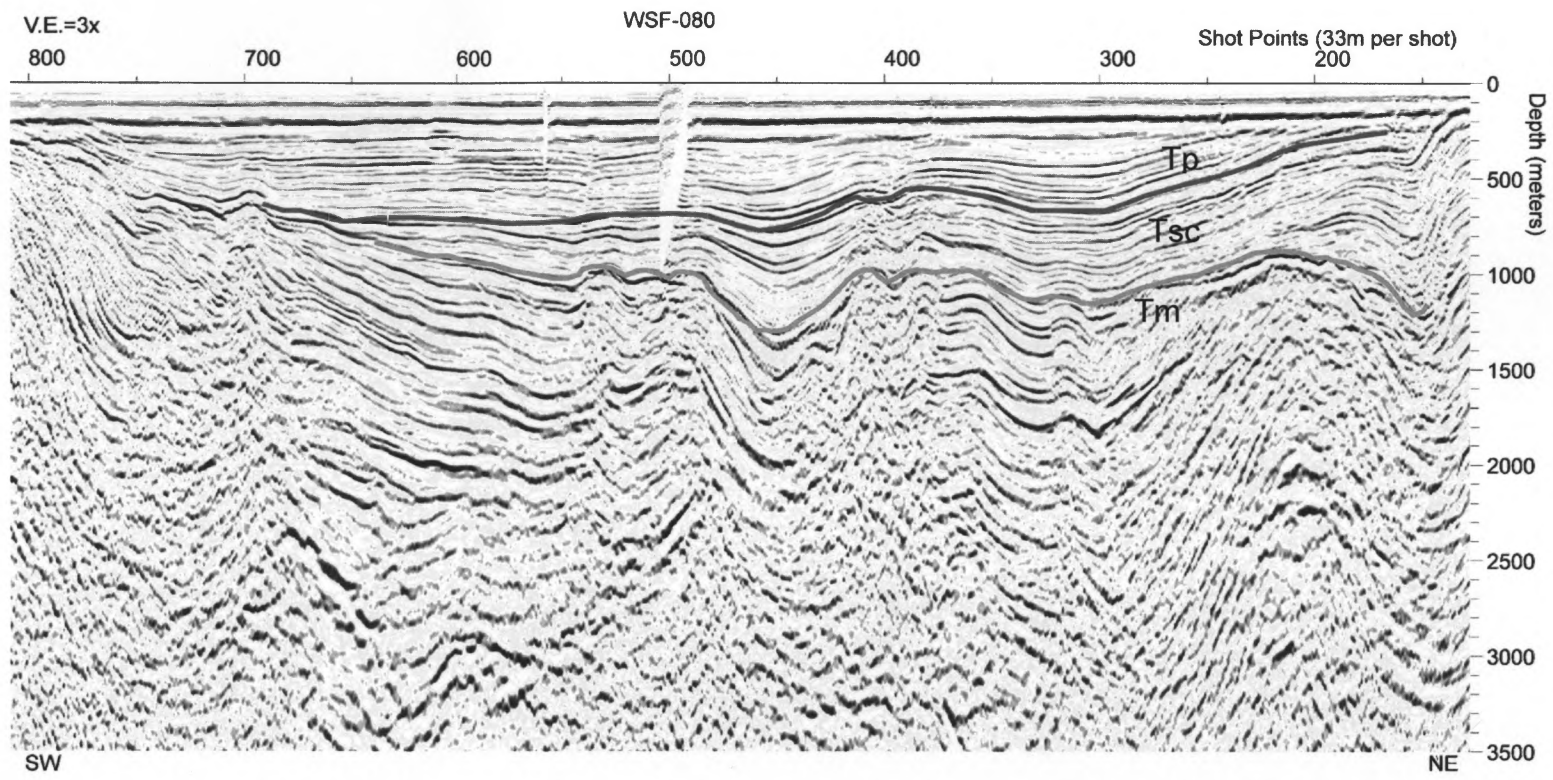


Figure 11: Depth converted MCS profile WSF-080. Dark blue is top of the Santa Cruz Mudstone; green is top of the Monterey Formation. Location of profile shown in Fig. 4.

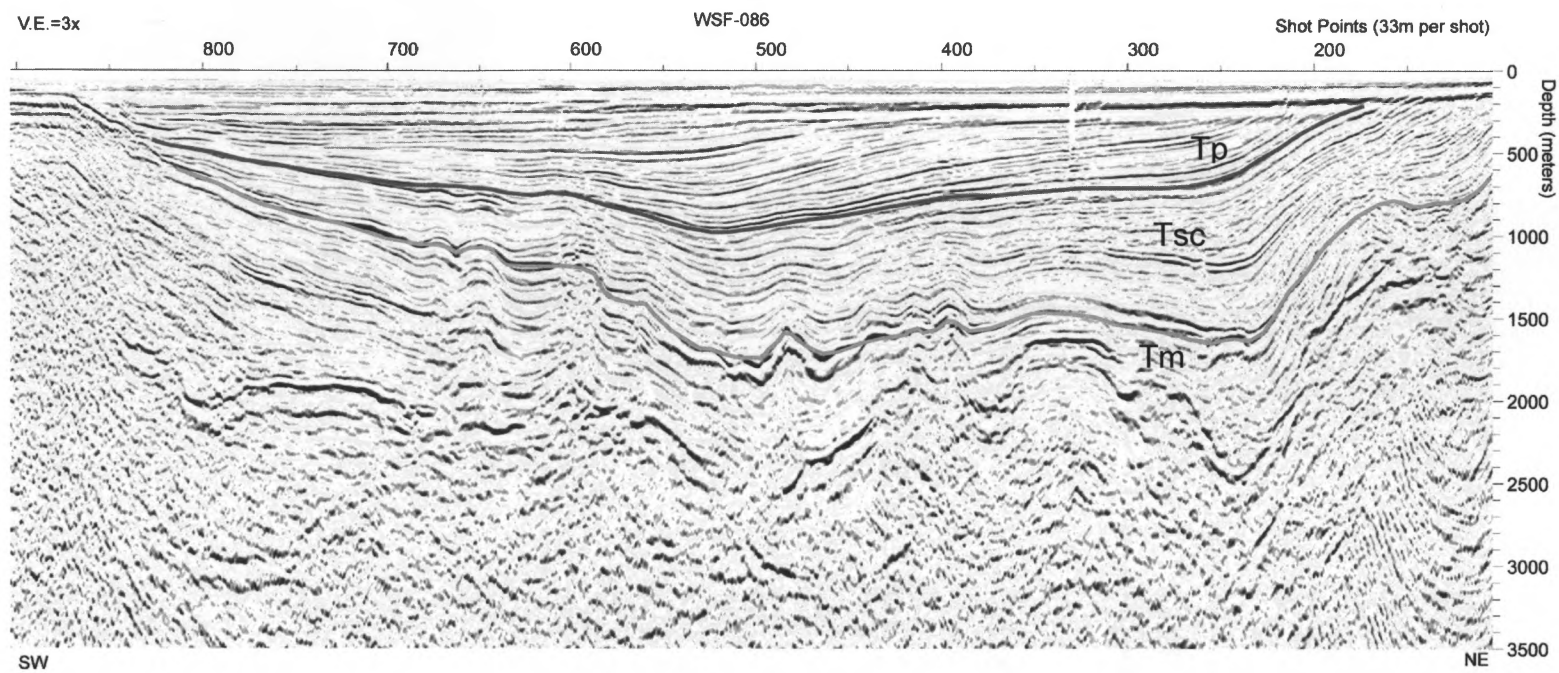


Figure 12: Depth converted MCS profile WSF-086. Dark blue is top of the Santa Cruz Mudstone; green is top of the Monterey Formation. Location of profile shown in Fig. 4.

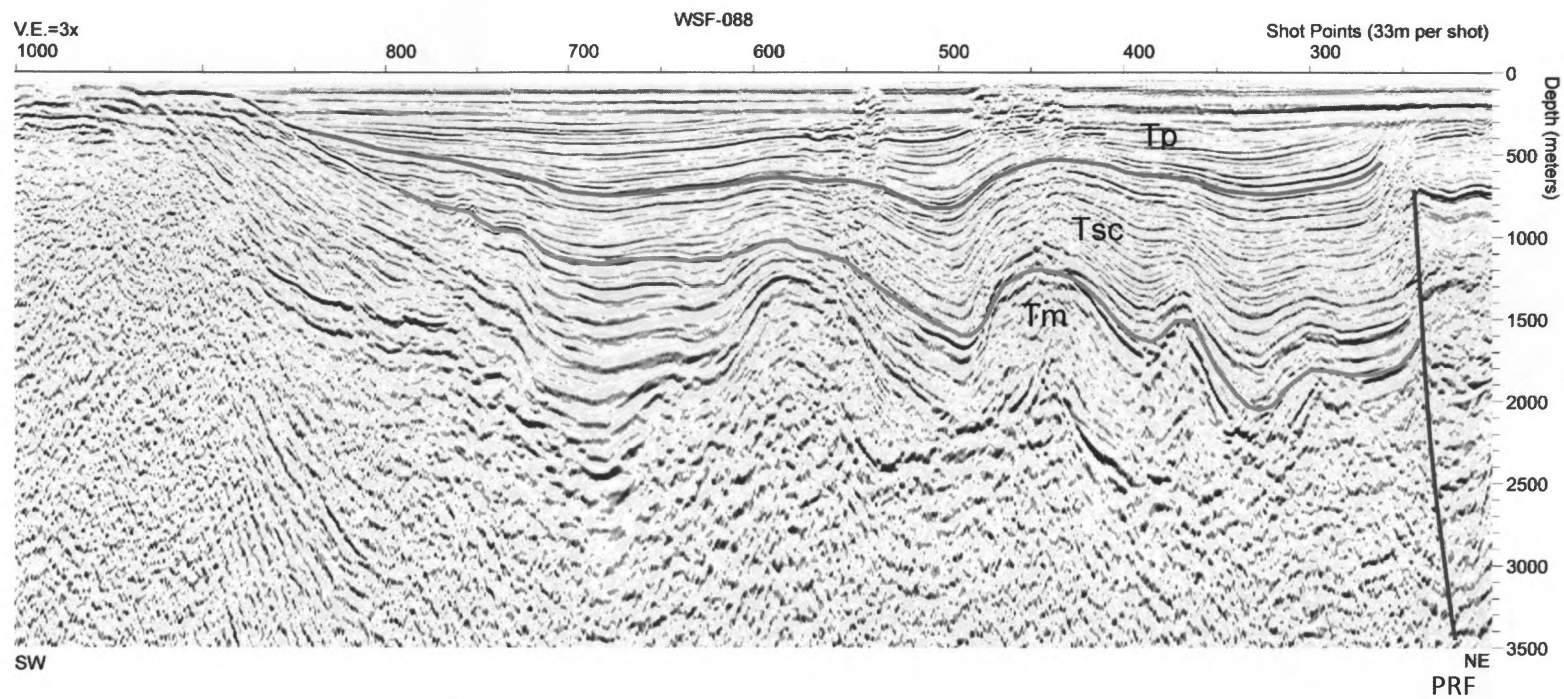


Figure 13: Depth converted MCS profile WSF-088. Dark blue is top of the Santa Cruz Mudstone; green is top of the Monterey Formation; red is the PRF. Location of profile shown in Fig. 4.

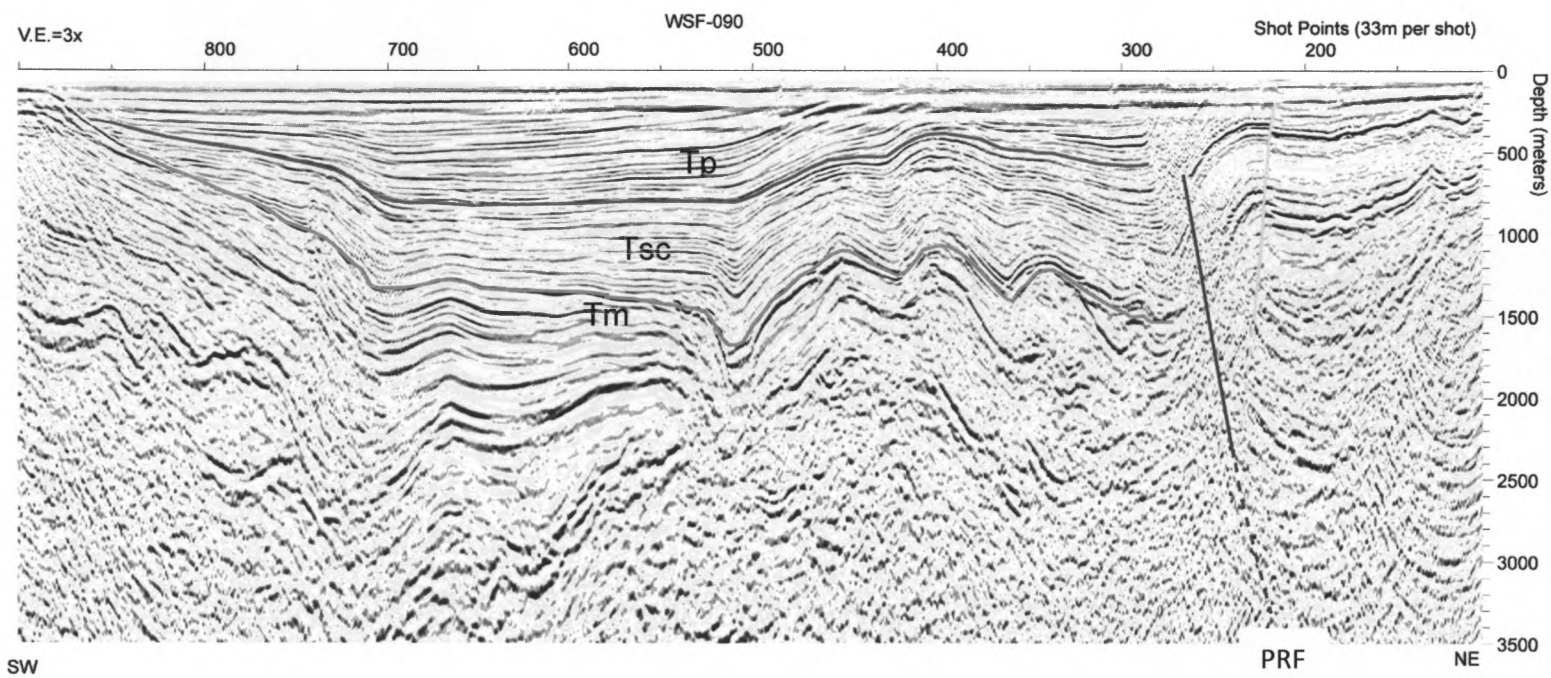


Figure 14: Depth converted MCS profile WSF-090. Blue is top of the Santa Cruz Mudstone; green is top of the Monterey Formation; red is the PRF; yellow is a reverse fault with opposite vergence to the PRF. Location of profile shown in Fig. 4.

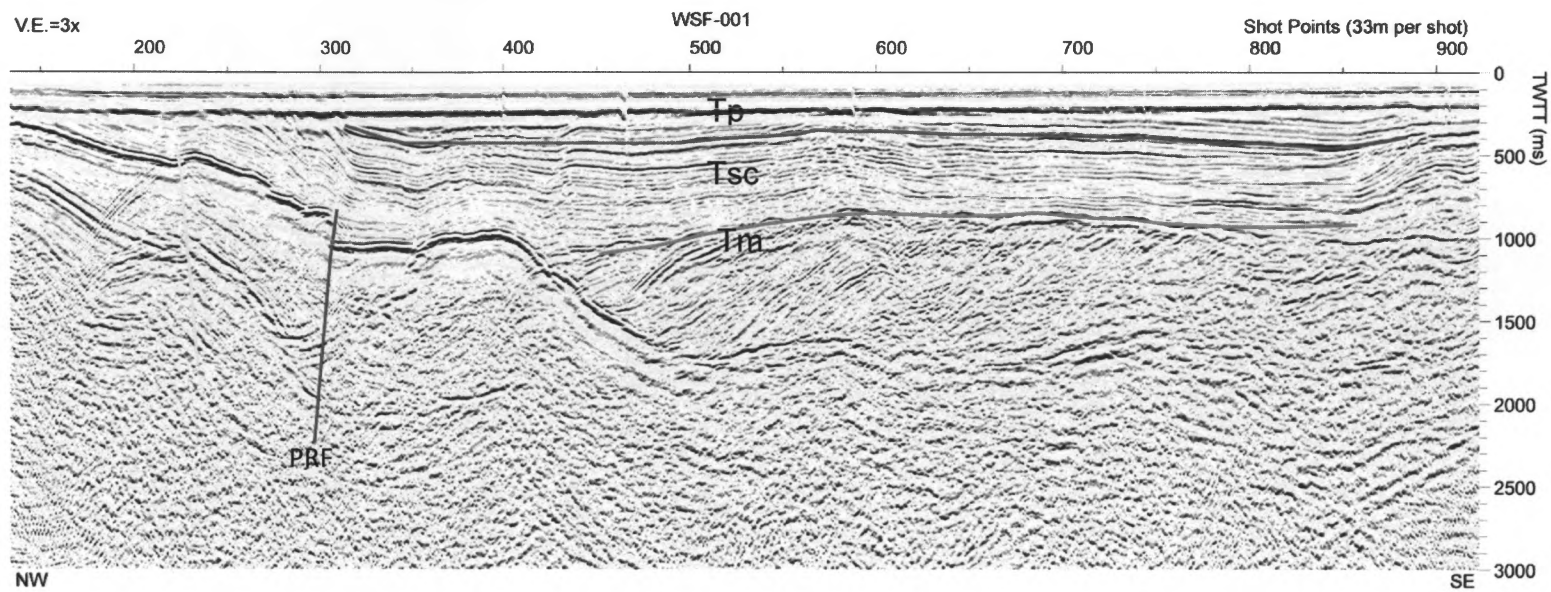


Figure 15: MCS profile WSF-001 (in TWTT). Dark blue is top of the Santa Cruz Mudstone; green is top of the Monterey Formation; red is the PRF; yellow is a reverse fault with opposite vergence to the PRF. Location of profile shown in Fig. 4.

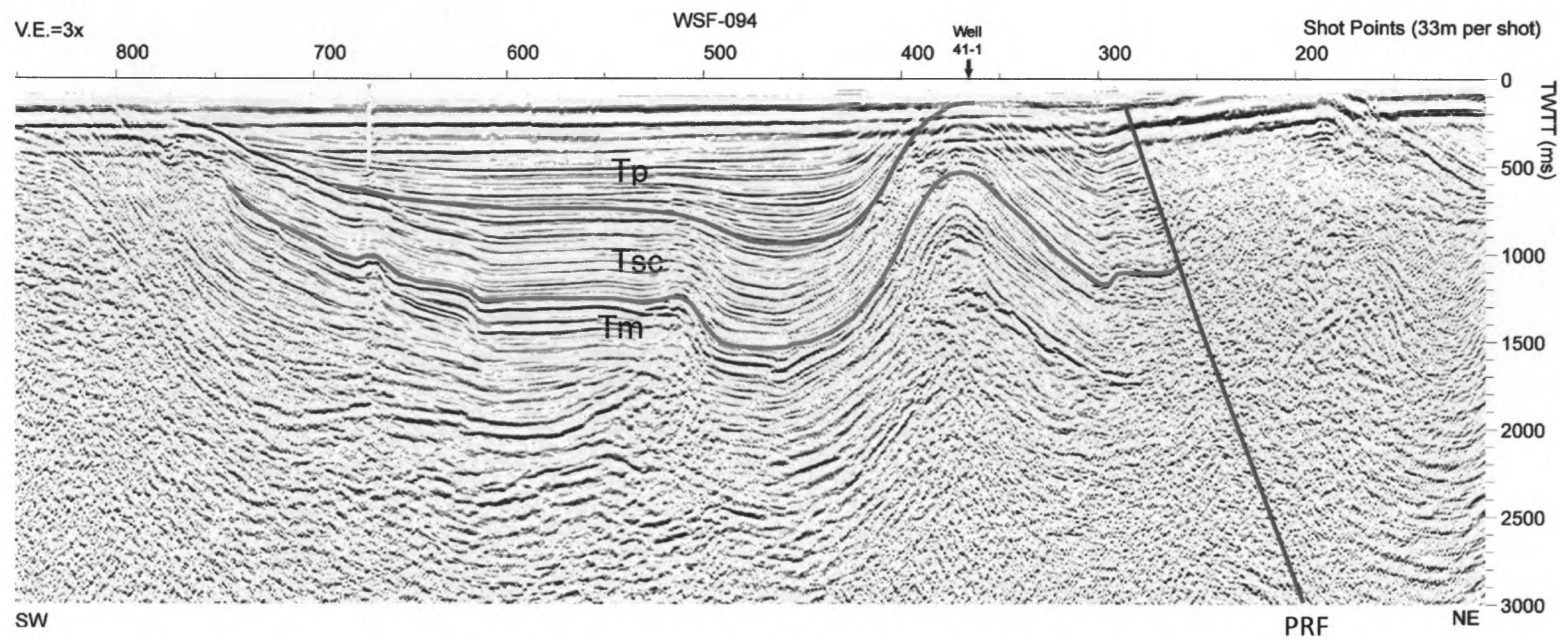


Figure 16: MCS profile WSF-094 (in TWTT). Light blue is top of the Santa Cruz Mudstone; green is top of the Monterey Formation; red is the PRF. Location of profile shown in Fig. 4.

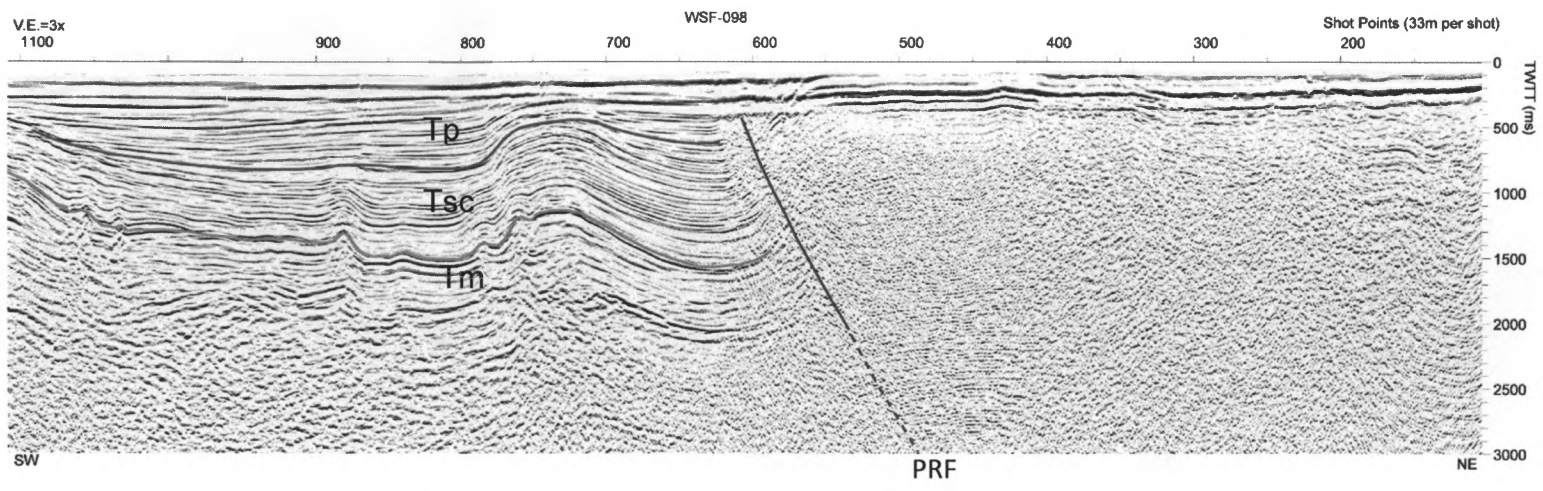


Figure 17: MCS profile WSF-098 (in TWTT). Dark blue is top of the Santa Cruz Mudstone; green is top of the Monterey Formation; red is the PRF. Location of profile shown in Fig. 4.

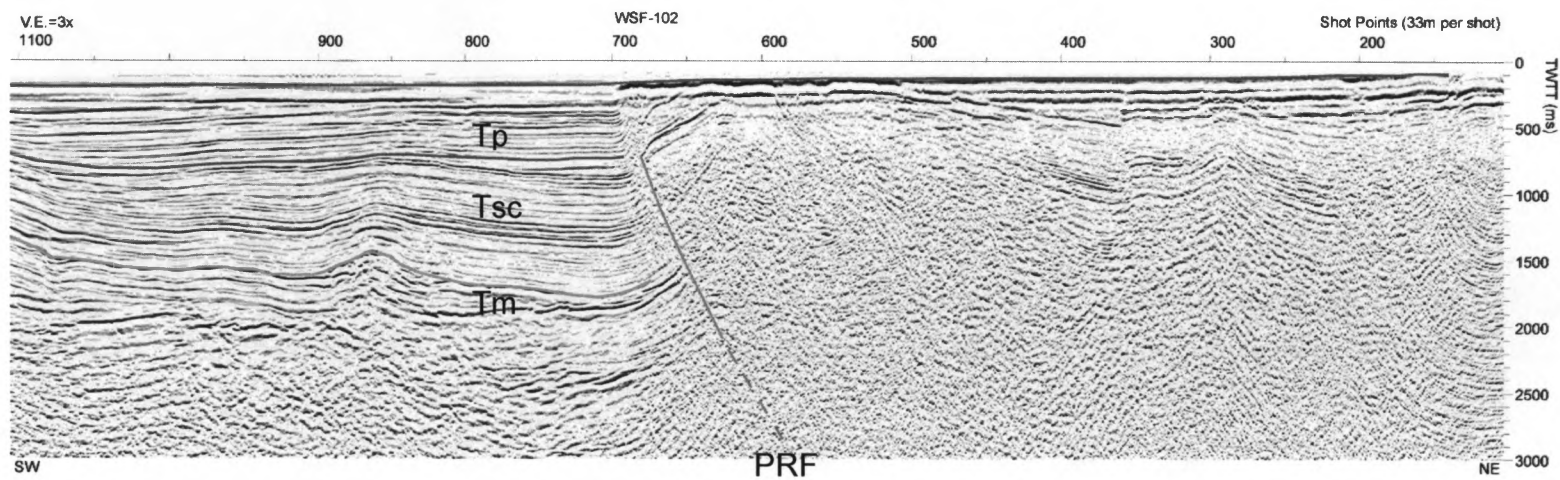


Figure 18: MCS profile WSF-102 (in TWTT). Dark blue is top of the Santa Cruz Mudstone; green is top of the Monterey Formation; red is the PPU; orange is the PRF. Location of profile shown in Fig. 4.

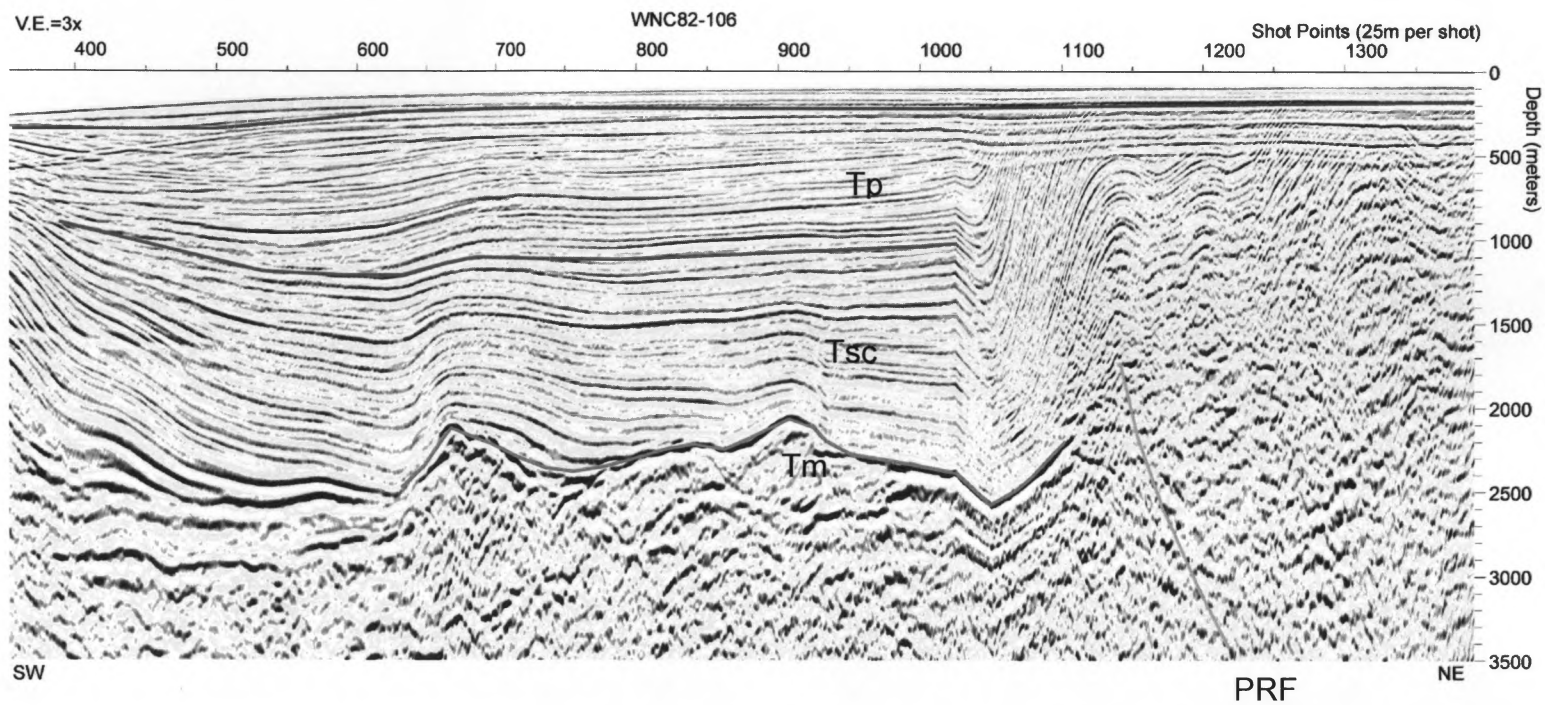


Figure 19: Depth converted MCS profile WNC82-106. Dark blue is top of the Santa Cruz Mudstone; green is top of the Monterey Formation; red is the PPU; orange is the PRF. Location of profile shown in Fig. 4.

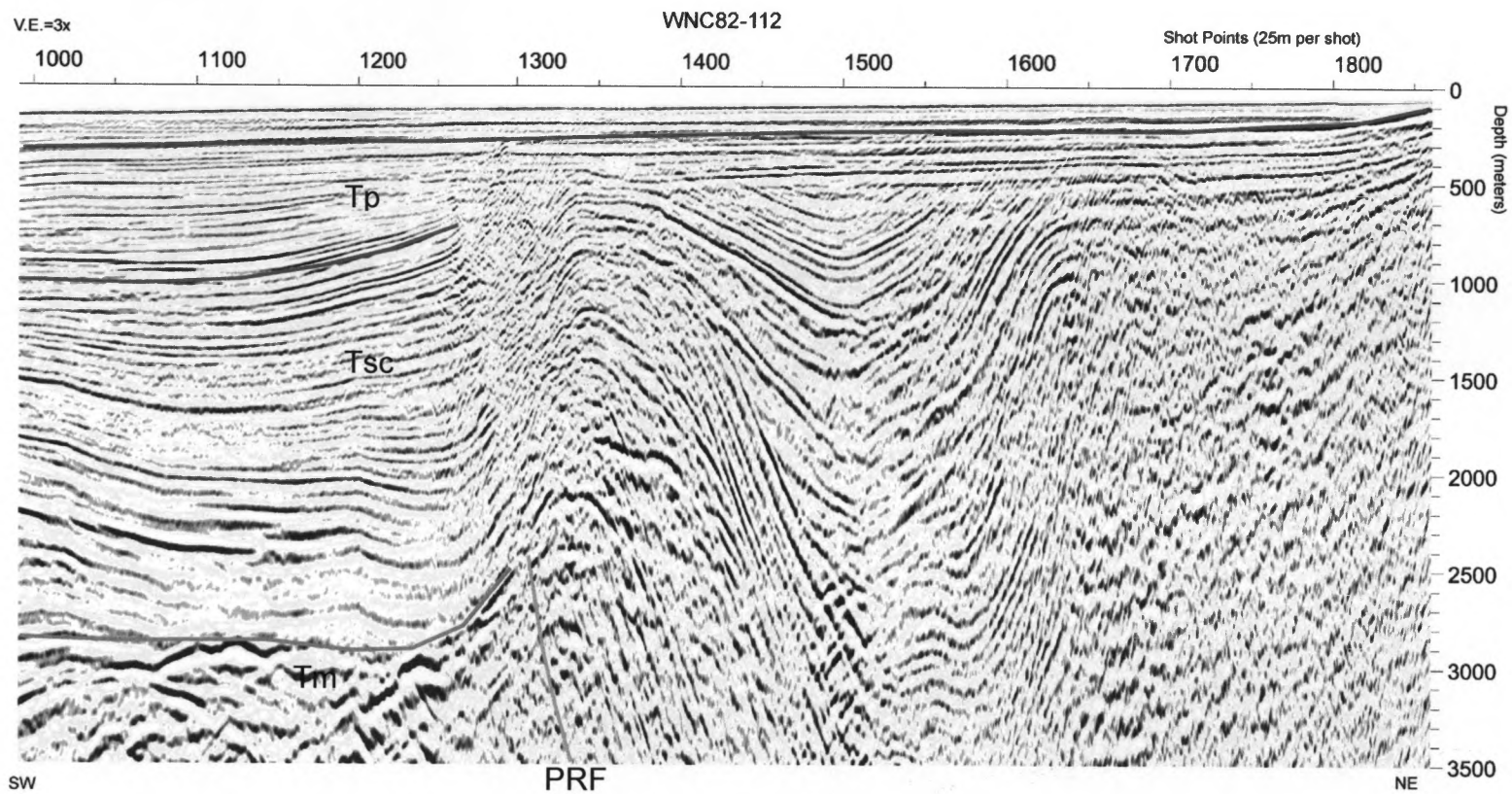


Figure 20: Depth converted MCS profile WNC82-112. Dark blue is top of the Santa Cruz Mudstone; green is top of the Monterey Formation; red is the PPU; orange is the PRF. Location of profile shown in Fig. 4.

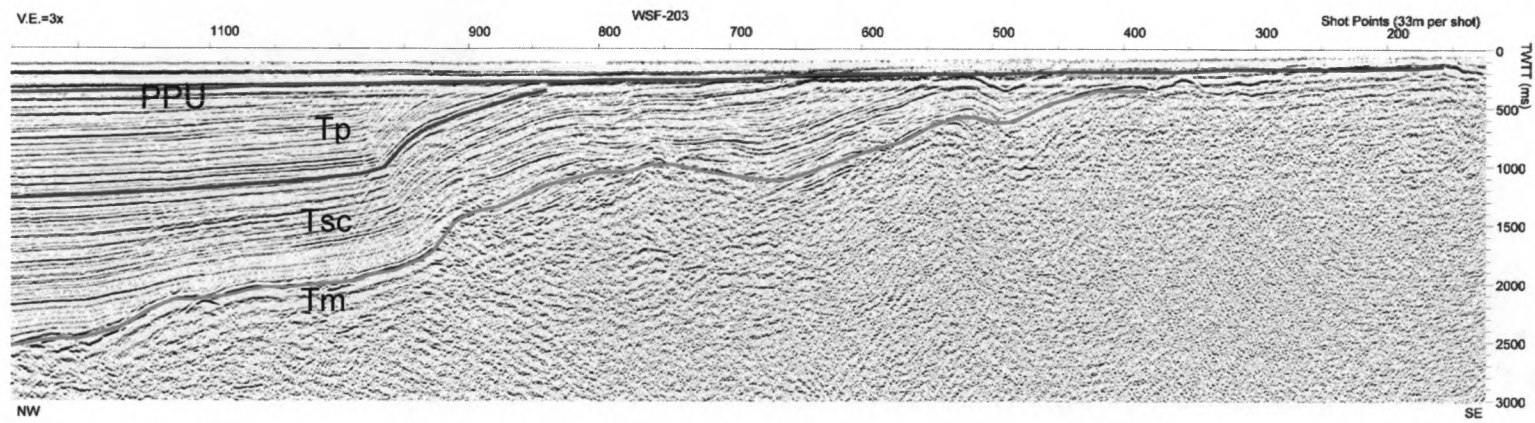


Figure 21: MCS profile WSF-203 (in TWTT). Dark blue is top of the Santa Cruz Mudstone; green is top of the Monterey Formation; red is the PPU. Location of profile shown in Fig. 4.

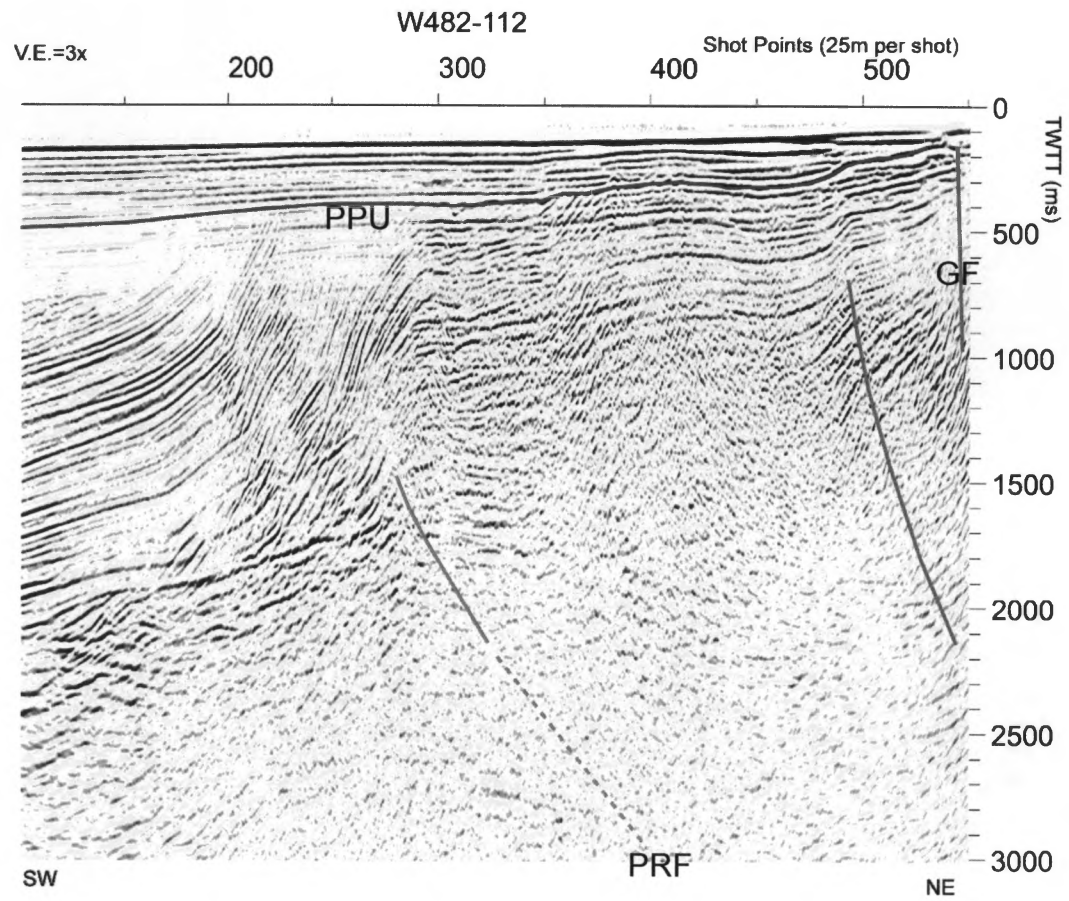


Figure 22: MCS profile W482-112 (in TWTT). Red is the PPU; orange is the PRF; grey is an unnamed fault; pink is the Gualala fault. Location of profile shown in Fig. 4.

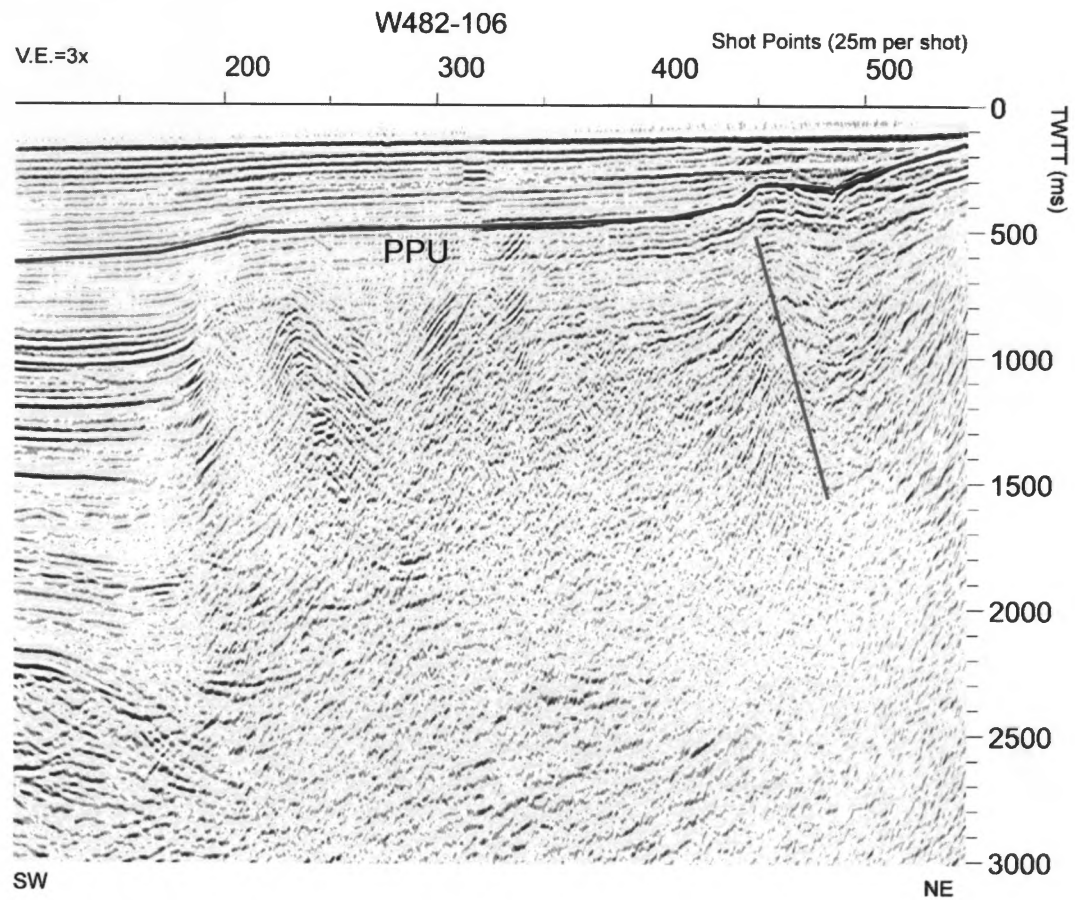


Figure 23: MCS profile W482-106 (in TWTT). Red is the PPU; grey is an unnamed fault. Location of profile shown in Fig. 4.

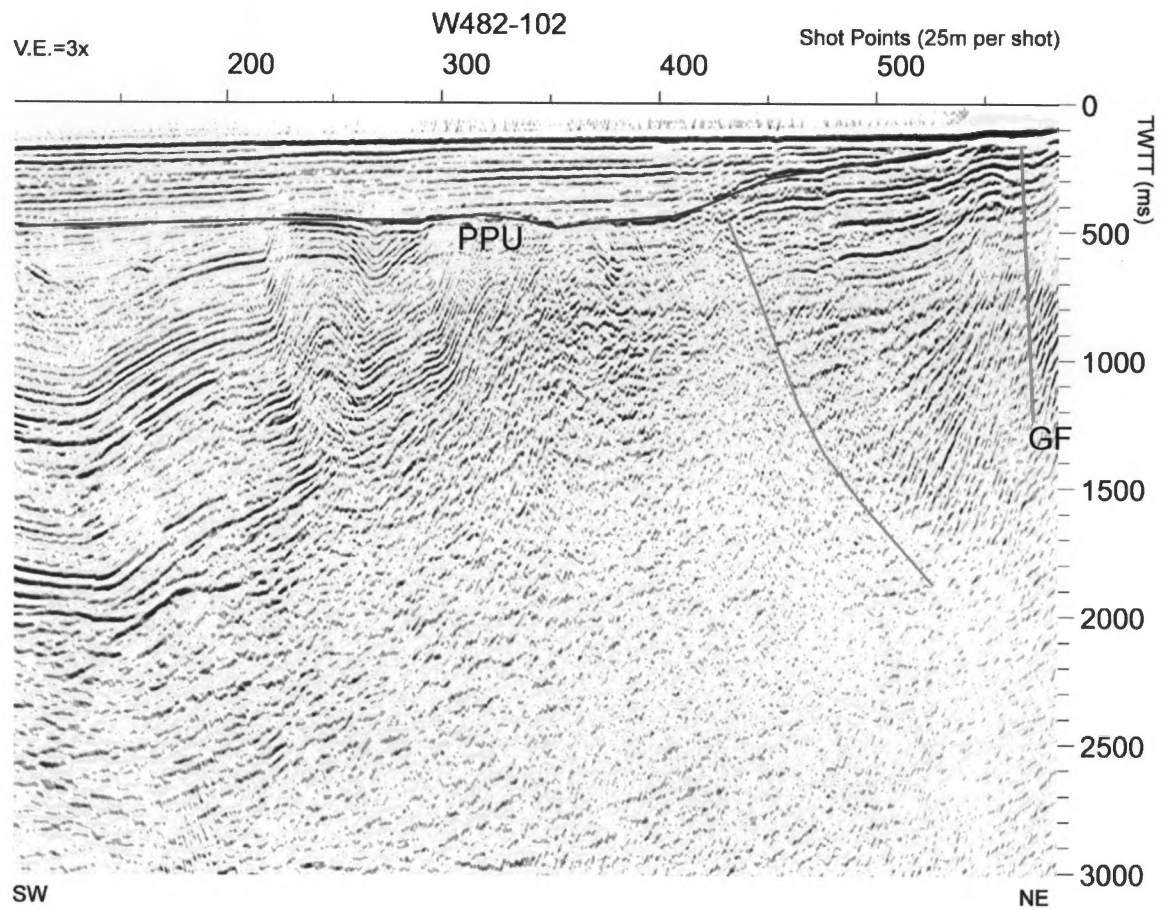


Figure 24: MCS profile W482-102 (in TWTT). Red is the PPU; grey is an unnamed fault; pink is the Gualala fault. Location of profile shown in Fig. 4.

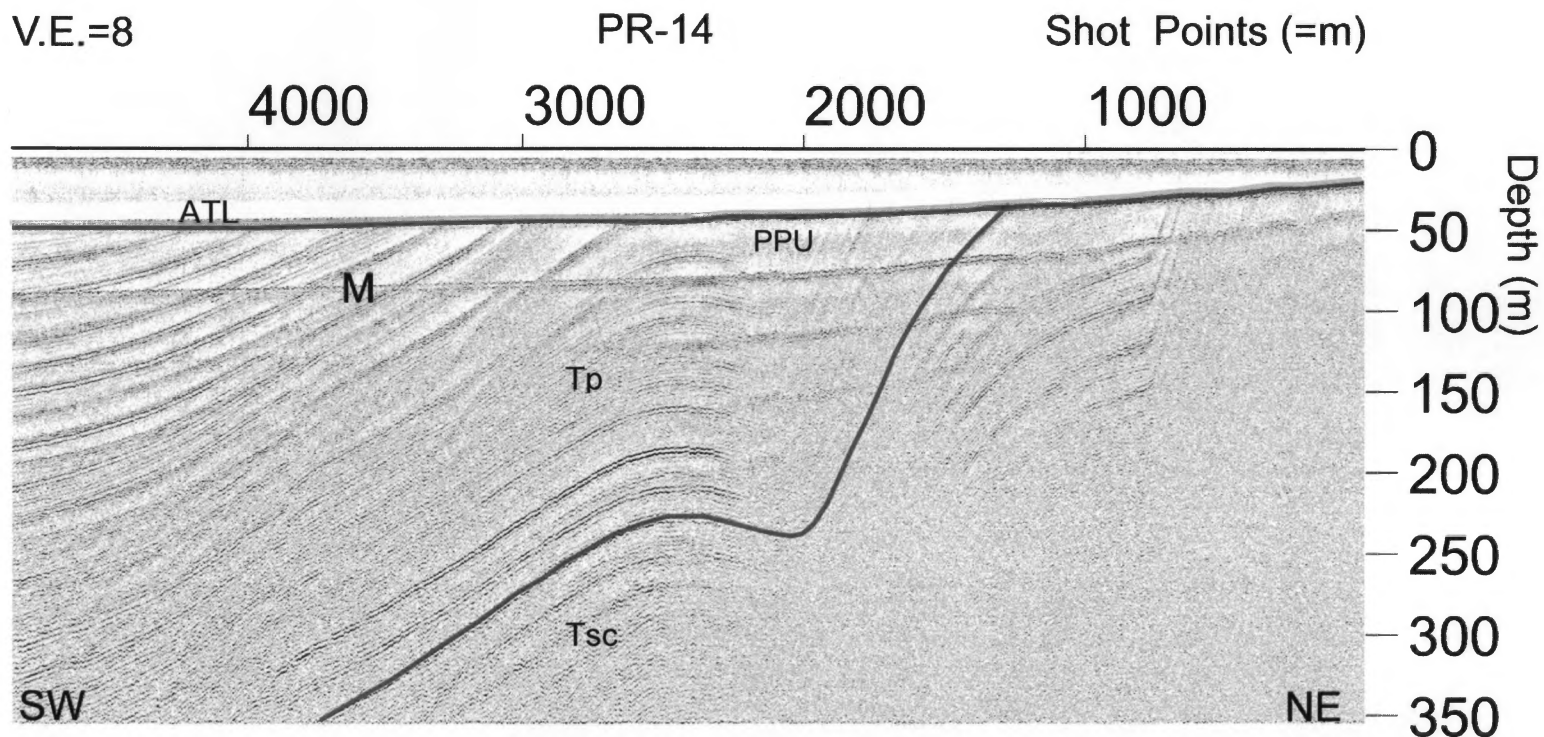


Figure 25: Depth converted mini-sparker seismic reflection profile PR-14. Blue is top of the Santa Cruz Mudstone; red is the PPU; green is the base of the ATL; M denotes the water bottom multiple. Location of profile shown in Fig. 4.

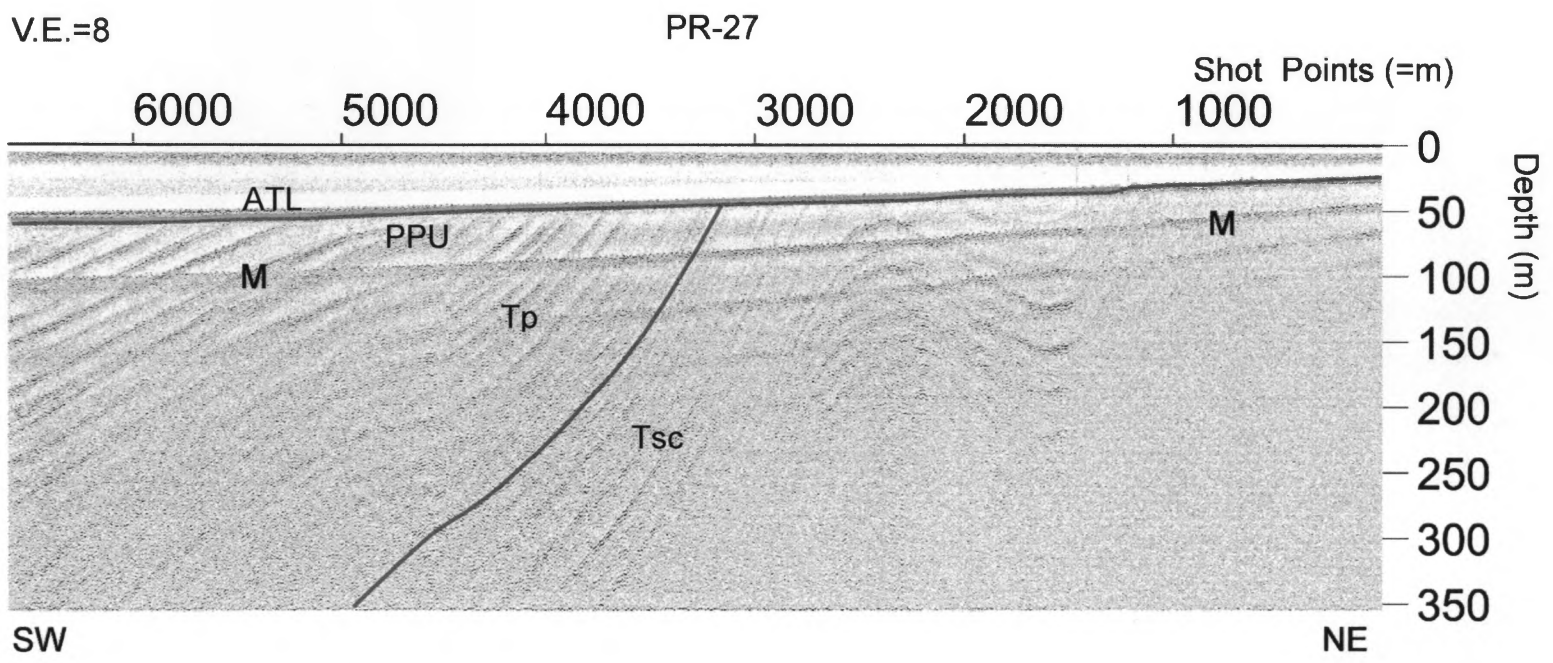


Figure 26: Depth converted mini-sparker seismic reflection profile PR-27. Blue is top of the Santa Cruz Mudstone; red is the PPU; green is the base of the ATL; M denotes the water bottom multiple. Location of profile shown in Fig. 4.

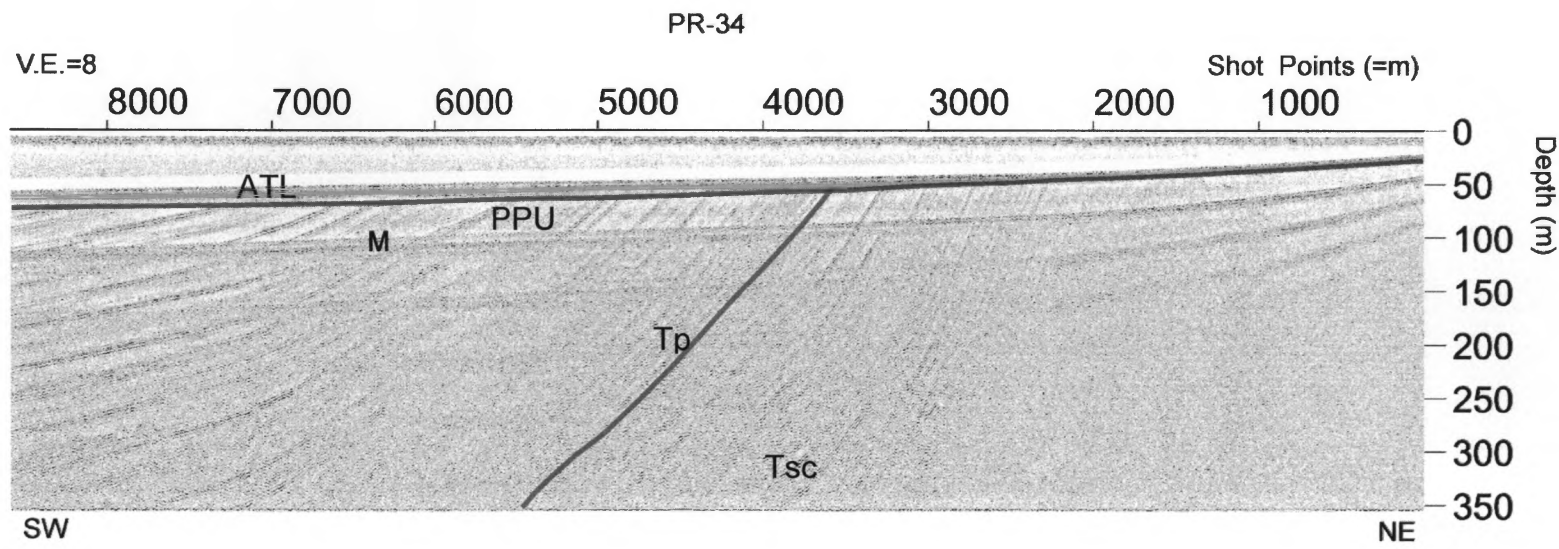


Figure 27: Depth converted mini-sparker seismic reflection profile PR-34. Blue is top of the Santa Cruz Mudstone; red is the PPU; green is the base of the ATL; M denotes the water bottom multiple. Location of profile shown in Fig. 4.

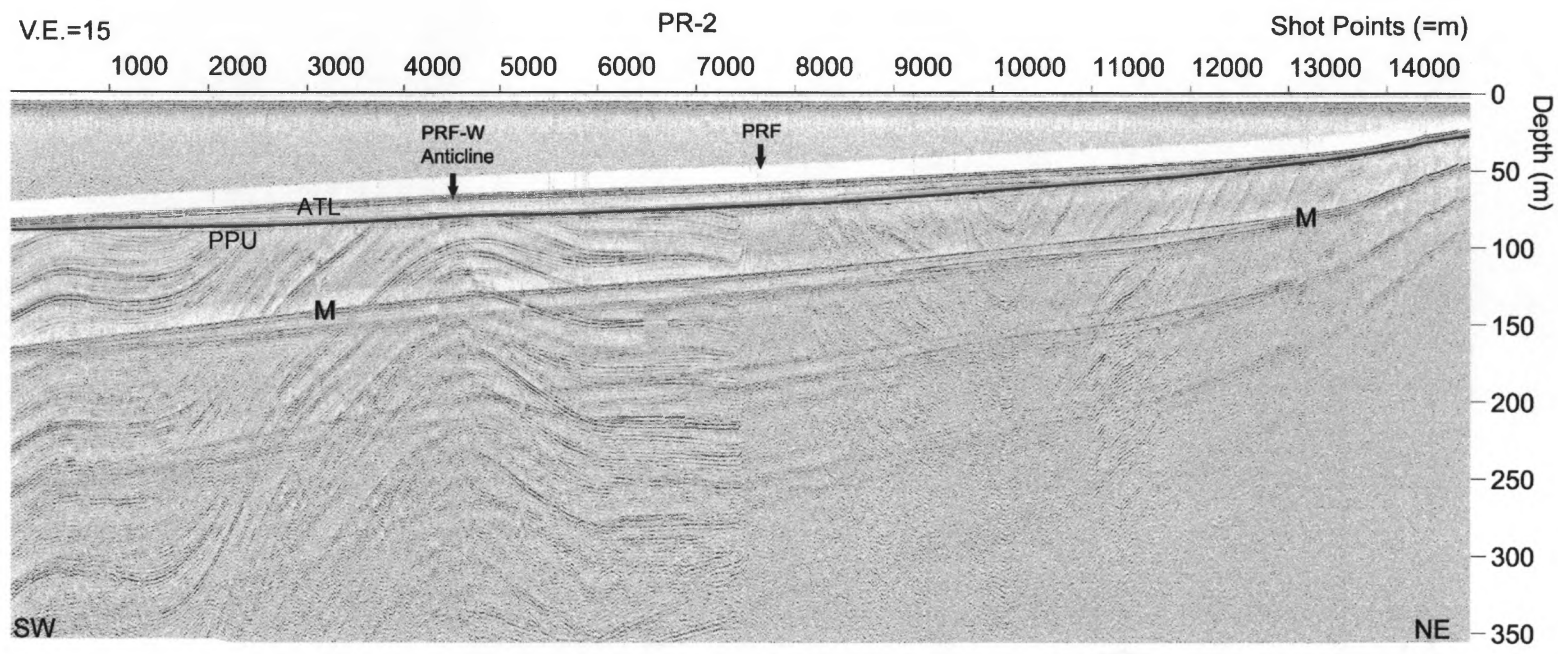


Figure 28: Depth converted mini-sparker seismic reflection profile PR-2. Red is the PPU; green is the base of the ATL; M denotes the water bottom multiple. Location of profile shown in Fig. 4.

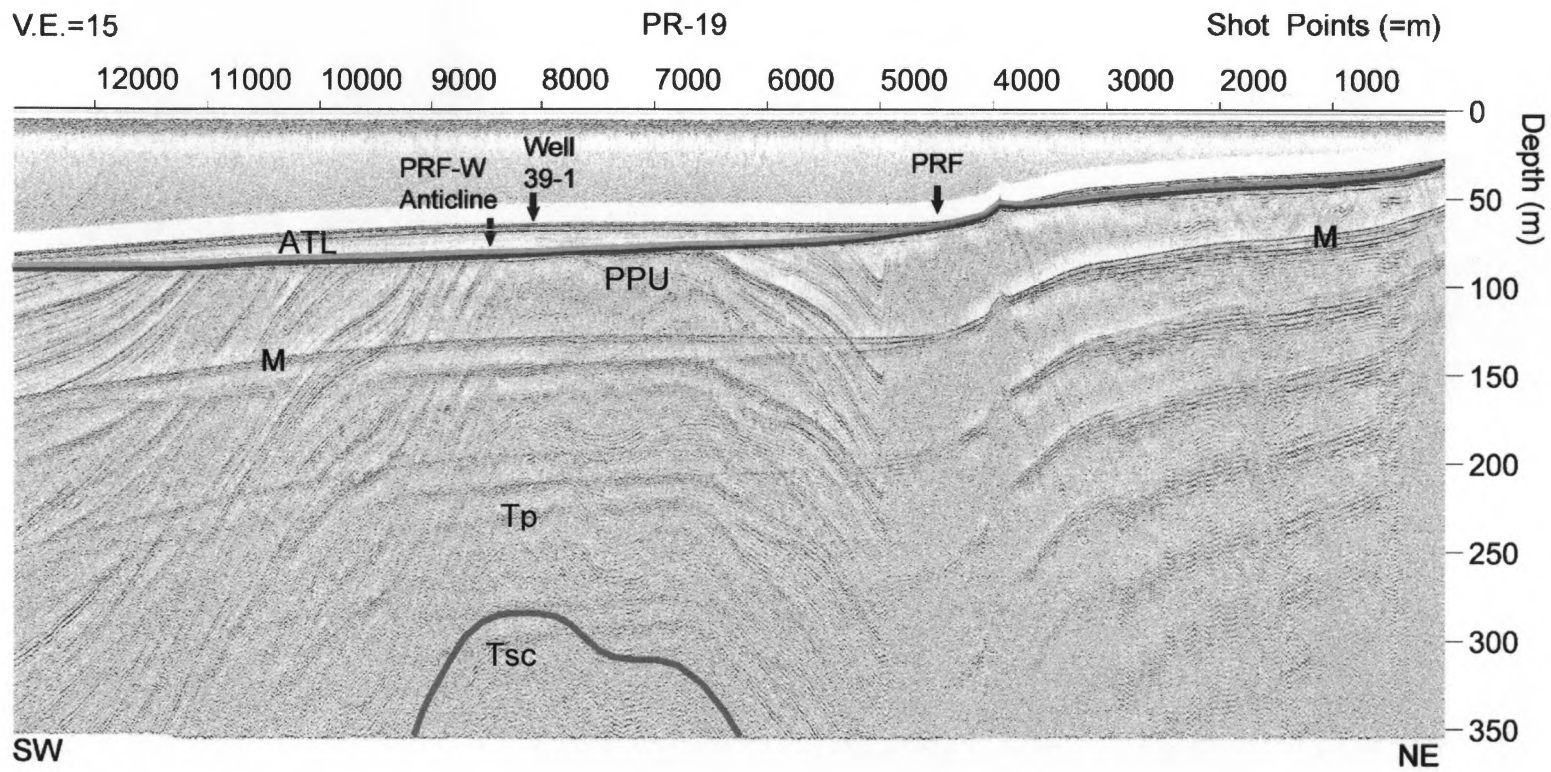


Figure 29: Depth converted mini-sparker seismic reflection profile PR-19. Blue is top of the Santa Cruz Mudstone; red is the PPU; green is the base of the ATL; M denotes the water bottom multiple. Location of profile shown in Fig. 4.

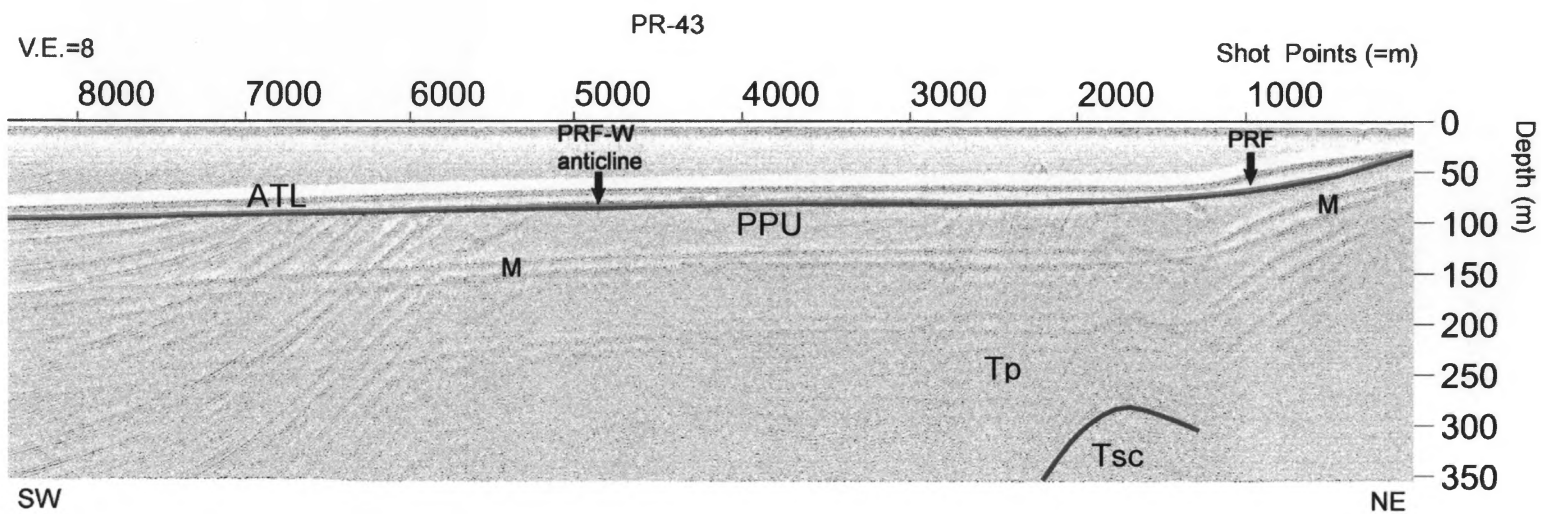


Figure 30: Depth converted mini-sparker seismic reflection profile PR-43. Blue is top of the Santa Cruz Mudstone; red is the PPU; green is the base of the ATL; M denotes the water bottom multiple. Location of profile shown in Fig. 4.

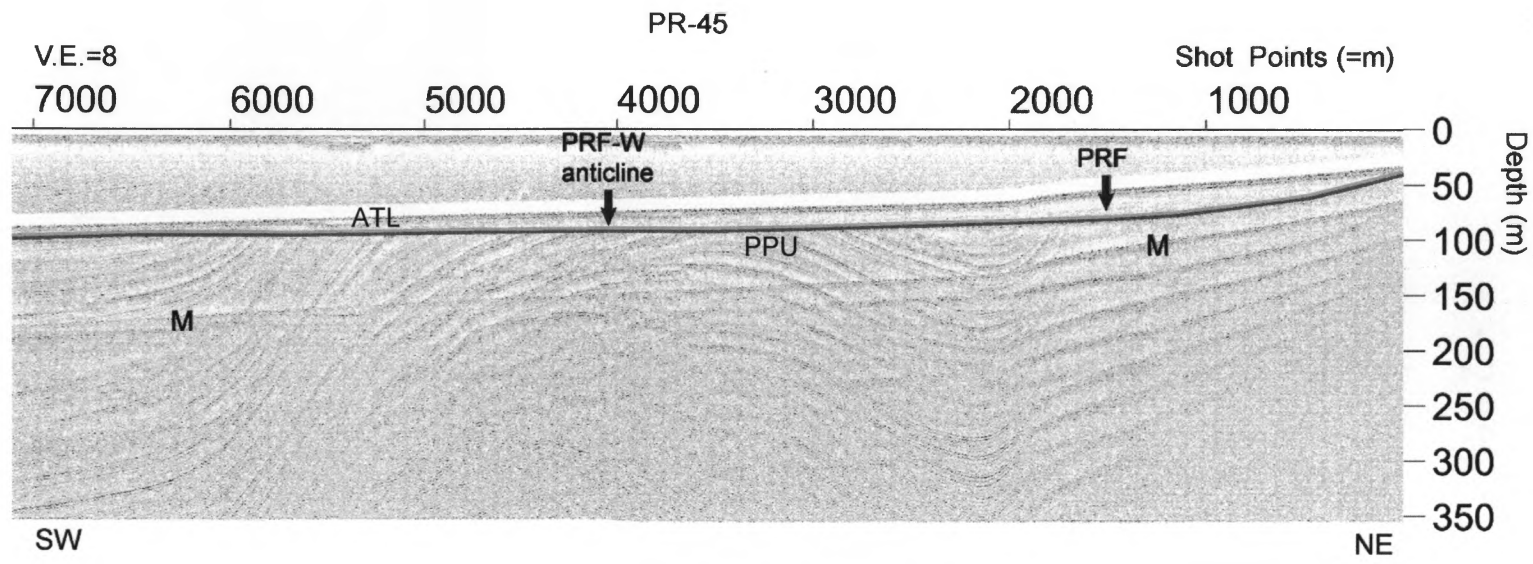


Figure 31: Depth converted mini-sparker seismic reflection profile PR-45. Red is the PPU; green is the base of the ATL; M denotes the water bottom multiple. Location of profile shown in Fig. 4.

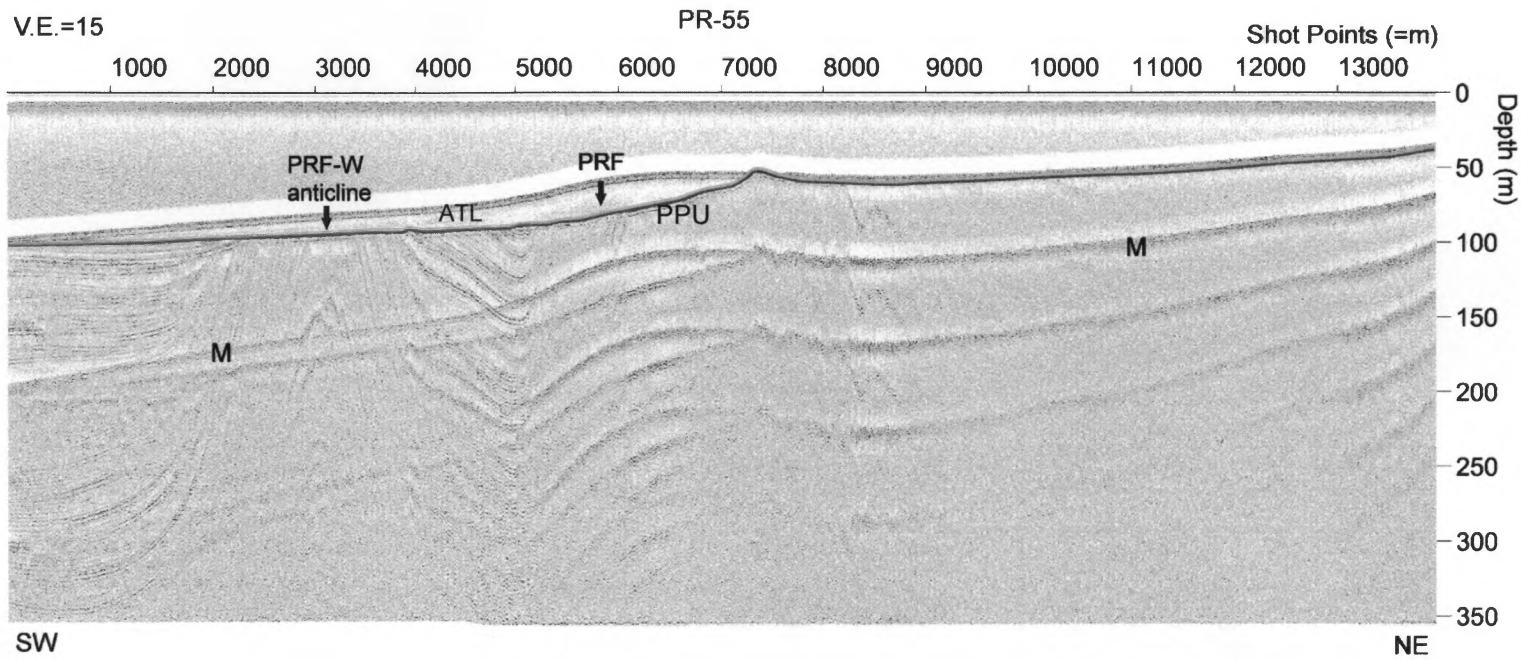


Figure 32: Depth converted mini-sparker seismic reflection profile PR-55. Red is the PPU; green is the base of the ATL; M denotes the water bottom multiple. Location of profile shown in Fig. 4.

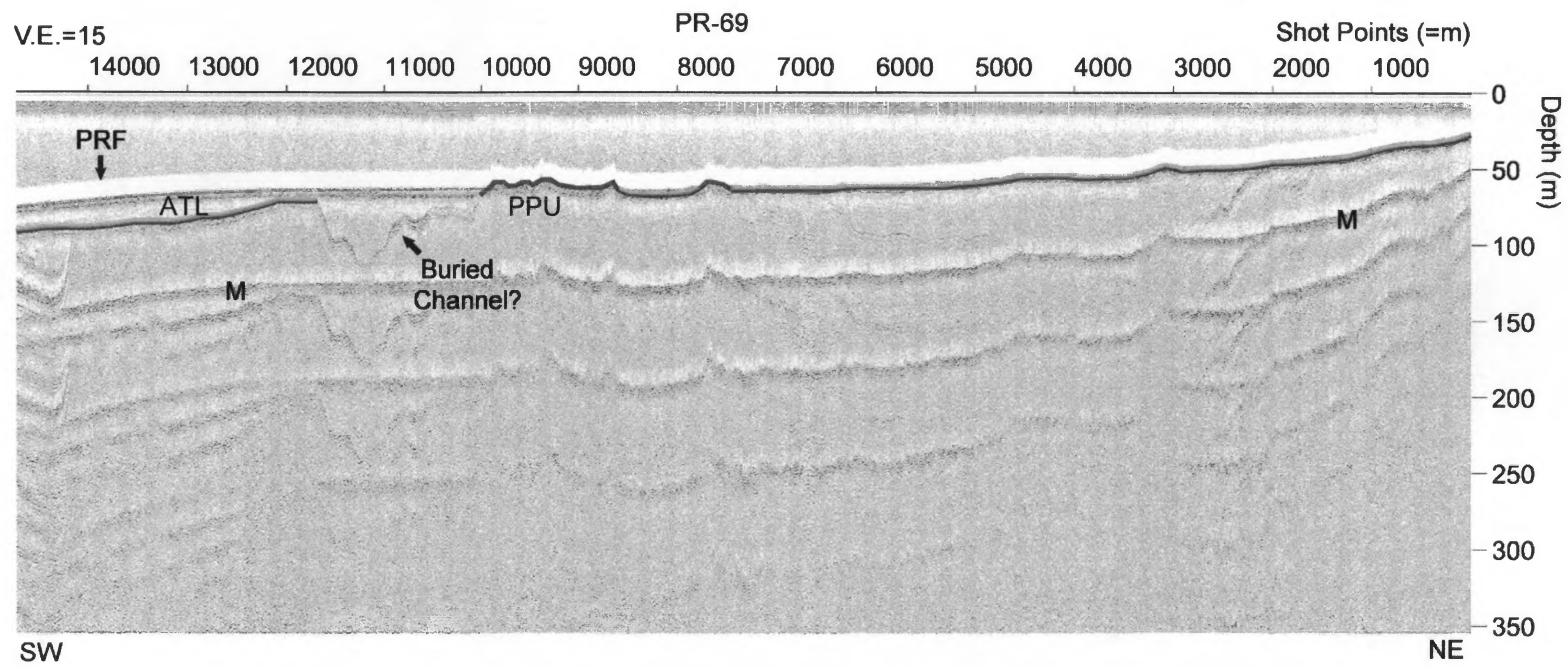


Figure 33: Depth converted mini-sparker seismic reflection profile PR-69. Red is the PPU; green is the base of the ATL; M denotes the water bottom multiple. Location of profile shown in Fig. 4.

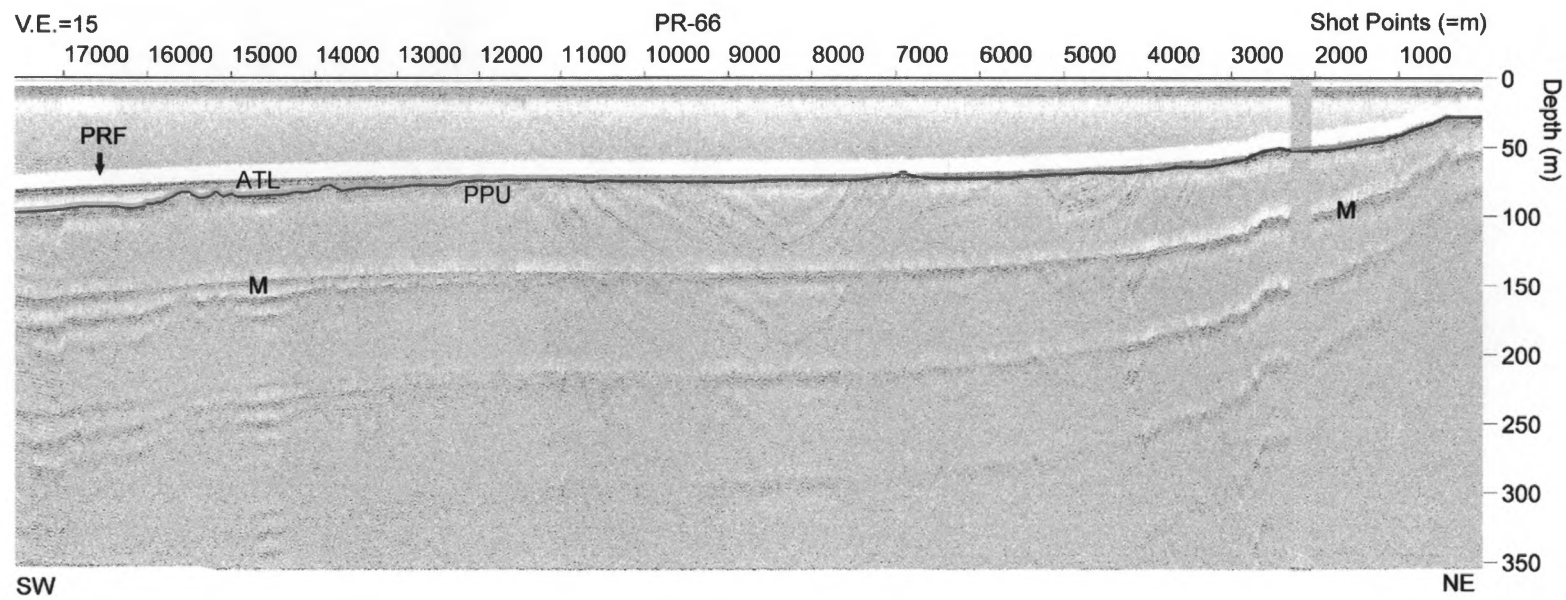


Figure 34: Depth converted mini-sparker seismic reflection profile PR-65. Red is the PPU; green is the base of the ATL; M denotes the water bottom multiple. Location of profile shown in Fig. 4.

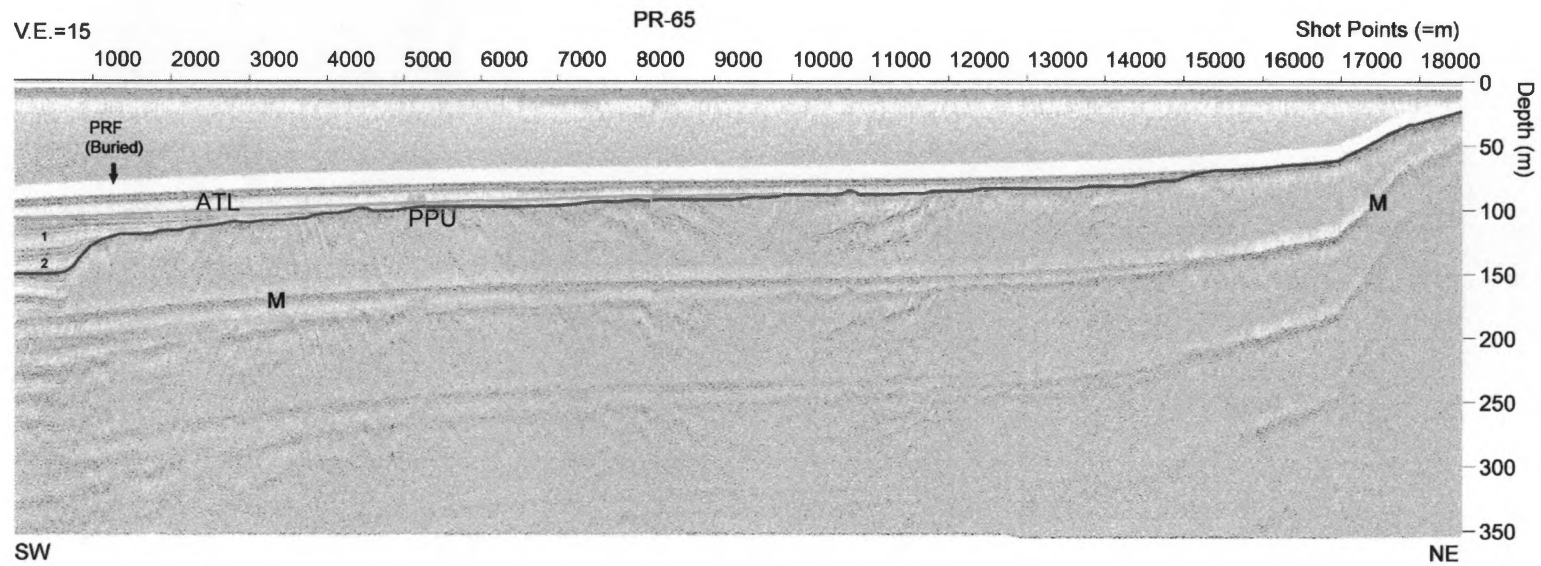


Figure 35: Depth converted mini-sparker seismic reflection profile PR-65. Red is PPU; green is the base of the ATL; M denotes the water bottom multiple. Location of profile shown in Fig. 4.

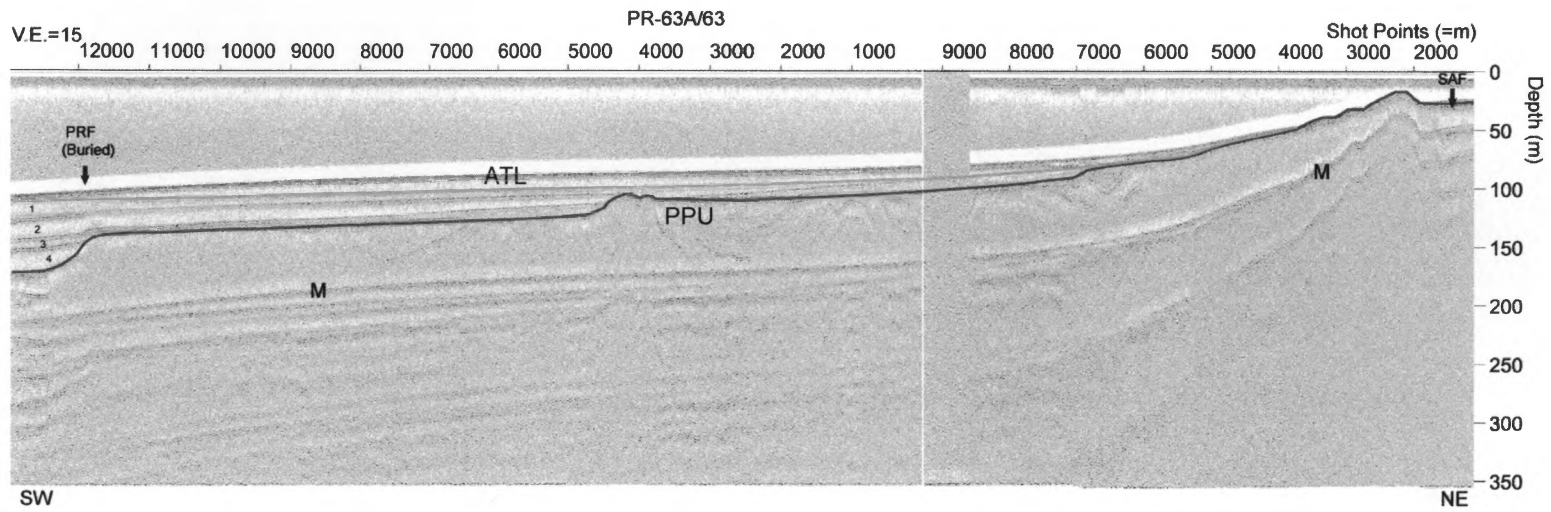


Figure 36: Depth converted mini-sparker seismic reflection profile PR-63A/63. Red is the PPU; green is the base of the ATL; M denotes the water bottom multiple. Location of profile shown in Fig. 4.

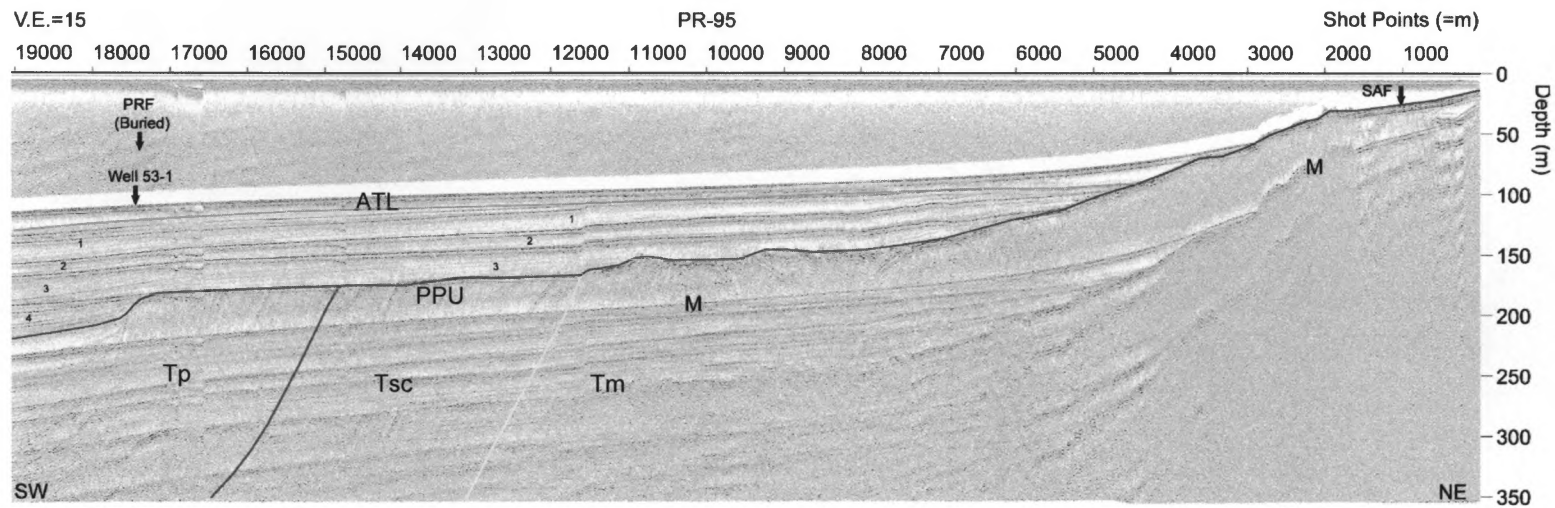


Figure 37: Depth converted mini-sparker seismic reflection profile PR-95. Red is the PPU; green is the base of the ATL; blue is top of the Santa Cruz Mudstone; yellow is top of the Monterey Formation; M denotes the water bottom multiple. Note the relatively undeformed sequences preserved above the PPU. Location of profile shown in Fig. 4.

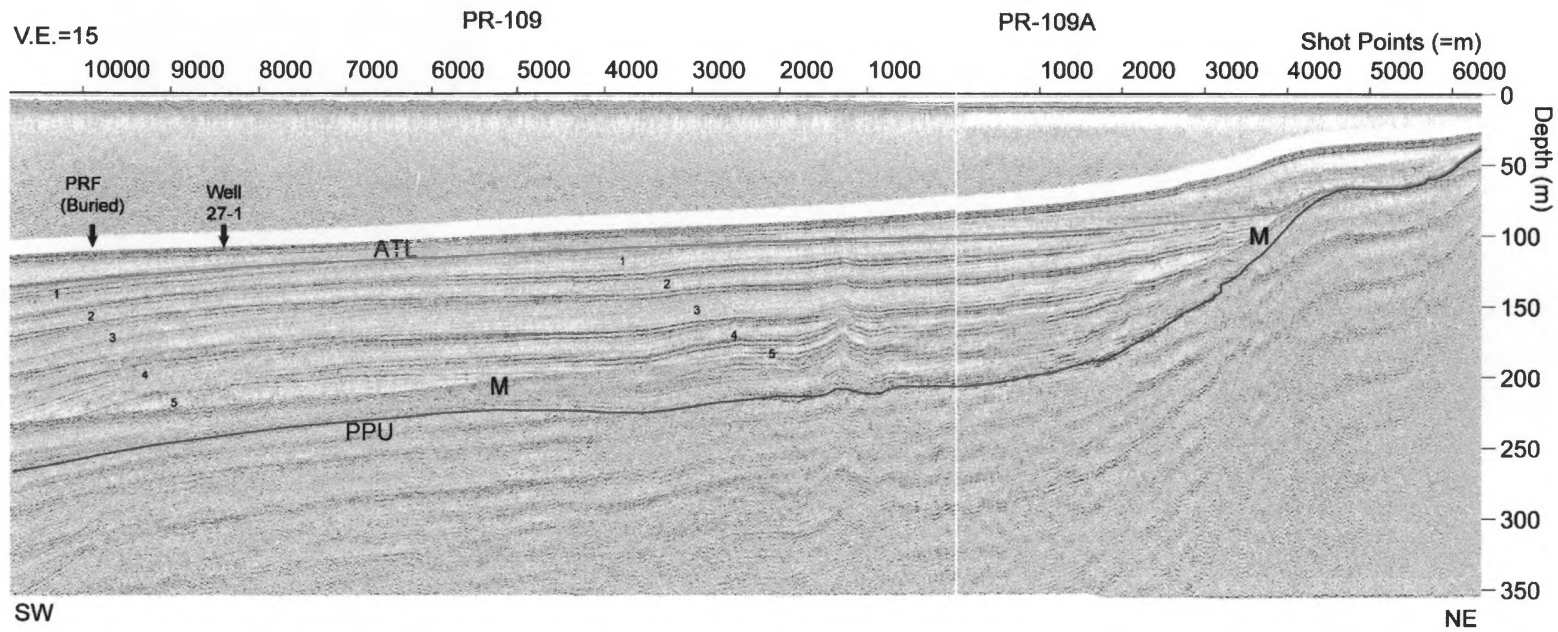


Figure 38: Depth converted mini-sparker seismic reflection profile PR-109/109A. Red is the PPU; green is the base of the ATL; M denotes the water bottom multiple. Location of profile shown in Fig. 4.

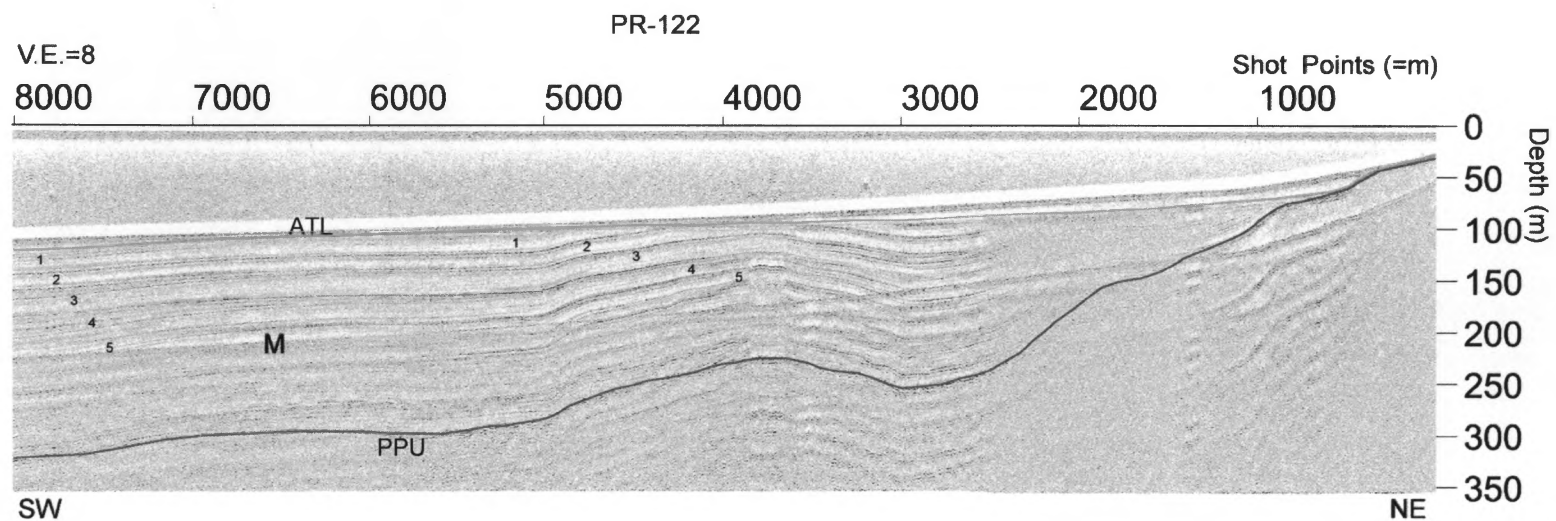


Figure 39: Depth converted mini-sparker seismic reflection profile PR-122. Red is the PPU; green is the base of the ATL; M denotes the water bottom multiple. Note the shortening of the Quaternary sequences and the PPU surface. Location of profile shown in Fig. 4.

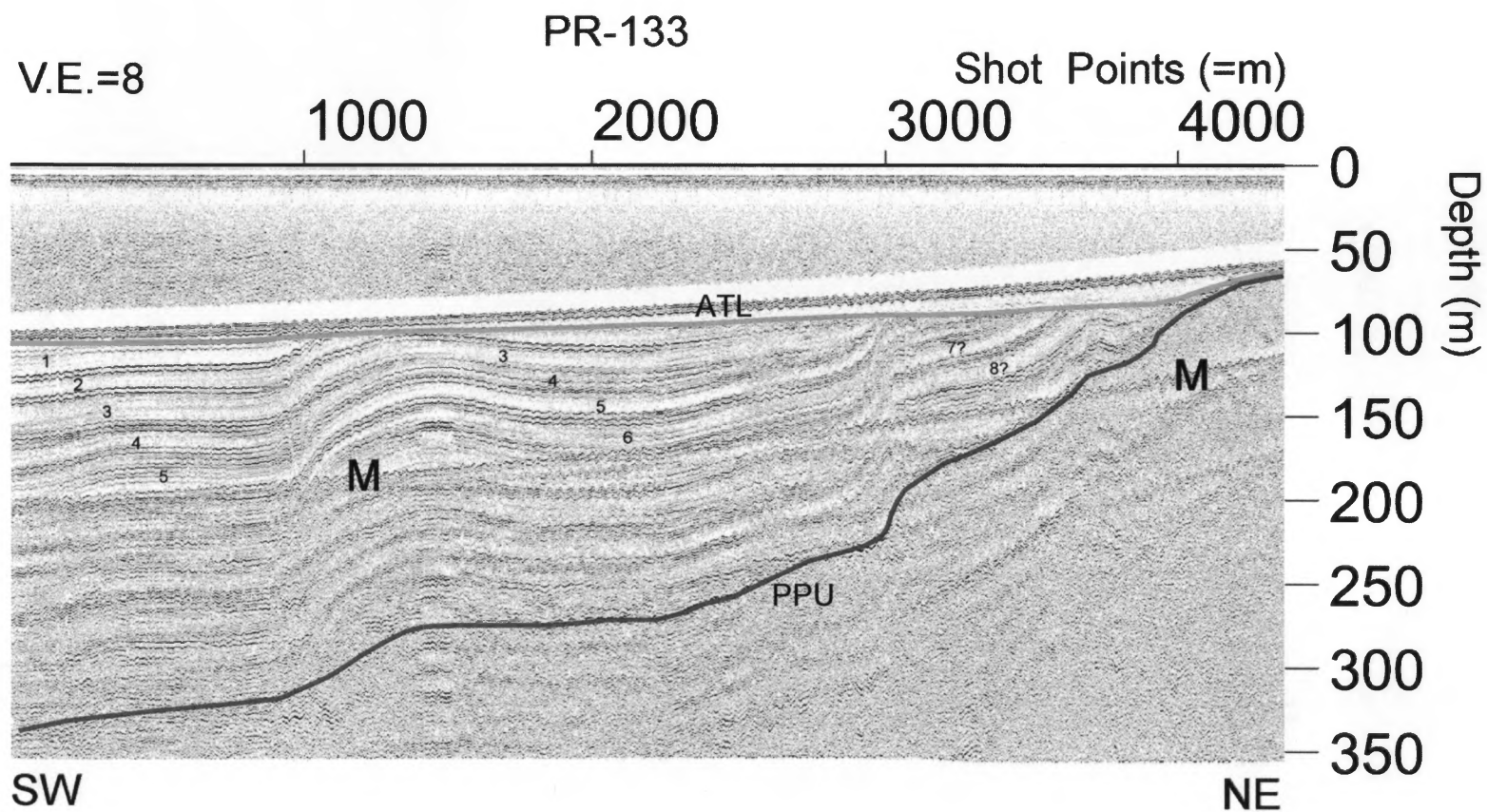


Figure 40: Depth converted mini-sparker seismic reflection profile PR-133. Red is the PPU; green is the base of the ATL; M denotes the water bottom multiple. Location of profile shown in Fig. 4.

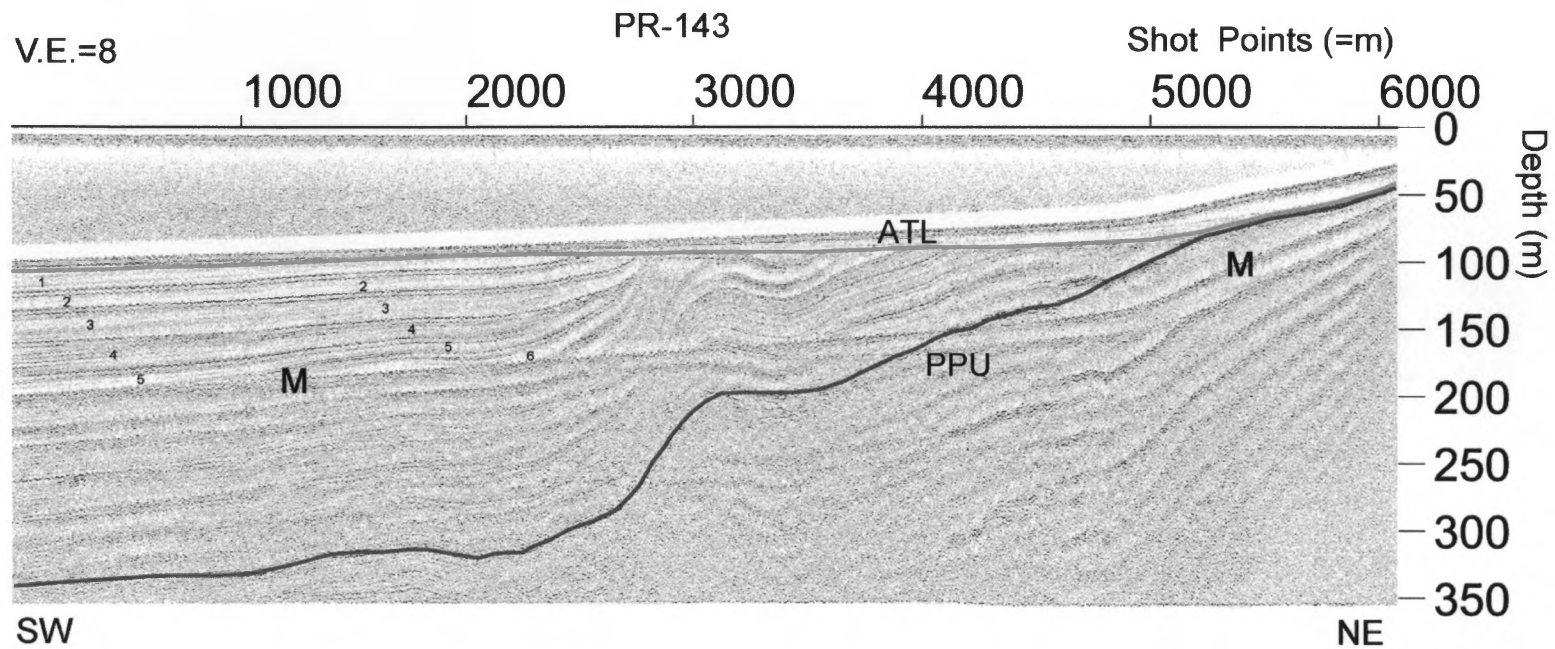


Figure 41: Depth converted mini-sparker seismic reflection profile PR-143. Red is the PPU; green is the base of the ATL; M denotes the water bottom multiple. Location of profile shown in Fig. 4.

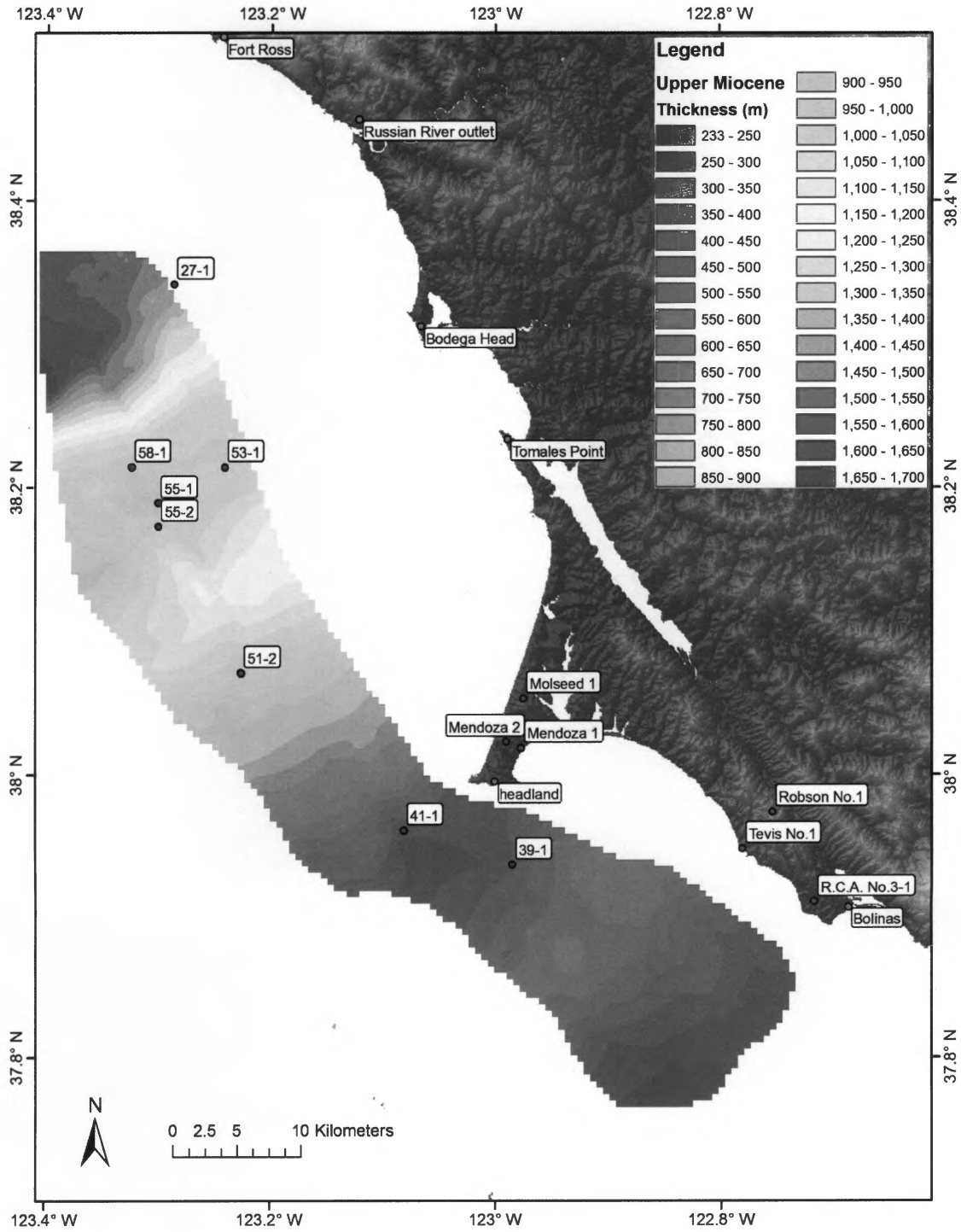


Figure 42: Isopach map of Upper Miocene units

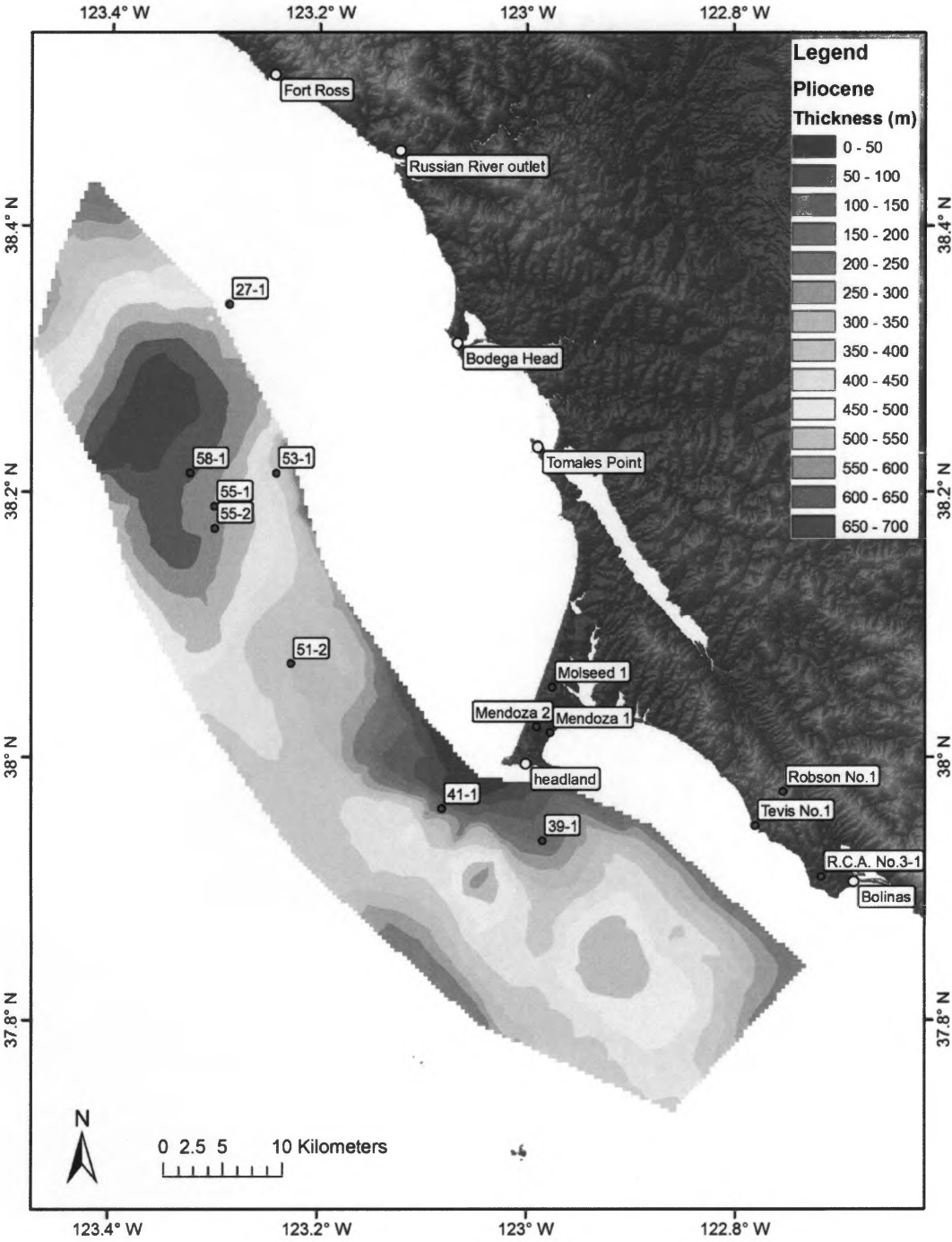


Figure 43: Isopach map of Pliocene units

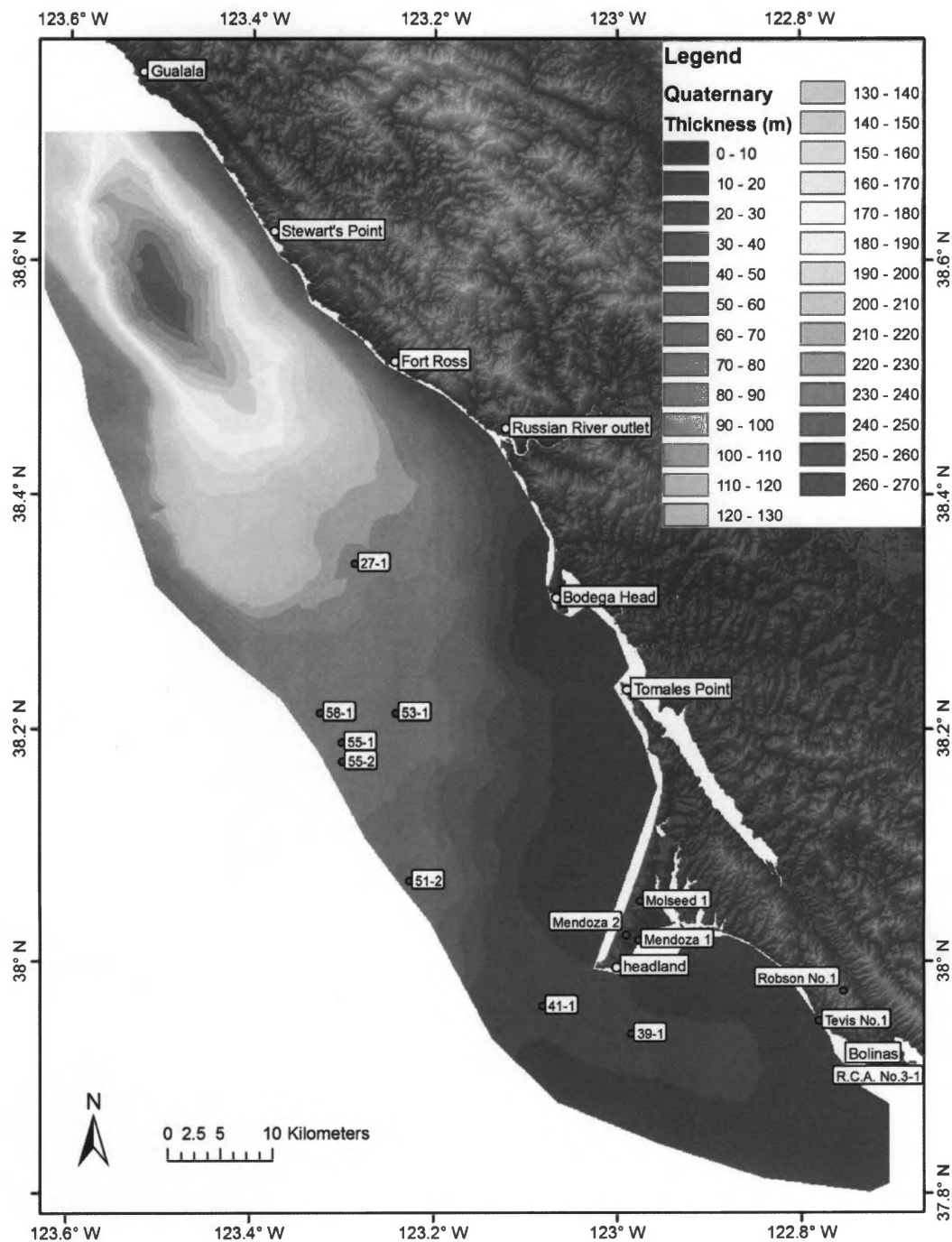


Figure 44: Isopach map of Quaternary units

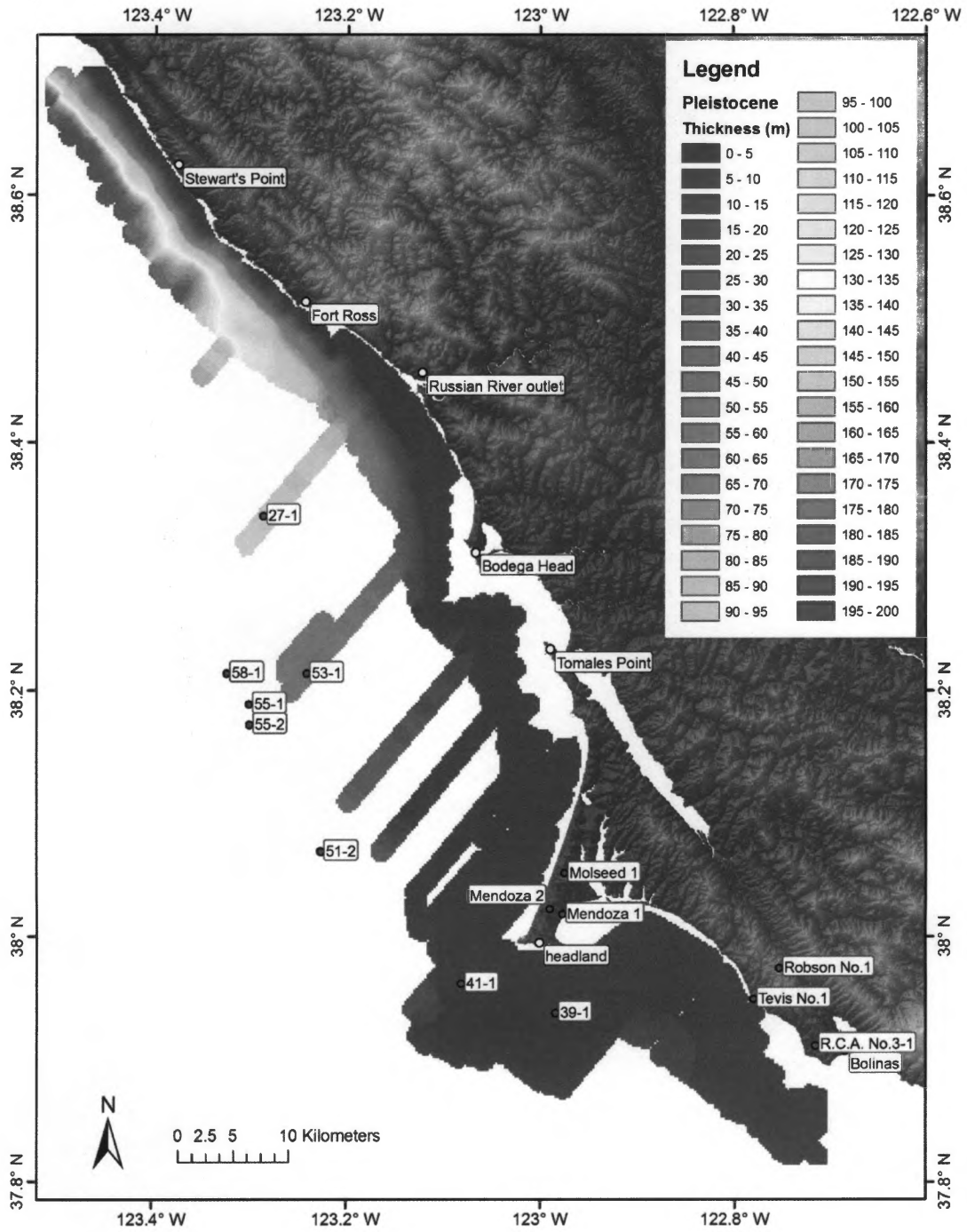


Figure 45: Isopach map of Pleistocene units

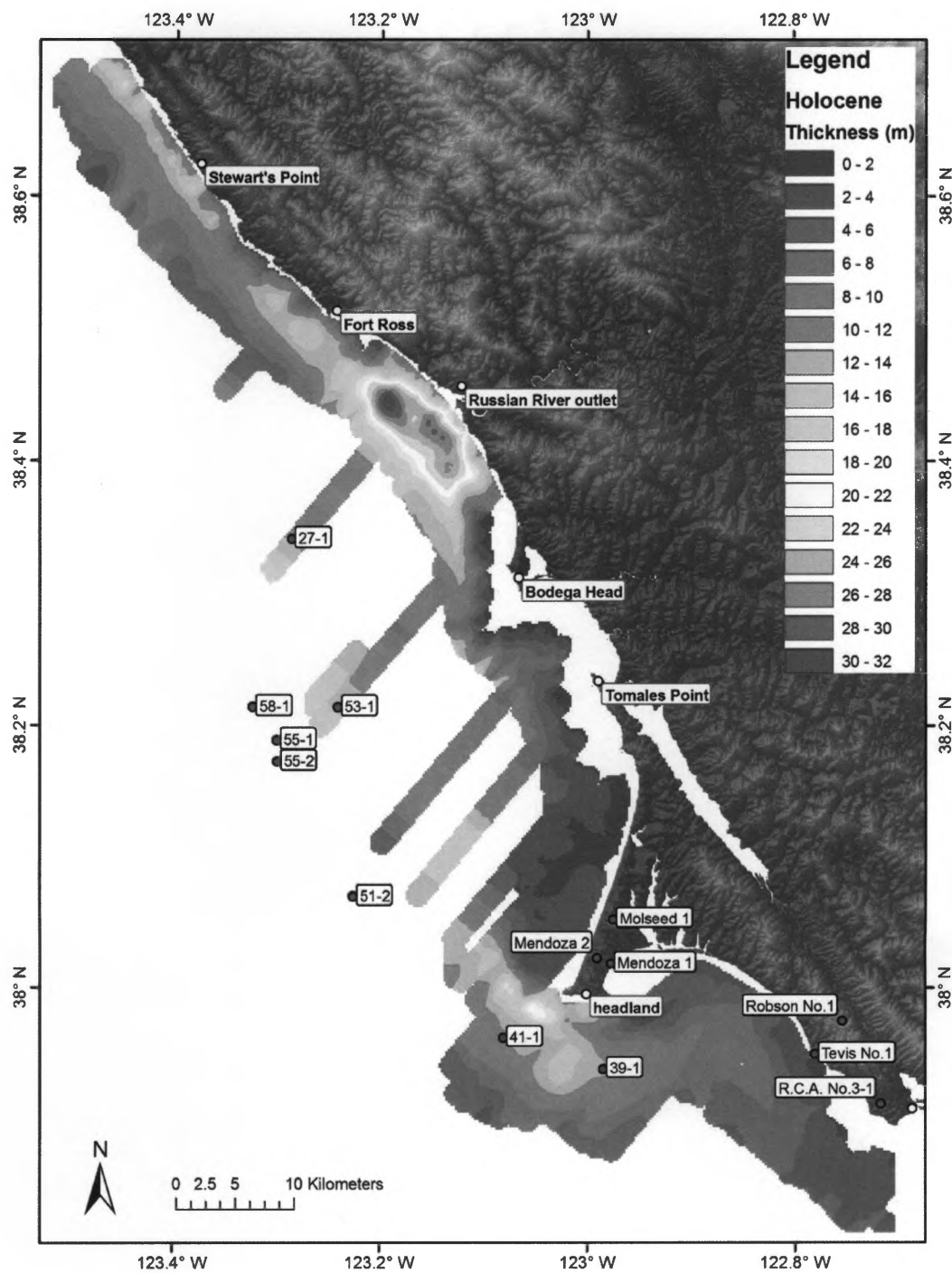


Figure 46: Isopach map of Holocene units

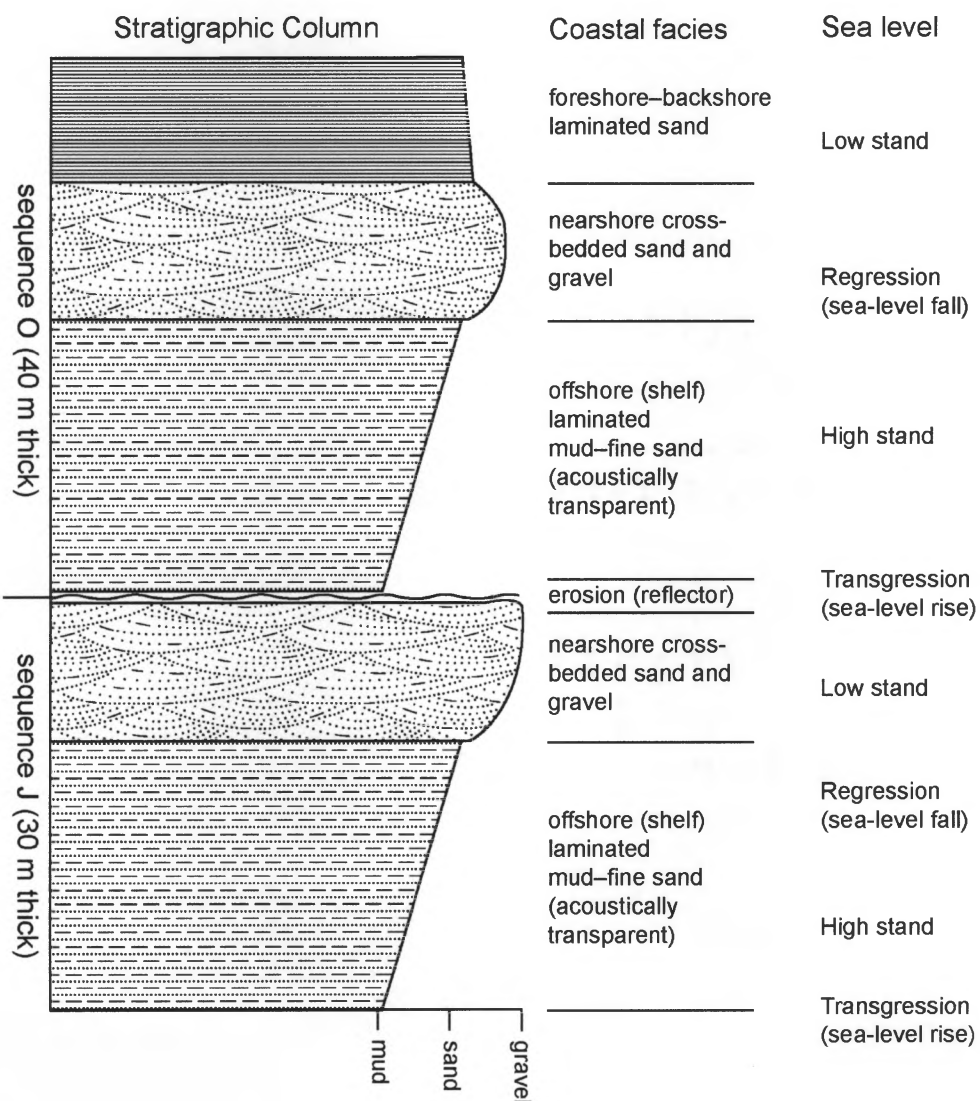


Figure 47: Two sequences to illustrate relation between sediment type, sea level, and acoustic response. No seismic reflectors are produced within homogeneous fine-grained sediments formed during sea-level high stands and gradually coarsening-upward sediments formed during regressions. Strong seismic reflectors occur between low-stand and high-stand deposits, where rising sea level moves high-energy nearshore zone across the shelf to create an erosional unconformity. Sequences J and O are from the Pleistocene Merced Formation (Hunter et al., 1984), which is exposed in the coastal cliffs along the western edge of the San Francisco Peninsula and is an analogue for offshore sequences preserved north of the Point Reyes Peninsula.

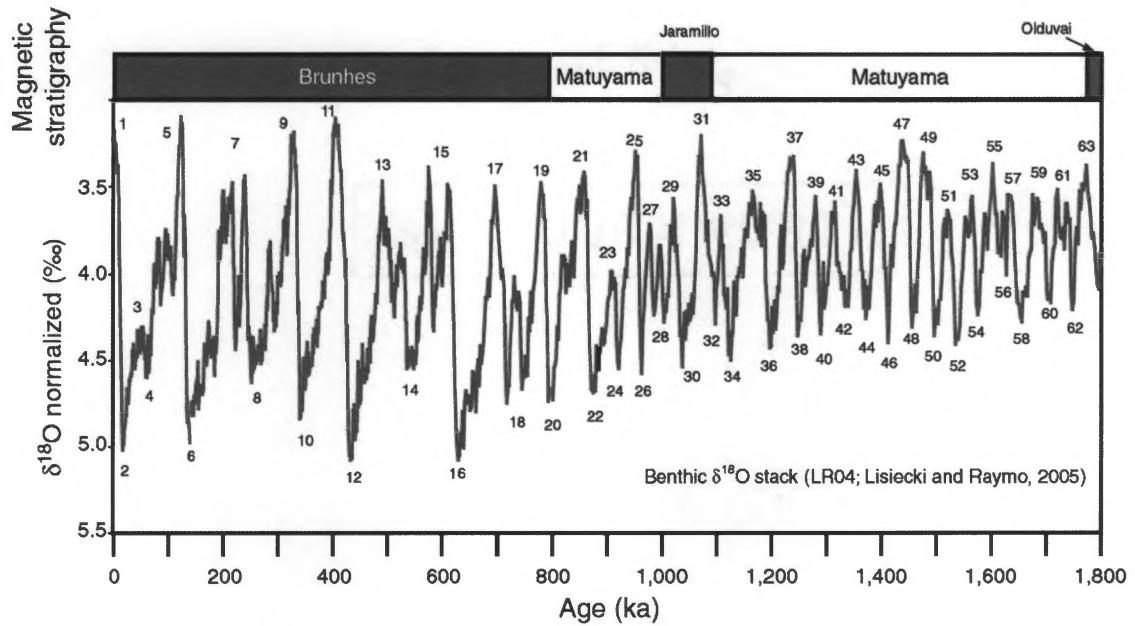


Figure 48: Marine Isotope Stage (MIS) curve from Bassinot (2007). Odd numbers are interglacial periods when sea level is high; even numbers are glacial periods when sea level is low.

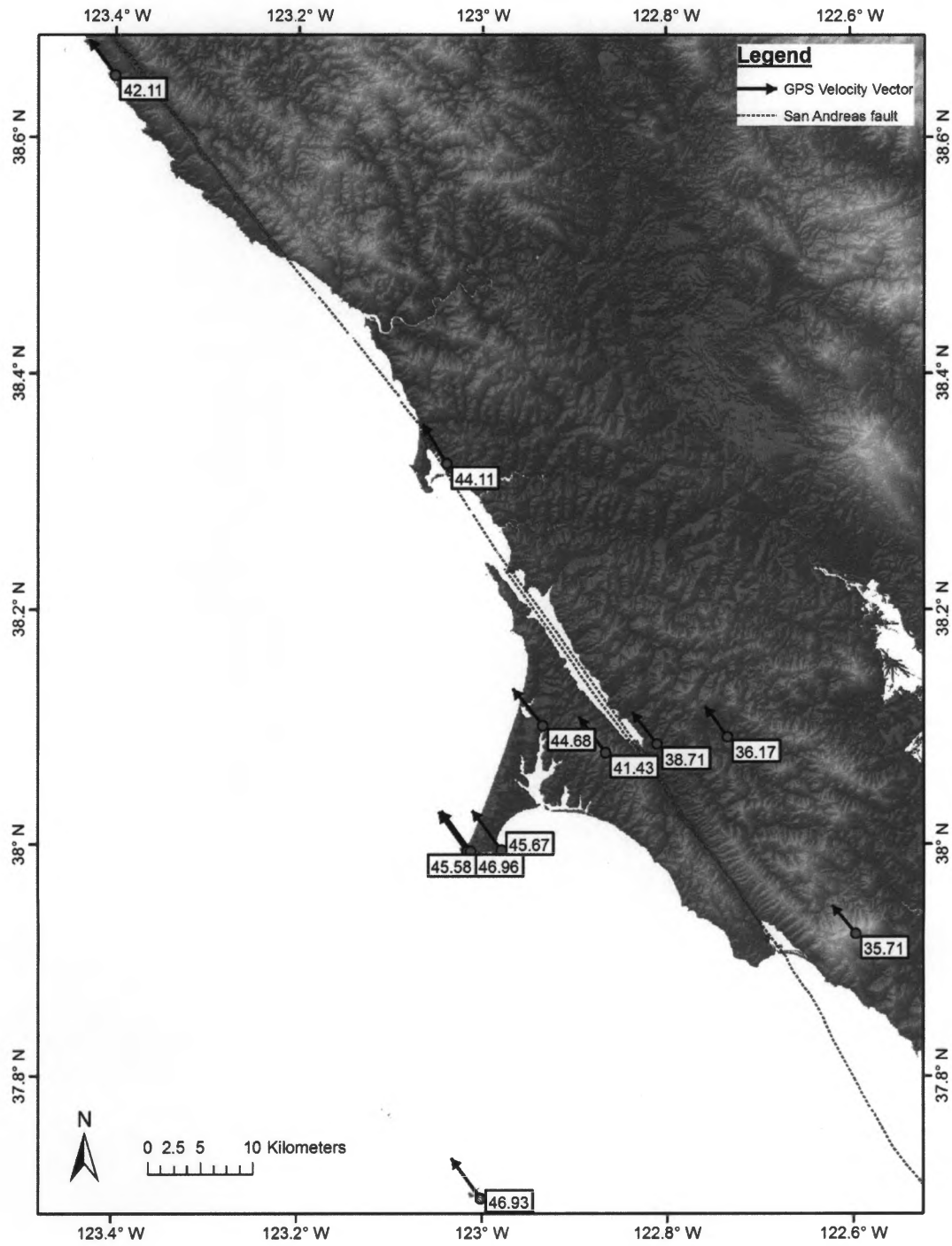


Figure 49: GPS velocity field vectors (with velocity in mm/yr) compiled by the WGCEP (<http://www.wgcep.org/>).

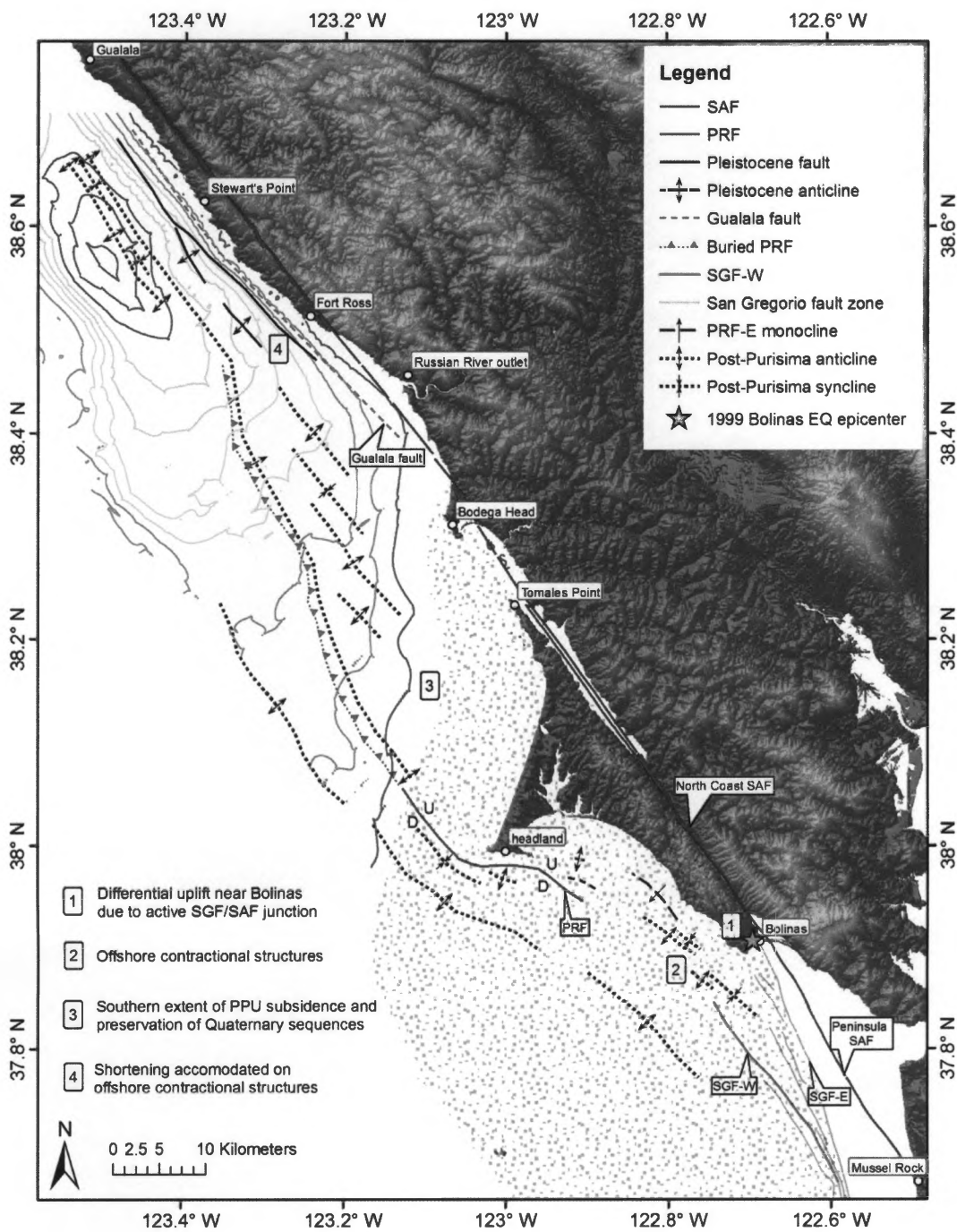


Figure 50: Late Quaternary deformation summary. Ten-meter bathymetric contours indicate a region of subsidence; contours are simplified from isopach map of Quaternary units (Fig. 44). The stippled pattern represents region of no subsidence or uplift.

## 8.0 Appendices

### *A. Velocity Models for Offshore Wells*

TWTTs for geologic units where there are no velocity data in the well logs, generally above a depth of 150–750, were estimated by using each well's regression equation for velocities above the top of the Monterey Formation; only velocities above the Monterey Formation were used as there is a pronounced increase in velocity at the top of the Monterey Formation. Where it was recorded, the velocity was measured every one-half foot (0.1524 m) using a borehole compensation technique that averages multiple measurements along the drill stem, and is reported in m/s. The individual well velocity regression models (Appendix C) estimate acoustic-wave velocities where they were not recorded by forcing a regression line through the available velocity data and 1,500 m/s at the sea floor (acoustic-wave velocity through water). The regression equations were based on a second-order polynomial line fit to the measured velocity data (Appendix A). The only exception to this method was for well 27-1, where the velocity of the pre-log sediment overlying the Monterey Formation was estimated with a linear regression through the velocity data forced through 1,500 m/s (velocity of water) at the seafloor. Tops of the units were then estimated by using the mid-point velocities estimated from each well model (Appendix C) for the overlying unit and including the total additive TWTTs from

other overlying units and water column (Equation 1). TWTTs to the tops of formations were calculated by Equation 1. Estimated TWTTs and recorded TWTTs are included in Tables 1–8.

(1) *TWTT to top of formation =*

$$\begin{aligned} & (TWTT \text{ above overlying } Fm) + \frac{(2 * \text{thickness of overlying } Fm)}{(\text{model velocity for middle of overlying } Fm)} \end{aligned}$$

To convert the seismic profiles from TWTT to depth, a velocity regression model for the Bodega Basin was required. A velocity regression was created for units above the top of the Monterey Formation, a major basin-wide unconformity (Fig. 8). To calculate the basin-wide velocity regression, the entire velocity measurement database was compiled, excluding wells numbered 27, 39 and 41, which were drilled on the periphery of the basin. The units in these wells, located on either the eastern side of the PRF, or to the south of the Point Reyes Peninsula, give an elevated velocity signature at shallow depths because uplift on the hanging wall of the fault has placed highly compacted older geologic units in the shallow subsurface. A velocity average was also calculated for units below the Monterey unconformity (Fig. 9). For the units above the Monterey Formation, the resulting second order polynomial function, when forced through the y-axis (sea level) at 1500 m/s (the average acoustic wave velocity through water), gives an estimate of a basin-wide velocity regression model (Equation 2).

$$(2) \quad \text{Velocity} = (479 \cdot \text{TWTT}^2) - (46 \cdot \text{TWTT}) + 1500$$

The velocity regression for post-Monterey units (as a function of TWTT) was set at the seafloor, and the velocity average for below the Monterey unconformity was set at the top of the Monterey Formation. To take into account the large amount of uplift across the PRF, the basin was divided into two grids: one for the western side of the PRF which includes the thick Neogene section, and one for eastern side of the PRF, in the region of Shell offshore wells 27, 39, and 41, where the Miocene-aged strata have been uplifted to the shallow subsurface. The uncertainties in the depths to horizons determined by using the velocity regression, are presented in Appendix B.

### ***B. Uncertainty in the Velocity Regression Equations***

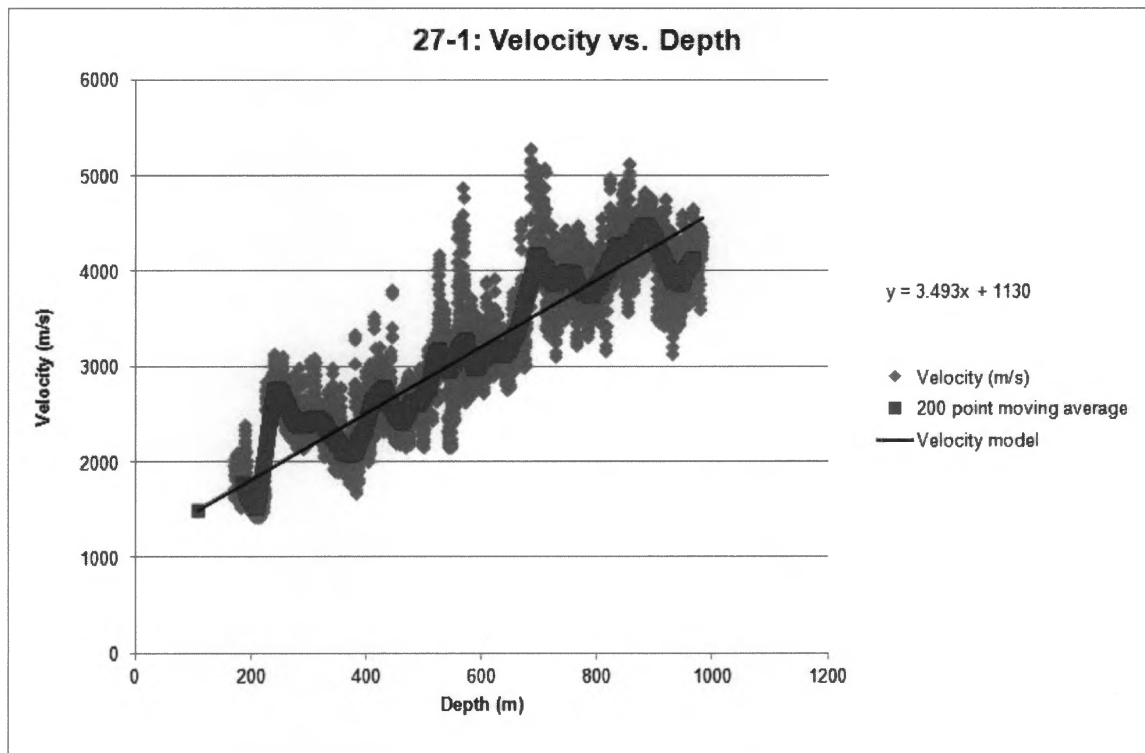
Uncertainty in the velocity regression equations can be quantified in multiple ways. For the basin-wide velocity curve, the standard error for both variables, TWTT (46) and TWTT<sup>2</sup> (479), are 3.7 and 2.4, respectively. A R-squared value can also be calculated from the basin-wide velocity curve, by not forcing the y-axis forcing 1500 m/s. A true r-squared value cannot be measured when the regression line is forced through a point on the y-axis. Removal of the y-axis forcing yielded a r-squared value of approximately 0.81. To test whether the 2<sup>nd</sup> order polynomial was the best fit to the raw velocity data above the Monterey Formation, a linear regression was fit through the data. The linear

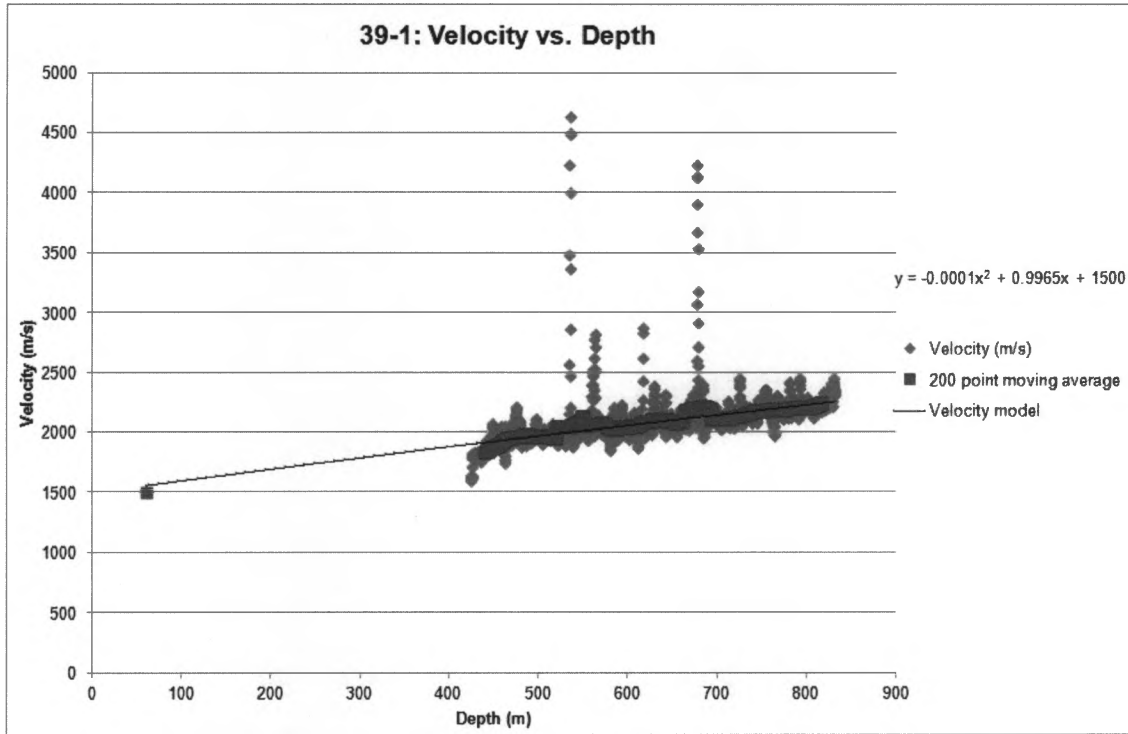
regression yielded a r-square value of 0.79. Although the r-squared value for the linear regression was very close to the r-squared value of the 2<sup>nd</sup> order polynomial, the higher value for the 2<sup>nd</sup> order polynomial regression, with the Y-axis forcing removed, confirms that it is the more appropriate regression line to use when fitting a regression line to velocity data measurements of marine sedimentary units.

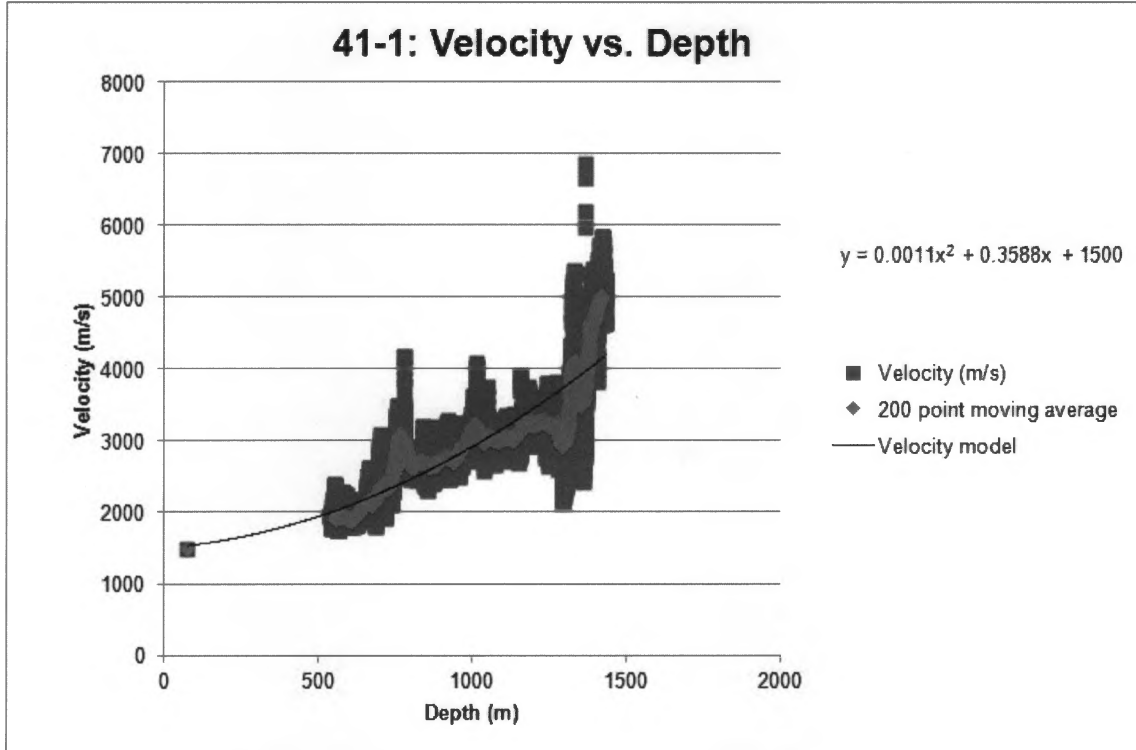
Uncertainty associated with the velocity regression models stems from a variety of sources. A poorly detailed borehole compensation technique that was used when the data were collected in the 1960s includes an unquantifiable amount of uncertainty. This uncertainty is probably not significant, however, because of the large number of measurements (collected every one-half foot or 0.1524 meters). The nature of the rock types, which includes alternating sandstone, siltstone and mudstone, will create localized fluctuations in velocity measurements when measured at one-half foot intervals.

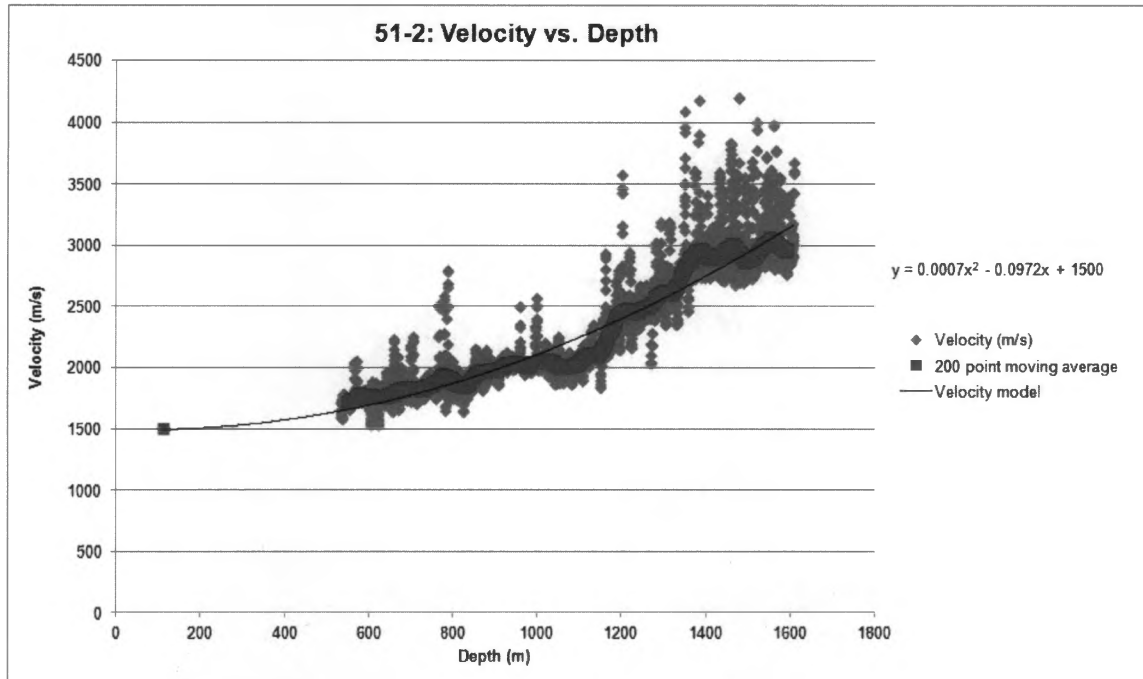
Uncertainty calculations for the regression equations do not appear to be significant and a more practical method for estimating uncertainty is to measure miss-ties on the seismic reflection profiles between multiple well locations. It is expected that most of this uncertainty is below a 30-meter seismic reflection resolution, particularly at depth.

### C. Individual Well Velocity Models

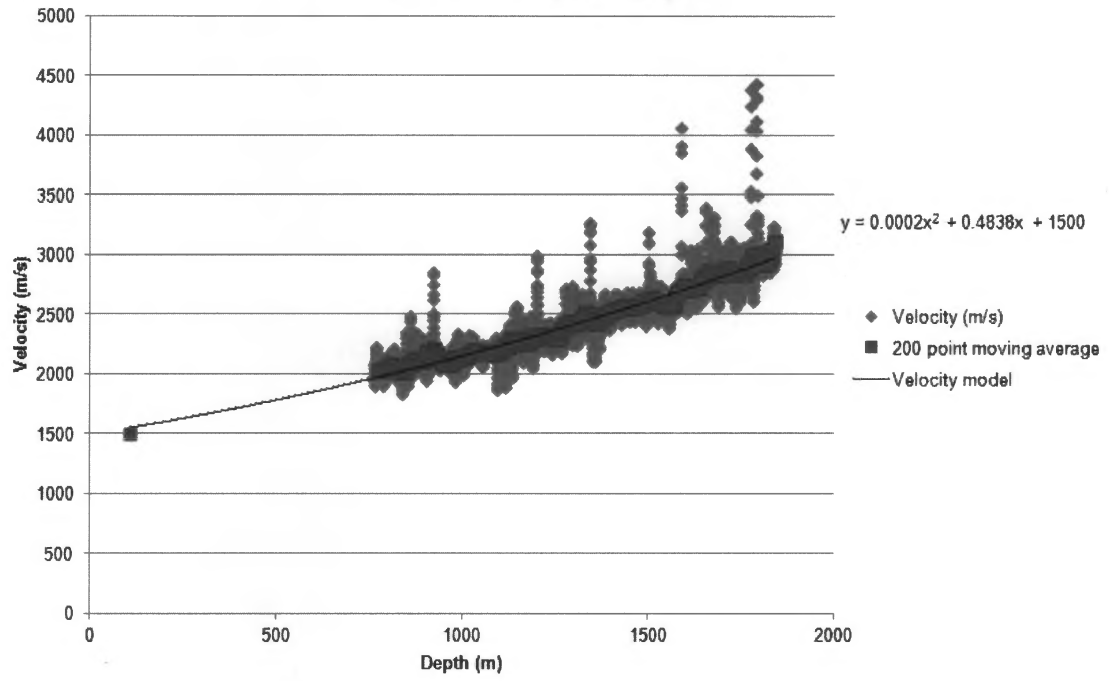


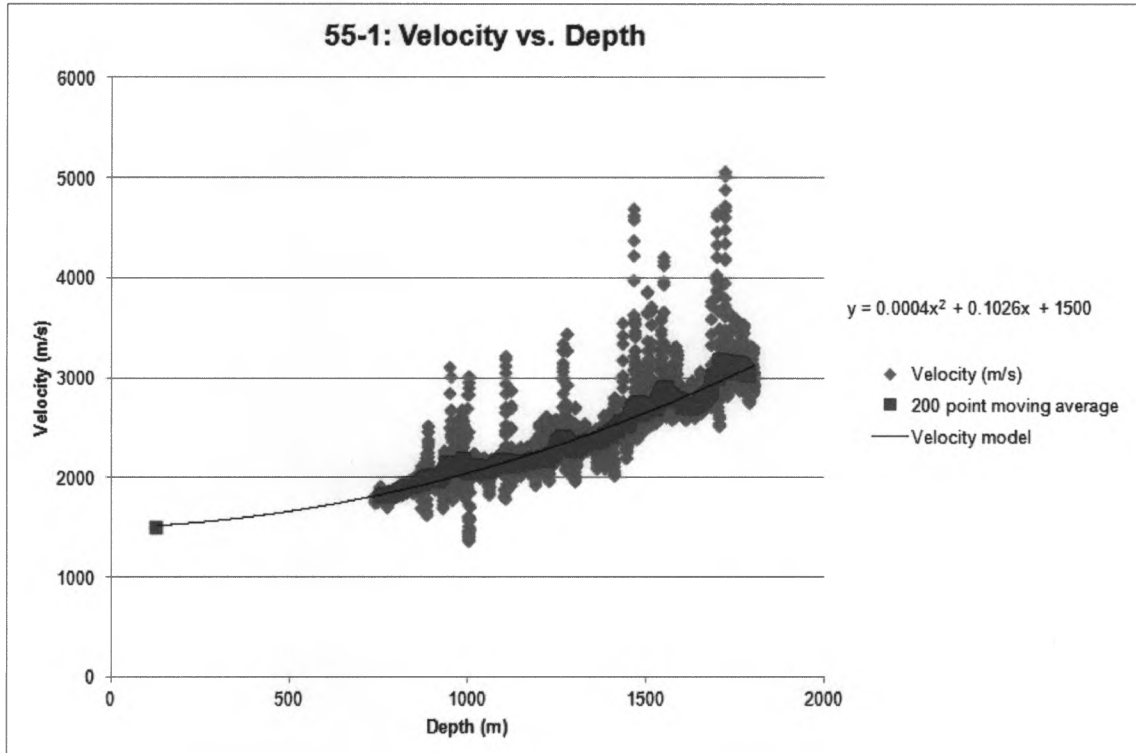






53-1: Velocity vs. Depth





55-2: Velocity vs. Depth

